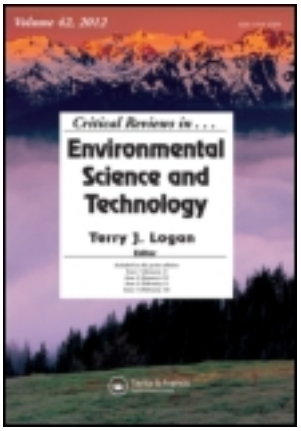

Critical Reviews in Environmental Science and Technology
Publication details, including instructions for authors and subscription information:
http://www.tandfonline.com/loi/best20

Field Approaches to Measure Hg Exchange Between Natural Surfaces and the Atmosphere—A Review

Jonas Sommar [a], Wei Zhu [a b], Che-Jen Lin [c d] & Xinbin Feng [a]

[a] State Key Laboratory of Environmental Geochemistry, Institute of Geochemistry, Chinese Academy of Sciences, Guiyang, China

[b] University of Chinese Academy Sciences, Beijing, China

[c] Department of Civil Engineering, Lamar University, Beaumont, Texas, USA

[d] College of Environmental Science and Engineering, South China University of Technology, Guangzhou, China

Accepted author version posted online: 08 Nov 2012.Published online: 12 Jul 2013.

To cite this article: Jonas Sommar, Wei Zhu, Che-Jen Lin & Xinbin Feng (2013) Field Approaches to Measure Hg Exchange Between Natural Surfaces and the Atmosphere—A Review, Critical Reviews in Environmental Science and Technology, 43:15, 1657-1739, DOI: 10.1080/10643389.2012.671733

To link to this article: http://dx.doi.org/10.1080/10643389.2012.671733

Critical Reviews in Environmental Science and Technology, 43:1657–1739, 2013

ISSN: 1064-3389 print / 1547-6537 online
DOI: 10.1080/10643389.2012.671733

Field Approaches to Measure Hg Exchange Between Natural Surfaces and the Atmosphere—A Review

JONAS SOMMAR,[1] WEI ZHU,[1,2] CHE-JEN LIN,[3,4] and XINBIN FENG[1]

[1]*State Key Laboratory of Environmental Geochemistry, Institute of Geochemistry, Chinese Academy of Sciences, Guiyang, China*

[2]*University of Chinese Academy Sciences, Beijing, China*

[3]*Department of Civil Engineering, Lamar University, Beaumont, Texas, USA*

[4]*College of Environmental Science and Engineering, South China University of Technology, Guangzhou, China*

This review focuses on a vital part of Hg (Hg) atmosphere-natural surface exchange field observational studies, namely the theory, applications, strengths, and limitations of the various experimental methodologies applied to gauge the flux process. We present an in-depth review, a comprehensive literature synthesis, and methodological and instrumentation advances for terrestrial and marine Hg flux studies in recent years. In particular, we outline the theory of a wide range of measurement techniques and detail the operational protocols.

KEY WORDS: air-water exchange, flux footprint, flux measurement tools, gaseous elemental mercury, mercury, micrometeorological techniques, terrestrial ecosystems

INTRODUCTION

Mercury (Hg) is a neurotoxic bioaccumulative trace element of human concern due to potential high-level exposure of methylHg primarily by fish consumption.[1] In the rather chemical inert elemental form (Hg^0), it has extraordinary volatility among the heavy metals.[2] Atmospheric transport of Hg^0

Address correspondence to Jonas Sommar, State Key Laboratory of Environmental Geochemistry, Institute of Geochemistry, Chinese Academy of Sciences, Guiyang 550002. E-mail: jonas@mails.gyig.ac.cn

associated with a generally slow oxidation allows Hg to be (dry or wet) deposited in areas very far (hemispherical scale) from where it was originally emitted to the atmosphere,[3] Therefore, Hg is considered a global pollutant. Nevertheless, the turnover time of Hg in the atmosphere (~1 year) is short compared to the oceanic[4] and terrestrial systems.[5] Human activities have influenced its natural cycling in two interrelated ways: by altering the rate at which Hg is transported between different environmental compartments and by altering Hg into more labile, short-lived pools from those in which it was originally deposited. This implies that transformation of deposited Hg into volatile Hg species and secondary emissions of legacy Hg (deposited from anthropogenic emissions in the past) to the atmosphere occurred—so called re-emissions. Natural emission process and re-emissions are not distinguishable by analytical techniques and will here as elsewhere be treated together. In turn, natural emissions can be sub-divided into inputs of geogenic Hg sources such as volcanoes, weathering processes of Earth crust and forest fires, and the recycling of deposited Hg from the oceans and terrestrial environment. Together, these processes account for a large fraction (up to 60% of the total) of the global atmospheric Hg budget.[6]

In contrast to anthropogenic Hg emissions consisting of a mixture of Hg^0, semi-volatile gaseous inorganic Hg^{II} compounds (gaseous oxidized Hg [GOM] aka reactive gaseous Hg [RGM]. GOM will be used in this review as it is a more appropriate term than RGM[7]) and Hg associated with aerosols (Hg-p), natural emissions occur predominantly as Hg^0. The actual speciation-fractionation of airborne Hg is essential to observe as it has a significant influence on depositional patterns to environmental surfaces. Dry deposition occurs due to turbulent transport and is therefore highly dependent on surface and meteorological conditions. Concerning Hg-p, coarse particles ($d_p > 2.5\ \mu m$) deposit faster than those belonging to the accumulation mode ($0.1 < d_p < 1\ \mu m$). The corresponding velocity (w_d, see Eq. 1) is generally in the order GOM > Hg-p ($0.1 < d_p < 1\ \mu m$) $\geq Hg^0$. Dry deposition velocities of Hg^0 are generally very low, such as < 0.1 cm s^{-1} over bare soil, grasslands, snow, and water surfaces.[8] Concerning Hg^0, the transfer processes at the interfaces of the lithosphere, atmosphere, hydrosphere, and biosphere are largely bi-directional (i.e., potentially include both emission and dry deposition events).

To better understand the biogeochemical cycle of Hg in the natural environment, it is important to determine spatial and temporal variability in the air-surface exchange of Hg^0 as it relates to environmental, physicochemical, meteorological factors as well as surface characteristics. The interactions between all these factors lead to highly variable Hg^0 flux, making it imperative to perform experimental studies in a diversity of surfaces (landscapes, oceans, etc.) over a sufficiently long time-scale to pinpoint crucial regulating mechanisms. Over the last three decades, this field has attracted substantial research activities. The state of knowledge has been summarized in review papers including general overviews of Hg emissions from natural sources[9,10] and more specifically for exchange of Hg between air and natural

terrestrial surfaces,[11–13] Hg air-water flux over oceans,[14,15] Hg air-surface exchange in polar regions,[16,17] Hg emissions from volcanoes[18] and biomass burning[19] as well as the current understanding of dry deposition of atmospheric Hg species.[8] This review article focus on a vital part of Hg atmosphere-natural surface exchange field observational studies, namely the theory, applications, strengths, and limitations of the various experimental methodologies applied to gauge the flux process. Here, we present an in-depth review including a comprehensive literature synthesis and document methodological and instrumentation advances for terrestrial and marine Hg flux studies in recent years. In particular, we outline the theory of a wide range of measurement techniques and detail the operational protocols.

Fluxes of Hg are expressed as emission or deposition rates per unit surface area, typically in nanograms per meter squared per hour. The sign convention treats an emission as a positive flux and a deposition as a negative flux. The flux (F_{Hg}) can be defined as the product of air concentration (C_{Hg}, typically in ng m^{-3}) and a bidirectional vertical surface-exchange velocity (w, m s^{-1}):

$$F_{Hg}(z) = C_{Hg}(z) \cdot w(z) \tag{1}$$

There exists various experimental approaches to gauge Hg environmental flux. Each approach has its niche:

1. Enclosure methods for small plots and small gas fluxes;
2. Optical long-path spectroscopic techniques (light detection and ranging [LIDAR], in differential absorption mode [DIAL] or ultraviolet differential optical absorption spectroscopy [UV-DOAS]) for point, line or small, well-defined, strong areal sources;
3. Micro-meteorological (relaxed eddy accumulation, modified Bowen-ratio and aerodynamic) methods for larger landscapes with homogeneous surface sources;
4. Bulk methods with major application for gas exchange over larger fresh- and sea-water bodies.

In Figure 1 the approximate length- and time-scales within which the various methods are operating are displayed. Each measurement method noted has its share of benefits and drawbacks (see Table 1 for a summary). Nevertheless, in addition to the given method categories, for specific areal sources or meteorological conditions, other approaches have in some instances been employed. Reviewed later in the section "Conservative tracers for non-turbulent conditions" is a ^{222}Rn tracer technique used during periodswith a stable nocturnal boundary layer and found to be suitable in situations where the fluxes are small, or the surface is highly heterogeneous.[20] For relatively small, spatially heterogeneously distributed source areas, such as working face landfills, simple models have been implemented.[21–23] They

TABLE 1. Evaluation of various techniques to measure mercury exchange between air and natural surfaces

	Enclosure	Flux-gradient methods	Relaxed Eddy Accumulation	Differential absorption LIDAR
Spatial scale		See Figure 1		
Sampling frequency	Typically 5 min[a]	10–20 Hz	1[b]–20 Hz	20 Hz
Time resolution of flux	Typically 10–20 min	Typically 20–90 min	Typically 10–30 min (3–6 hr[b])	Typically 1 hr
Weaknesses	• Modification of microclimate. • Perturbations to gas concentration gradients and associated diffusion. • Potential physical damage to biological structures.	• Relying on measurements of often small gradients. • Different footprints for various sensor heights. • Not applicable for low u^*.[c] • Function of anemometer sensitive to rain. • Co-location of sources/sinks for the reference quantity with those for Hg.[c]	• Offset from $\bar{w} = 0$ causes bias, which cannot be removed from the data with later processing.[d] • Pressure and flow fluctuations in the sampling system must be avoided. • Function of anemometer sensitive to rain.	• Complex and less compact. • Labor-intensive construction.
Financial expenses	Relatively less costly (in coupling with automatized Hg analyzer high[e])	High[f]	High[f]	Very high[g]
Personal expertise	Introduction education	Good knowledge in micrometeorological and measuring technique.	Good knowledge in micrometeorological and measuring technique.	Expertise in photonics, optics, laser spectroscopy, etc. No stand-alone commercial apparatus available.

Requirements	Tight seal to surface plot. Uniform flow over surface.	• Scalar similarity. • Recommended ratio between sampling heights $z_2/z_1 \sim 4–8$ [c]	• Sampling made at constant flow rate. • Valve switching at accurate time. •Scalar similarity	Measurement of vertical wind field.
General restrictions in application	Limited use for flux estimate of larger areas.	• Turbulent conditions. • Difficult to apply on tall vegetation. • Sufficient footprint area.	• Turbulent conditions. • Sufficient footprint area	Restricted to point, line or small, well-defined strong areal sources.
Gas sampling and analytical system	Chambers can potentially be operated using battery power and require in a basic version no on-line gas measurement.	Analyzers need high precision, robust samples are required with sequential sampling at different heights to avoid the effect of tube dead volumes.	Analyzers need high precision, conditional sampling system require strict pressure and flow control measures. Bias between conditional sampling lines should be (regularly) investigated and corrected for.	Require high-power, narrow-bandwidth tuneable lasers.

[a]Automatized Hg analysis.
[b]Applies to REA with denuder front samplers (GOM).
[c]Mainly concerns MBR-method.
[d]Different strategies in order to filter out vertical bias from the w signal have been applied (see Bowling et al.[117]).
[e]~15–60 k€.
[f]Includes automatized Hg analyzer ~50–110 k€.
[g]A rough estimate based on individual new components only: 300 k€ and up.

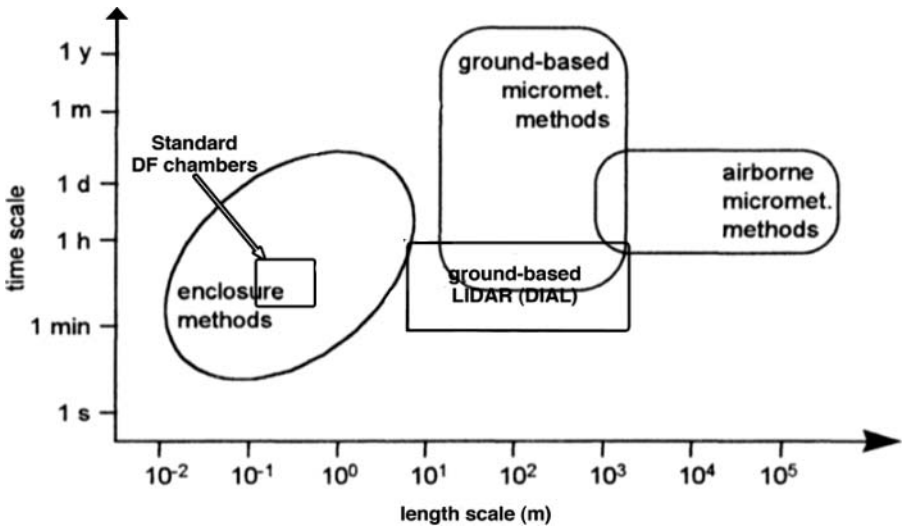

FIGURE 1. Time- and length-scale niches of various methodologies to measure natural fluxes of trace gases.

involve single point Hg air sampling up- and downwind the area source combined with on-site meteorological data as input to predict dispersion parameters. These models are not explicitly discussed in this review and more information can be found elsewhere.[24,25] However, they have points of contact with the source area models relevant for micro-meteorological techniques (see section "Footprint (source area) of MM-techniques") and are included in the summary of published articles on air-natural surface exchange of Hg presented in Table 2. Description of techniques utilized for estimating Hg emissions from natural high temperature processes (e.g., biomass wild-fires or volcanic activity) is beyond the scope of this review and can be retrieved elsewhere.[18,19,26]

STRUCTURE OF ATMOSPHERIC BOUNDARY LAYER

The trace gas exchange at the Earth's surface creates local concentration surplus or deficit in the adjacent air layers. Usually, these effects are distributed very fast (in the timescale of min to hr) throughout the planetary boundary layer (PBL) by turbulent mixing. An idealized PBL thus represents a well-mixed closed chamber and the surface flux can be described according to Eq. 2. However, in real conditions (especially during daytime), the PBL is not constant in height and continuously mixes with overlying air layers while growing.[27] Additionally, horizontal advection cannot be neglected. The lowest 10% of the PBL height, where most of flux measurements are made, is

TABLE 2. A summary of air-surface mercury flux measurements for various marine, limnological, and terrestrial ecosystems reported in the literature. The flux values are in general given as mean, mean ± standard deviation or as a min–max range if not otherwise stated.

Surface/source	Location	Season	Species[a]	Method	Flux	Remarks	Citation
			Contaminated sites				
Hg cell chlor-alkali plant	EKA Nobel, Bohus, Sweden	— May 2002 August–September, 2001 January, 2002 June 2003	Hg^0	DIAL	30 g h^{-1} 31 g h^{-1} 10.5 g h^{-1} 6 g h^{-1} 11 g h^{-1}	Emission factor 0.5–1.0 g Hg/ton Cl_2 produced.	Edner et al.,[79] Edner et al., [203] Sjöholm et al.,[81] Wängberg et al.,[204] Grönlund et al.[82]
Hg cell chlor-alkali plant	Norsk Hydro, Stenungsund, Sweden	May 2002	Hg^0	DIAL	1.9–8.1 g h^{-1}		Edner et al.[203]
Hg mining complex	Almadén, Spain	September 1993	Hg^0	DIAL	600–1200 g h^{-1}	Hg-tot soil concentration ~700 μg g^{-1}.	Ferrara et al.[205]
Old roasted cinnabar banks		August 1993	TGM	DFC	80000–110000 ng m^{-2} h^{-1}		Ferrara et al.[206]
Abandoned Hg mining complex	Mt. Amiata, Italy	July 1995	Hg^0	DIAL	60–100 g h^{-1}	Strong seasonal variation. Hg-tot soil concentration ~180 μg g^{-1}.	Ferrara et al.[207]
Roasted cinnabar banks		February, May, August 1992	TGM	DFC	30–10000 ng m^{-2} h^{-1}		Ferrara et al.[206]
Hg cell chlor-alkali plant	Rosignano Solvay, Italy	September 1990 February 2002 July, 2003	Hg^0	DIAL	43 g h^{-1} 20 g h^{-1} 54 g h^{-1} 48–54 g h-1	Emission factor 1.8–4.8 g Hg/ton Cl_2 produced. Range refers to various approaches to assess the vertical wind profile. The low range value derived by doppler-LIDAR.	Ferrara et al.[208] Sjöholm et al.[81] Grönlund et al.[82] Bennett et al.[85]
Hg cell chlor-alkali plant	Zakłady Azotowe, Tarnów, Poland	August 2003	Hg^0	DIAL	28 g h^{-1}	Emission factor 8.8 g Hg/ton Cl_2 produced.	Grönlund et al.[82]

(*Continued on next page*)

TABLE 2. A summary of air-surface mercury flux measurements for various marine, limnological, and terrestrial ecosystems reported in the literature. The flux values are in general given as mean, mean ± standard deviation or as a min–max range if not otherwise stated. *(Continued)*

Surface/source	Location	Season	Species[a]	Method	Flux	Remarks	Citation
Hg cell chlor-alkali plant	Southeast USA	Fall 2006	Hg^0	DOAS	410 ± 168 g day^{-1}	Three bistatic UV-DOAS instruments with a horizontal distance of 220 m between light source and receiver employed.	Thoma et al.[83]
Abandoned Hg mining complex	Idrija, Slovenia	November 2003	Hg^0	DIAL	2 g h^{-1}	Distillation plant only, low temperatures prevailing.	Grönlund et al.[209]
Contaminated soil	Idrija town, Slovenia	September 2004	Hg^0	DFC	20–240 ng m^{-2} h^{-1}	Hg-tot substrate conc. 333 μg g^{-1}	Kotnik et al.[210]
Mine/retort surface	New Idria, CA, USA	September 1998, October 1999	TGM	DFC	119–3267 ng m^{-2} h^{-1}	Hg-tot substrate conc. 11–535 μg g^{-1}	Coolbaugh et al.[211]
Landfills	Southern Florida, USA	1997–1999, 2001–2002	TGM	DFC		Seven landfills investigated.	Lindberg and Price[23]
Final/temporary cover					<1–~20 ng m^{-2} h^{-1}		Lindberg et al.[22]
Waste surface					<1–~150 ng m^{-2} h^{-1}		
Working face surface				DM[b]	~200–400 mg h^{-1}	Extrapolated to uniform surface flux in the order of magnitude 10–100 μg m^{-2} h^{-1}.	
Landfill covered by clean soil and equipped with passive gas drainage	Nan-Ji-Do, Seoul, Korea	Spring 2000	TGM	AER	254 ± 224 ng m^{-2} h^{-1} −1164 ± 1276 ng m^{-2} h^{-1}	Strong emission prevailing. Dry deposition observed when plume of landfill gas vent impacting fetch.	Kim et al.[145]
Landfill	Bang Chun, Daegu, Korea	January 2004	TGM	AER	39 ± 43 ng m^{-2} h^{-1} [c] −60 ± 80 ng m^{-2} h^{-1} [c]	K-values estimated from a parameterization incl. wind speed.	Nguyen et al.[46]

Landfills Final/temporary cover Waste surface Working face surface	Guiyang, Guizhou, China Wuhan, Hubei, China	2003–2006	TGM	DFC DM[b]	−1–20 ng m^{-2} h^{-1} [d] ~500–600 ng m^{-2} h^{-1} [d] ~2–370 g $year^{-1}$	Five landfills investigated. Multi-plot short time studies. Presence of vegetation tends to dampen evasion flux.	Li et al.[21]
Landfills covered with coal combustion products Blended coal fly ash landfill Lignite derived fly ash landfill FGD material + fly ash	Great Lakes area, USA Midwestern USA	October 2003 September 2004	TGM	DFC	0.2–5.4 ng m^{-2} h^{-1} [e] −0.2–4.9 ng m^{-2} h^{-1} [e] 0.7–22.2 ng m^{-2} h^{-1} [e]	Diurnal patterns in flux with predominant overall net emission.	Xin et al.[212]
Chlor-alkali waste repository	Bohus, Sweden	June 2002	TGM	REA	6270 ± 5484 ng m^{-2} h^{-1}	Diurnal pattern linked to solar radiation rather than soil surface layer temperature. Hg^0 detected in the surface soil (~13%) of Hg-tot conc. 28–183 μg g^{-1}	Olofsson et al.[92]
Land-applied stabilized harbour dredged sediment material (SDM)	Bayonne, NJ, USA	August 2001-November 2002	TGM	AER	−13–1040 ng m^{-2} h^{-1}	Flux significantly correlated with solar radiation. Hg-tot SDM conc. 1.3 −2.6 μg g^{-1}	Goodrow et al. [148]
Hg-gold amalgamation mining areas	Cuyuni river basin, Bolivar state, Venezuela	May 2004	Hg^0	DFC	0.7–420 μg m^{-2} h^{-1}	Soil, waste rock and mud surfaces Hg-tot concentrations 0.5–500 μg g^{-1}	Garcia-Sanchez et al.[51]

(*Continued on next page*)

TABLE 2. A summary of air-surface mercury flux measurements for various marine, limnological, and terrestrial ecosystems reported in the literature. The flux values are in general given as mean, mean ± standard deviation or as a min–max range if not otherwise stated. *(Continued)*

Surface/source	Location	Season	Species[a]	Method	Flux	Remarks	Citation
Hg mining areas	Lanmuchang, Guizhou, China	December 2002 and May 2003	TGM	DFC	−623–10544 ng m^{-2} h^{-1}	Hg refining activities until 1958. Fluxes correlated by Hg air conc. during day and occasionally anti-correlated during night.	Wang et al.[213]
	Wanshan, Guizhou, China	November 2002 July–August 2004			−9434–27827 ng m^{-2} h^{-1}	Multi-site short time studies including cinnabar slag heaps, natural enriched bedrock, contaminated and agricultural soils.	Wang et al.[214]
	Wuchuan, Guizhou, China	December 2003 December 2004			−5493–140 ng m^{-2} h^{-1}	Five locations investigated. Hg flux and air TGM concentration significantly anti-correlated.	Wang et al.[215]
Open pit gold mining areas	Cortez-pipeline and Twin Creeks mines, NV, USA	February 2008–March 2009	TGM	DFC	19–377 ng m^{-2} h^{-1}	Hg-tot concentrations 0.6–3.5 μg g^{-1}	Eckley et al.[216]
Waste rock piles					37–28500 ng m^{-2} h^{-1} [f]	19–177 μg g^{-1}	
Tailings					490–13000 ng m^{-2} h^{-1}	~35-fold higher flux compared to pre- and post-application periods	
Active cyanide leach pads							
Mine waste	Ivanhoe Au mine, CA, USA	Fall 1999	TGM	DFC	101–546 ng m^{-2} h^{-1}	Hg-tot conc. 11.8–30.5 μg g^{-1}	Engle et al.[55]
	McLaughlin mine, CA, USA				214–2101 ng m^{-2} h^{-1}	Hg-tot conc. 81–497 μg g^{-1}	Gustin et al.[135]
	Sulphur Bank superfund site, CA, USA				188–8404 ng m^{-2} h^{-1}	Hg-tot conc. 105–1120 μg g^{-1}	

Tailings	Sulphur Bank superfund site, CA, USA		TGM	DFC	4060–11000 ng m^{-2} h^{-1}	Hg-tot conc. 500–530 μg g^{-1} Extremely high GOM conc.– ~76 ng m^{-3} associated with measurements.	Nacht et al.[217]
Mill tailings	Carson River superfund site, NV, USA			MBR	50–3000 ng m^{-2} h^{-1}	Hg-tot conc. 20 μg g^{-1}	Gustin et al.[135]
Processed mill tailings					0–150 ng m^{-2} h^{-1}	Hg-tot conc. 0.3 ± 0.07 μg g^{-1}	
Contaminated floodplains	Lower River Elbe, lower Saxony, Germany	August 1995	TGM	DFC	43 ± 5 ng m^{-2} h^{-1}	Single day sampling	Wallschläger et al.[52]
				SDM[g]	53 ± 17 ng m^{-2} h^{-1}	Hg-tot conc. ~10 μg g^{-1}	
	Central River Elbe, Thuringia, Saxony, Germany	2005–2006	TGM	SFC[b]	10–800 ng m^{-2} h^{-1}	Co-located DFCs were operated simultaneously. Hg-tot conc. 3.5–15.6 μg g^{-1}	Rinklebe et al.[42] Rinklebe et al.[218]
Contaminated forested floodplains	Oak Ridge, TN, USA	Spring and fall 1993	TGM	MBR	86 ± 72 ng m^{-2} h^{-1}	Best-fetch flux data given.	Lindberg et al.[93]
Freshwater surfaces							
Boreal forest lakes	Gårdsjön, Sweden	May–June 1988–1989 June 1994	TGM	DFC MBR	8.0 ± 2.5 ng m^{-2} h^{-1}	Emission fluxes totally dominant	Xiao et al.[33]
					8.5 ± 6.5 ng m^{-2} h^{-1}		Lindberg et al.[130]
	Three adjacent lakes	May–June 1988		DFC	7.8 ± 5.4 ng m^{-2} h^{-1}		Xiao et al.[33]
	Eagle Lake, NW Ontario, Canada	July 1986	TGM-DGM	GEM[i]	~4.5 ng m^{-2} h^{-1}	Derived from spiking sediment with Hg^0.	Schroeder et al.[174]

(*Continued on next page*)

TABLE 2. A summary of air-surface mercury flux measurements for various marine, limnological, and terrestrial ecosystems reported in the literature. The flux values are in general given as mean, mean ± standard deviation or as a min–max range if not otherwise stated. *(Continued)*

Surface/source	Location	Season	Species[a]	Method	Flux	Remarks	Citation
Acidic forest lakes	Kejimkujik Nat. Park, NS, Canada						
	North Cranberry Lake	August 1997	TGM	DFC	1.1 ng m^{-2} h^{-1}	Lake low in DOC[j]	Boudala et al.[219]
					5.4 ng m^{-2} h^{-1}	Lake rich in DOC[j]	
	Big Dam West Lake	Summer 2000			−0.2–6.5 ng m^{-2} h^{-1}	Various multivariate models employed to fit the DFC flux data. A generalized approach using time-shifted solar radiation data to predict DGM for GEM proposed.	O'Driscoll et al.[220]
	Puzzle lake	Summers 1999, 2000			−4.6–9.0 ng m^{-2} h^{-1}		
Reservoir	Cane Creek Lake, TN, USA	June 2003–May 2004	TGM	DFC	~1.2 ng m^{-2} h^{-1} (summer)	Seasonality in DGM level followed a mean solar radiation trend	Zhang et al.[224]
					~0.5 ng m^{-2} h^{-1} (winter)		
High Arctic (74°N) lakes	Cornwallis Island, Nunavut, Canada	August 1998	TGM-DGM	GEM[k]	0.4–2.8 pmol m^{-2} h^{-1}	DGM production promoted by UV radiation and labile Hg^{II}(aq) species.	Amyot et al.[226]
Acidic, oligotrophic forest lake	Ranger lake, Canada	May–October 1994	TGM-DGM	GEM[k]	0.2–6.4 pmol m^{-2} h^{-1}	High DOC. Actinic shortwave radiation has limited effect on DGM formation.	Amyot et al.[227]
Oligotrophic headwater lake	Experimental Lakes Area (ELA), Ontario, Canada	September 2002	TGM (^{202}Hg)	DFC	2.9 ± 1.8 ng m^{-2} h^{-1}	Spike $^{202}HgCl_2$ (2.4 μg m^{-2}) added every two weeks for 18 weeks	Southworth et al.[228]
		June 2003			4.0 ± 1.8 ng m^{-2} h^{-1}		
		August 2003			4.3 ± 1.9 ng m^{-2} h^{-1}		
		September 2003			3.9 ± 1.0 ng m^{-2} h^{-1}		

Great lakes, North America	Lake Michigan	1994–1995	TGM	GEM	120 ± 70 pmol m^{-2} day^{-1}	520 kg a^{-1} derived from k_{tot} = 0.8 m day^{-1} and DGM 150 fM	Mason and Sullivan[229]
	Lake Ontario, North shore	July 1998	TGM-DGM	GEM^{l}	~0–2.8 ng m^{-2} h^{-1}	Air gradient measurements indicate episodically moderate dry deposition.	Poissant et al.[122]
	Lake Ontario, South shore				0.9–9.1 ng m^{-2} h^{-1}		
Seepage lake	Spring lake, MN, USA	2001–2002	TGM-DGM	GEM	−0.9–25 pmol m^{-2} h^{-1}	Approach by Schroeder et al.[155]	Hines and Brezonik[230]
					−4.8–74 pmol m^{-2} h^{-1}	Approach by Poissant et al.[105]	
Arctic tundra lakes	Toolik lake, AK, USA	July 2000	TGM-DGM	GEM^{l}	300–100 pmol m^{-2} day^{-1}	DGM formation largely controlled by organic matter.	Tseng et al.[231]
	Nine adjacent smaller lakes				60 –190 pmol m^{-2} day^{-1}		
River surface	Sites at St. Lawrence River						
	St. Anicet Quay, QC, Canada	Summer 1995	TGM	DFC	−0.5–1.0 ng m^{-2} h^{-1}	Evasion predominant	Poissant and Casimir[199]
	Near Cornwall, Ontario, Canada	May 2005			0.2–1.1 ng m^{-2} h^{-1}	Highest cross-correlation (R^2~0.63) between flux and DGM with a lag time 1–2.5 h corresponding to surface water eddy diffusion time.	O'Driscoll et al.[232]
	Upper St. Lawrence River	July 1998	TGM-DFC	GEME	0.02–9.3 ng m^{-2} h^{-1}	Air gradient measurements indicate episodically weak dry deposition.	Poissant et al.[122]

(*Continued on next page*)

TABLE 2. A summary of air-surface mercury flux measurements for various marine, limnological, and terrestrial ecosystems reported in the literature. The flux values are in general given as mean, mean ± standard deviation or as a min–max range if not otherwise stated. *(Continued)*

Surface/source	Location	Season	Species[a]	Method	Flux	Remarks	Citation
Stream surface	Knobesholmsån, Sweden	August 1999	TGM	DFC	−2.5–88.9 ng m^{-2} h^{-1}	Evasion predominant	Gårdfeldt et al.[45]
			Urban settings				
Residential area soil	Yang Jae, Seoul, Korea	September 1997	TGM	AER	103 ± 80 ng m^{-2} h^{-1} −92 ± 128 ng m^{-2} h^{-1}	K-values estimated from a parameterisation incl. wind speed. Hg-tot soil concentrations 0.07–0.69 $\mu g\ g^{-1}$. Evasion predominant.	Kim and Kim[147]
Urban soil Suburban soils	Guiyang city, Guizhou, China	May–June 2003	TGM	DFC	31.8 ng m^{-2} h^{-1} 44.4 ng m^{-2} h^{-1} 15.0 ng m^{-2} h^{-1} 0.4 ng m^{-2} h^{-1}	Median TGM conc. 6–8 ng m^{-3} (CV 30–50%) at four sampling sites. Soil Hg-tot conc. (0.15–0.63 $\mu g\ g^{-1}$) and solar radiation important parameters.	Feng et al.[49]
Dense urban	Basel city center, Switzerland	March 2004 Sept.–Oct. 2004	TGM	^{222}Rn-tracer	7.5 ± 1.5 ng m^{-2} h^{-1m} 5.2 ± 1.0 ng m^{-2} h^{-1m}	Measurement at 38 m a g l. (above urban structures). Stable NBL occurred ~42% of the nights sampled.	Obrist et al.[20]

Toronto pavement	Toronto, Canada	2005–2006	TGM	DFC	1.0 ng m^{-2} h^{-1}[n]	Spatial flux variability was significantly related to the street dust concentrations (10–45 ng g^{-1}).	Eckley and Branfireun[57]
Austin pavement	Austin, TX, USA				0.8 ng m^{-2} h^{-1}[n]		
Toronto roofs					0.7 ng m^{-2} h^{-1}[n]		
Toronto windows					0.2 ng m^{-2} h^{-1}[n]		
Toronto soils					6.2 ng m^{-2} h^{-1}[n]		
Austin soils					7.8 ng m^{-2} h^{-1}[n]		
Urban bare soil	Tuscaloosa, AL, USA	Entire year	TGM	DFC	5.69 ± 5.79 ng m^{-2} h^{-1} [o]	Meteorological effects contribute to 24% of signature for pavement, 53% for turf and 60% for soil.	Gabriel and Williamson[233]
Turf grass					0.53 ± 1.25 ng m^{-2} h^{-1}[o]		
Pavement					0.26 ± 0.41 ng m^{-2} h^{-1}[o]		
			Coastal sea/Estuarine waters				
Open fjord water	Gullmarsfjorden, Sweden	1997–1998	TGM	DFC	−2.7–8.8 ng m^{-2} h^{-1}	Evasion predominant	Gårdfeldt et al.[45]
	Kongsfjorden, Ny-Ålesund, Spitsbergen	May 2002	TGM-DGM	GEM[p]	0.1–7 ng m^{-2} h^{-1}	DGM conc. 12.2–70.4 pg L^{-1} corresponding to supersaturation.	Sommar et al.[234]
Coastal waters	Halifax harbour, NS, Canada	Summer 1999	TGM	DFC	0.7 ng m^{-2} h^{-1}		Schroeder et al.[235]
	Long Island Sound	August 1995	TGM-DGM	GEM[q]	64/520/1230 pmol m^{-2} day^{-1}	Quantitatively, evasion (80 ± 25 kg a^{-1}) is equivalent with ~35% of the total input and over three times that of direct dry deposition.	Rolfhus and Fitzgerald[237]
		February 1996 October 1996			75/210/550 pmol m^{-2} day^{-1}		
		May 1997			170/530/780 pmol m^{-2} day^{-1}		
		October 1997			180/340/390 pmol m^{-2} day^{-1}		
					8/68/150 pmol m^{-2} day^{-1}		
	West of Mace Head, Ireland	September 1999	TGM-DGM	GEM[p]	0.4–6.4 ng m^{-2} h^{-1}	TGM conc. from Mace Head Atmospheric Research Station	Gårdfeldt et al.[166]

(*Continued on next page*)

TABLE 2. A summary of air-surface mercury flux measurements for various marine, limnological, and terrestrial ecosystems reported in the literature. The flux values are in general given as mean, mean ± standard deviation or as a min–max range if not otherwise stated. *(Continued)*

Surface/source	Location	Season	Species[a]	Method	Flux	Remarks	Citation
	Tyrrhenian Sea	August 1998	TGM	DFC	8.2; 44.0[r] ng m^{-2} h^{-1}	Limited number of data	Ferrara and Mazzolai[238]
	Near a chlor-alkali plant				0.1; 35.0[r] ng m^{-2} h^{-1}		
	Unpolluted water						
	Yellow Sea	October 2008	Hg^0-DGM	GEM[p]	0.9 ± 1.8 ng m^{-2} h^{-1}	Water samples collected a few meters from shore.	Ci et al.[239]
	Eastern tip of Shandong peninsula	January 2009			−0.1 ± 0.6 ng m^{-2} h^{-1}		
		April–May 2009			0.3 ± 0.7 ng m^{-2} h^{-1}	Maximum DGM conc. during summer.	
		August 2009			0.9 ± 1.4 ng m^{-2} h^{-1}		
Estuaries	Tokyo Bay	December 2003, October 2004 and January 2005	TGM-DGM	GEM[p]	140 ± 120 ng m^{-2} day^{-1}	Average DGM and TGM levels of seven locations were 52 ± 26 pg L^{-1} and 1.9 ± 0.6 ng m^{-3} resp.	Narukawa et al.[167]
	San Francisco Bay	1999–2000, Winter	TGM-DGM	GEM[p]	~3–12 ng m^{-2} h^{-1}	The SF bay estimated to be a net source of mercury to the atmosphere of 40–240 kg $year^{-1}$	Conaway et al.[240]
		Summer			~12–46 ng m^{-2} h^{-1}		
	Pettaquamscutt estuary, RI, USA	August 1991	TGM-DGM	GEM[s]	20–40 ng m^{-2} day^{-1}		Mason et al.[241]
	Scheldt estuary	Winter 1993–4	TGM-DGM	GEM[t]	45–57 ng m^{-2} day^{-1}	Flux was positively related with phytoplankton pigments	Baeyens and Leermakers[180]
		Summer 1993–4			100–141 ng m^{-2} day^{-1}		
	Chesapeake Bay, ML, USA	February, July 1997	TGM-DGM	GEM[s]	0.05–0.7 nmol m^{-2} day^{-1}		Mason et al.[242]

Mesotidal lagoon	Arcachon Bay, France	March 2005 May 2006 Sept.–Oct. 2007	TGM-DGM	GEM[u]	4.2–11.6 ng m^{-2} h^{-1} 0.4–14.5 ng m^{-2} h^{-1} 1.4–13.5 ng m^{-2} h^{-1}	Multiple station study	Bouchet et al.[53]
			Open sea waters				
Atlantic Ocean	North Atlantic	August 1993	TGM-DGM	GEM	15.9 ± 10.8 ng m^{-2} h^{-1}	Average gas transfer velocity 2.3 m day^{-1}. DGM conc. 120 ± 78 pg L^{-1}	Mason et al.[244]
	North Atlantic (~60°N, 5°E–40°W)	July 2005	TGM-DGM	GEM[v]	-0.6–2.5 ng m^{-2} h^{-1}	TGM and DGM with 10 min. time resolution. DGM 5.6–17.2 pg L^{-1}.	Andersson et al.[245]
	50–80°N, 16°W–16°E	June–July 2004		GEM[p]	~0–2.4 ng m^{-2} h^{-1}	DGM conc. 10–32 pg L^{-1}	Temme et al.[246]
	78–85°N, 15°W–10°E	July–August 2004			~0–6.1 ng m^{-2} h^{-1}	DGM conc. 15–53 pg L^{-1}	
	Equatorial and southern Atlantic	May-June 1996	TGM-DGM	GEM[p]	~80 ng m^{-2} h^{-1}	DGM conc. 100–800 pg L^{-1}.	Mason and Sullivan[247]
	Mid-Atlantic Bight adjacent to North America	July and September 1998	TGM-GEM	GEM[p]	2.5 ng m^{-2} h^{-1}		Mason et al.[248]
Arctic Ocean	Incl. Baffin Bay, NW Passages, Beaufort Sea, Chukchi Sea, Bering's str. and Greenland Sea.	July-September 2005	TGM-DGM	GEM[v]	−1.6–98 ng m^{-2} h^{-1}	Route through sea-ice excluded. Efflux of Hg^0 from ocean prevalent. DGM conc. 5–134 pg L^{-1}.	Andersson et al.[192]
Waters of Canadian Arctic archipelago	Resolute Bay, near Griffith Island, Nunavut, Canada	May 2004	TGM-GEM Me_2Hg	GEM[w]	~130 ± 30 ng m^{-2} day^{-1} 4.8 ± 0.6 ng m^{-2} day^{-1}	DGM conc. 129 ± 36 pg L^{-1} Me_2Hg conc. 11.1 ± 4.1 pg L^{-1}	St Louis et al.[249]
Pacific Ocean	Equatorial Pacific	June, July 1984	DGM	GEM[x]	8–148 ng m^{-2} day^{-1}	DGM conc. 5–46 pg L^{-1}	Kim and Fitzgerald[163]
	Equatorial Pacific (Panama to Samoa, 85–180°W, 5°N–12°S)	January, February 1990	DGM	GEM[x]	32–290 ng m^{-2} day^{-1}	DGM conc. 10–72 pg L^{-1}	Mason and Fitzgerald[250]

(*Continued on next page*)

TABLE 2. A summary of air-surface mercury flux measurements for various marine, limnological, and terrestrial ecosystems reported in the literature. The flux values are in general given as mean, mean ± standard deviation or as a min–max range if not otherwise stated. *(Continued)*

Surface/source	Location	Season	Species[a]	Method	Flux	Remarks	Citation
	North Pacific (Japan to Hawaii)	May 14–20 2002	Hg^0-DGM	GEM[p]	20.9 ± 18.4 ng m^{-2} day^{-1}	26 ± 14 pg L^{-1} (Tropical waters)	Laurier et al.[251]
		May 21–28 2002			26.0 ± 31.1 ng m^{-2} day^{-1}	12 ± 6 pg L^{-1} (Northern waters)	
		May 29–31 2002			59.8 ± 50.3 ng m^{-2} day^{-1}		
Mediterranean Sea	Western Mediterranean Sea	July–August 2000	TGM-DGM	GEM[p]	0.5–4.5 ng m^{-2} h^{-1}	DGM conc. tend to be higher in the East MS and in Strait of Sicily.	Gårdfeldt et al.[166]
	Tyrrhenian Sea				0.1–9.9 ng m^{-2} h^{-1}		
	Strait of Sicily				2.3–40.5 ng m^{-2} h^{-1}		
	Eastern Mediterranean Sea				1.6–15.2 ng m^{-2} h^{-1}		
	Main part of the basin	Summer 2003	TGM-DGM	GEM[v]	107 ng m^{-2} day^{-1}	High levels of Hg^0 supersaturation in the surface water (~150–3160%). Annual net emission from entire MS ~77 tons	Andersson et al.[168]
	Central Mediterranean Sea	Spring 2004			36 ng m^{-2} day^{-1}		
	Ionian and Adriatic Sea	Fall 2004			118 ng m^{-2} day^{-1}		
South China Sea	Northern basin	August 2007	TGM-DGM	GEM[v]	0.2–15.3 ng m^{-2} h^{-1}	Highest DGM conc. near mainland.	Fu et al.[252]
Yellow Sea	Incl. Northern East China Sea	July 2010	TGM-DGM	GEM[v]	3.2–44.0 ng m^{-2} h^{-1}	High levels of Hg^0 supersaturation (260–1300%) in surface water	Ci et al.[253]
North Sea	Southern bight	1995–1996	TGM-DGM	GEM[t]	21–223 ng m^{-2} day^{-1}	DGM conc. 42–154 pg L^{-1}	Baeyens and Leermakers[180]
	German bight				12 ng m^{-2} day^{-1}	DGM conc. 12 pg L^{-1}	
	Entire basin (stations also in Skagerrak and Norwegian Sea)	July 1991	TGM-DGM	GEM[y]	22–45 ng m^{-2} day^{-1}	DGM conc. 52 ± 22 pg L^{-1}	Coquery and Cossa[254]
Baltic Sea	Proper (Southern) Baltic	July1997	TGM-DGM	GEM[p]	6–89 ng m^{-2} day^{-1}	DGM conc. 14–26 pg L^{-1}	Wängberg et al.[165]
		March 1998			1–89 ng m^{-2} day^{-1}	DGM conc. 14–22 pg L^{-1}	

	Belt Sea, Arkona Sea, Bornholm Sea, and the western and eastern Gotland Sea	February, April, July, and November 2006	TGM-DGM	GEM[z]	50 ± 19 ng m^{-2} day^{-1}[aa]	The cruises covered ~60% of the entire Baltic Sea. Small near zero fluxes prevailing during winter.	Kuss and Schneider[190]
				Wetlands			
Cattail marsh	Florida Everglades, USA	April 1996–March 1998	TGM	MBR	31 ± 50/0.2 ± 15 ng m^{-2} h^{-1}[r]	Bimodal features in daytime flux with early peak coinciding with maximum in CH_4 flux.	Lindberg and Meyers[133]
Open water surface				DFC	2.7 ± 5.6 ng m^{-2} h^{-1}		Lindberg et al.[256]
Sawgrass marsh		June 1997		MBR	17 ± 29 ng m^{-2} h^{-1}	Flux over vegetation correlated with H_2O vapor flux.	Lindberg and Zhang[257]
Area w/ uprooted plants		March 1997			−4 ± 15 ng m^{-2} h^{-1}		Lindberg et al.[132] Lindberg et al.[132]
Wetland, dry	Lake St. François, QC, Canada	Aug.–Sept. 1999	TGM	DFC	−1.5–2.4 ng m^{-2} h^{-1}	Plants removed before application of DFC.	Poissant et al.[258]
flooded		May 2000			−0.5–7.1 ng m^{-2} h^{-1}		Zhang et al.[259]
		May–June 2003			−0.1–2.4 ng m^{-2} h^{-1}		
Mixed vegetation ~1.5 m height, dry conditions		Aug.–Sept. 2002	Hg^0 GOM Hg-p	MBR	−110–278 ng m^{-2} h^{-1}	GOM and Hg^0 flux significantly anti-correlated.	Poissant et al.[140]
River Bulrush stand, dry		August 2003	TGM	DFB[bb]	−26–1 ng m^{-2} h^{-1}	Condensation inside bag at night.	Zhang et al.[38]
flooded					−9–33 ng m^{-2} h^{-1}		
					–0.26 ± 0.28 ng m^{-2} h^{-1}		
					–0.33 ± 0.24 ng m^{-2} h^{-1}		
flooded			GOM		–2.8 ± 4.8 pg m^{-2} h^{-1}		
flooded			Hg-p		–3.3 ± 24.5 pg m^{-2} h^{-1}		
Mixed sawgrass-cattail marsh	Florida Everglades, USA	June 2000	TGM	AER	16 ± 30/−1 ± 4 ng m^{-2} h^{-1} [r]	Mostly emission during daytime and dry deposition during nighttime.	Marsik et al.[151]
Water surface				DFC	−0.3–2.8 ng m^{-2} h^{-1}		

(*Continued on next page*)

TABLE 2. A summary of air-surface mercury flux measurements for various marine, limnological, and terrestrial ecosystems reported in the literature. The flux values are in general given as mean, mean ± standard deviation or as a min–max range if not otherwise stated. *(Continued)*

Surface/source	Location	Season	Species[a]	Method	Flux	Remarks	Citation
Coastal salt marsh vegetated mainly by *Spartina patens* grass	Farm River, CT, USA	June-July 1997 March-July 1998	TGM	AER	−3.3–13.2 ng m^{-2} h^{-1}[cc]	Extrapolation for the whole year 2008 suggests the area to be a sink of −4 ± 7 μg m^{-2}.	Lee et al.[142]
Non-vegetated coastal salt marsh sediments	Secaucus H.S. Marsh, NJ, USA	Aug. 2005, May 2006, June 2007	TGM	AER	−375–677 ng m^{-2} h^{-1}	Hg fluxes peaked at midday. Cumulative fluxes strongly correlated with cumulative solar radiation (R^2 = 0.97, $p < 0.01$).	Smith and Reinfelder[149]
Dwarf *Spartina patens* grass salt marsh	Great Bay Estuary, NJ, USA	October 2007			−34–81 ng m^{-2} h^{-1}		
			Background soils				
Mixed forest soil	Walker Branch, TN, USA	1993	TGM	MBR	7.5 ± 7.0 ng m^{-2} h^{-1}	Emission fluxes dominant (70%)	Kim et al.[129]
		April–June 1995		DFC	−2.2 ± 2.4 ng m^{-2} h^{-1}	Solar radiation, soil temperature and moisture all have effect on flux.	Carpi and Lindberg[34]
	Watson Forest, TN, USA	June–August 1995			7.0 ± 1.9 ng m^{-2} h^{-1} 2.7 ± 0.5 ng m^{-2} h^{-1}		
Deciduous forest floor Coniferous forest soil	Gårdsjön, Sweden	August 1987	TGM	DFC	1.4 ± 0.5 ng m^{-2} h^{-1} 1.1 ± 0.4 ng m^{-2} h^{-1}	Soil temp. 10–11°C	Schroeder et al.[32]
		Dec.–April 1987			−0.9 ± 0.4 ng m^{-2} h^{-1}	Soil temp. −5–3°C	Xiao et al.[33]
		May–June 1987			0.3 ± 0.4 ng m^{-2} h^{-1}	Soil temp. 7–13°C	
		June 1994		MBR	−4.0–4.2 ng m^{-2} h^{-1}	Significant gradients only	Lindberg et al.[131]
Various forest soils	Kejimkujik Park, NS, Canada	Summer 1997 & 1999	TGM	DFC	−0.4–2.2 ng m^{-2} h^{-1}	Hg-tot soil conc. 0.15–0.33 μg g^{-1}	Schroeder et al.[235]

Mixed forest floor	Tahquamenon Watershed, MI, USA	June 1998	TGM	DFC	1.4 ± 1.4 ng m^{-2} h^{-1}	Overall mean of four forest sites	Zhang et al.[260]
Mixed forest soil	Sierra Nevada foothill, CA, USA	Dark	TGM	DFC	0.5 ± 0.03 ng m^{-2} h^{-1}	Four plots with Hg-tot soil concentrations 0.032–0.060 $\mu g\ g^{-1}$	Ericksen et al.[54]
		Light			1.5 ± 0.18 ng m^{-2} h^{-1}		
Glade with low vegetation	Experimental Lakes Area (ELA), Ontario, Canada	July/Sept./Oct. 2000	TGM (^{202}Hg)TGM	DFC	4.8/1.1/<0.1 ng m^{-2} h^{-1}	Spray application of 10.9 $\mu g\ m^{-2}$ ^{202}Hg in July.	Hintelmann et al.[261]
Blueberry sprigs					3.8/2.1/0.7 ng m^{-2} h^{-1}	Sporadic sampling at various daytime periods.	
Moss-covered soils			TGM (^{202}Hg)		2.9/0.3/0.1 ng m^{-2} h^{-1}		
			TGM		2.1/0.3/0.1 ng m^{-2} h^{-1}		
Pine forest soil	Yellowstone National Park, MT, USA	Dark	TGM	DFC	−0.1 ± 0.02 ng m^{-2} h^{-1}	One plot with Hg-tot soil concentration of 0.040 $\mu g\ g^{-1}$.	Ericksen et al.[54]
		Light			0.7 ± 0.18 ng m^{-2} h^{-1}		
Deciduous forest floor litters	Standing Stone State Forest, TN, USA	Jan.–Nov. 2004	TGM	DFC[dd]	0.4 ± 0.5 ng m^{-2} h^{-1}	Daytime measurements only. A seasonal trend of lower emissions in the presence of closed canopy relative to open one was observed.	Kuiken et al.[198]
Mixed forest floor litter		May–June 2005	TGM	DFC[dd]		Hg-tot soil (leaf litter) concentrations	Kuiken et al.[197]
	Ferry Beach Park, ME, USA	Day			−0.1–2.5 ng m^{-2} h^{-1}	0.069–0.105 (0.048) $\mu g\ g^{-1}$	
	Letchworth Park, NY, USA	Day + Night			−0.5–0.5 ng m^{-2} h^{-1}	0.050–0.149 (0.089) $\mu g\ g^{-1}$	
	Bald Eagle Park, PA, USA	Day + Night			−1.3–1.8 ng m^{-2} h^{-1}	0.033–0.219 (0.065) $\mu g\ g^{-1}$	
	Double Trouble Park, NJ, USA	Day			−0.3–0.7 ng m^{-2} h^{-1}	0.013–0.122 (0.047) $\mu g\ g^{-1}$	
	River Park North, NC, USA	Day			−4.4–1.5 ng m^{-2} h^{-1}	0.021–0.066 (0.034) $\mu g\ g^{-1}$	
	Myeartle Beach Park, SC, USA	Day + Night			−5.1–1.9 ng m^{-2} h^{-1}	0.047–0.142 (0.029) $\mu g\ g^{-1}$	

(*Continued on next page*)

TABLE 2. A summary of air-surface mercury flux measurements for various marine, limnological, and terrestrial ecosystems reported in the literature. The flux values are in general given as mean, mean ± standard deviation or as a min–max range if not otherwise stated. *(Continued)*

Surface/source	Location	Season	Species[a]	Method	Flux	Remarks	Citation
Broadleaf Forest floor	Eastern flank of Mt. Gongga area, Sichuan, China	August 2006	TGM	DFC	−6.2–21.1 ng m^{-2} h^{-1}	Five plots investigated with Hg-tot soil conc. 0.06–0.18 μg g^{-1}.	Fu et al.[262]
Deciduous forest floor	Adirondack Mountains, NY, USA	2005–2006	TGM	DFC	−2.5–27.2 ng m^{-2} h^{-1}	Cumulative estimated emission flux for 2006 ~7.0 μg m^{-2}	Choi and Holsen[58]
Boreal mixed forest floor	Hyytiälä, Finland	April–Sept. 2007	TGM	SFC[b]	1.2 ng m^{-2} h^{-1}		Kyllonen et al.[66]
Tropical forest soil	Negro river basin, Brazil	January 2003–2004	TGM	DFC		Sampling time 6–12 h	Magarelli and Fostier[196]
		Day/Night			0.2 ± 0.2/−0.4 ± 0.2[ee]	Frequently two co-located DFCs were operated simultaneously.	
Seasonally flooded		Day/Night			0.4 ± 0.4/−0.2 ± 0.2[ee]		
Deforested clearing		Day/Night			4.8 ± 0.6/2.6 ± 1.0[ee]		
Seasonally flooded		Day/Night			2.6 ± 2.0/1.6[ee]		
			Agricultural fields				
Bare agricultural field	Nelson field, TN, USA	June–August 1995	TGM	DFC	12.5 ± 5.4 ng m^{-2} h^{-1}	Grass removed before experiment	Carpi and Lindberg[34]
	Barn field, TN, USA	May 1995			44.8 ± 5.2 ng m^{-2} h^{-1}		
Bare agricultural field	Underwood, ND, USA	Light	TGM	DFC	1.2 ± 0.52 ng m^{-2} h^{-1}	Four plots with Hg-tot soil concentrations 0.029–0.035 μg g^{-1}	Ericksen et al.[54]
Paddy field	Chengjiang, Chongqing, China	April, May, June, October, 2008	Hg^0	DFC	23.8 ± 15.6 ng m^{-2} h^{-1}	Emissions decreased with the growth of crops and increased after harvesting.	Zhu et al.[263]
		November, 2008			6.3 ± 11.9 ng m^{-2} h^{-1}		
Bare paddy field	Kang Hwa Island, Korea	March 2001	TGM	AER	−136–1071 ng m^{-2} h^{-1}	Emission during daytime and intermittent dry deposition during night.	Kim et al.[143]

Rice paddy field, seedlings	Kang Hwa Island, Korea	April 2002	TGM	AER	−112–454 ng m^{-2} h^{-1}	Dry deposition mostly occurred during early morning or late evening.	Kim et al.[144]
Fallow field	Hopetown, Ontario, Canada	September 1999	TGM	AER	1.1 ng m^{-2} h^{-1}	Hg-tot soil conc. 0.10 μg g^{-1}	Schroeder et al.[235]
Cornfield	Rosemount, St. Paul, MN, USA	May–June 2001	TGM	REA	–92–191 ng m^{-2} h^{-1}	Significant diurnal variations.	Cobos et al.[115]
Soya bean/corn field amended with biosolids	Maryhill, Ontario, Canada	Fall 2004	TGM	AER	−2.9–3.6 ng m^{-2} h^{-1}	Peak dry deposition during biosolids application event.	Cobbett and Van Heyst[153]
Soya bean/corn field	Elora, Ontario, Canada	November 2006 –August 2007			−342–517 ng m^{-2} h^{-1}	Net evasion ~6.3 ng m^{-2} h^{-1} calculated on an annual basis.	Baya and Van Heyst[154]
Hg-enriched soil with/ without snow cover	Elora, Ontario, Canada	February–March 2000	TGM	DFC	8.3 ± 0.9 ng m^{-2} h^{-1} 295 ± 42 ng m^{-2} h^{-1}	Snow piled over soil. Soil after snow melt.	Schroeder et al.[235]
Agricultural fields	Eastern flank of Mt. Gongga area, Sichuan, China	Dec. 2005[ff] (Oct. 2006), April 2006[ff] (April 2006), Aug. 2006[gg] (Aug. 2006),	TGM	DFC	−22.5–17.6 (-1.4–18.5)[ee] 0.8 –118.1 (-4.5–14.8)[ee] 3.4 –57.5 (-3.6–23.3)[ee]	Two plots w/ Hg-tot soil conc. 0.10 μg g^{-1}. Moderate to elevated TGM conc.	Fu et al.[262]
Sewage sludge amended Salix field	Grästorp, Sweden	April 2003 July 2003	TGM	REA	830 ± 702 ng m^{-2} h^{-1} 211 ± 176 ng m^{-2} h^{-1}	Over bare field. Hg-tot soil conc. 0.45 μg g^{-1} Salix plant canopy height ~1.5 m	Olofsson et al.[92]
Sewage sludge amended fields	Oak Ridge, TN, USA	April 1995–February 1996	TGM	DFC MBR	170–700 ng m^{-2} h^{-1}	MBR measurements performed during limited time in fair comparison with DFC. Hg-tot soil conc. 0.6–6 μg g^{-1}	Carpi and Lindberg[200]
			MeHg	DFC	12–24 pg m^{-2} h^{-1}	MeHg substrate conc. 8.3 ng g^{-1}	Carpi et al.[264]

(*Continued on next page*)

TABLE 2. A summary of air-surface mercury flux measurements for various marine, limnological, and terrestrial ecosystems reported in the literature. The flux values are in general given as mean, mean ± standard deviation or as a min–max range if not otherwise stated. *(Continued)*

Surface/source	Location	Season	Species[a]	Method	Flux	Remarks	Citation
			Naturally enriched surfaces				
Shales	Thunder Bay, Ontario, Canada	July 1997 1998	TGM	DFC	9.1–213.5 ng m^{-2} h^{-1}	Hg-tot substrate conc. 0.36–1.6 μg g^{-1}	Schroeder et al.[235]
					28 ± 2.8 ng m^{-2} h^{-1}		
				AER	34 ± 6 ng m^{-2} h^{-1}		
	McMillan Pass, Yukon, Canada	July 2001		DFC	9 ± 0.6 ng m^{-2} h^{-1}		Edwards et al.[137]
				AER	7 ± 0.6 ng m^{-2} h^{-1}		
Mercury sulfides	Pinchi, BC, Canada	July 1998	TGM	DFC	92 ng m^{-2} h^{-1}	Hg-tot substrate conc. 179.5 μg g^{-1}	Schroeder et al.[235]
Mineralized soil	Clyde Forks, Ontario, Canada	August 1996	TGM	DFC	1760 ng m^{-2} h^{-1}	Hg-tot substrate conc. 124.6 μg g^{-1}	Schroeder et al.[235]
Volcanic rock	Ivanhoe Au Mining District, NV, USA	Fall 1999	TGM	DFC	−62–109 ng m^{-2} h^{-1}	Polycarbonate and Teflon DFCs compare favourably Hg-tot substrate conc. 0.02–9.7 μg g^{-1}	Engle et al.[57]
Geothermal area	Steamboat Springs, NV, USA	Nevada Study and Tests of the Release of Mercury From Soil, STORMS intercomparison Sept. 1–4, 1997	TGM	DFC	38–381 ng m^{-2} h^{-1} *bb*	Four groups using both MM and DFC techniques in one cluster and three groups using DFCs only in another. Hg-tot soil conc. 0.1–15 μg g^{-1} if the total fetch of MM flux measurements considered.	Gustin et al.,[41] Wallschläger et al.,[43] Edwards et al.,[50] Poissant et al.[134]
				AER	89–141 ng m^{-2} h^{-1} *bb*		
				MBR	263–364 ng m^{-2} h^{-1} *bb*		
Hot ground Sinter		September–November 1998		DFC	1734–16374 ng m^{-2} h^{-1}	Hg-tot soil conc. 732 μg g^{-1}	Coolbaugh et al.[211]
					49.7–499.5 ng m^{-2} h^{-1}	Hg-tot soil conc. 4.9–29.3 μg g^{-1}	

			Grasslands/pasture				
Pasture	St. Anicet, Québec, Canada	Summer 1995	TGM	DFC MBR	3.0 ± 2.2 ng m^{-2} h^{-1}	MBR measurements run in parallel with DFC show good correlation during daytime.	Poissant and Casimir[199]
Pasture	Hopetown, Ontario, Canada	September 1999	TGM	AER	1.1 ng m^{-2} h^{-1}	Hg-tot soil conc. 0.047 μg g^{-1}	Schroeder et al.[235]
Prairie grassland	Central Oklahoma, USA	Dark	TGM	DFC	2.7 ± 0.18 ng m^{-2} h^{-1}	Four plots with Hg-tot soil concentrations <0.01–0.022 μg g^{-1}	Ericksen et al.[54]
	Near Wichita Mountains, OK, USA	Light			2.4 ± 0.17 ng m^{-2} h^{-1}		
		Dark			1.2 ± 0.05 ng m^{-2} h^{-1}	Four plots with Hg-tot soil concentrations 0.011–0.020 μg g^{-1}	
		Light			1.5 ± 0.13 ng m^{-2} h^{-1}		
	Black Kettle Grasslands Preserve, Cheyenne, OK, USA	Dark			0.7 ± 0.07 ng m^{-2} h^{-1}	Four plots with Hg-tot soil concentrations ≤0.010 μg g^{-1}	
		Light			1.1 ± 0.08 ng m^{-2} h^{-1}		
	Cherokee National Grasslands, CO, USA	Light			0.5 ± 0.05 ng m^{-2} h^{-1}	Four plots with Hg-tot soil concentrations <0.01–0.019 μg g^{-1}	
	Wisconsin, USA	Dark			0.0 ± 0.03 ng m^{-2} h^{-1}	Nine plots with Hg-tot soil concentrations <0.01–0.028 μg g^{-1}	
		Light			0.5 ± 0.09 ng m^{-2} h^{-1}		
	Underwood, ND, USA	Light			0.1 ± 0.09 ng m^{-2} h^{-1}	Three plots with Hg-tot soil concentrations 0.042–0.055 μg g^{-1}	
Subalpine grassland	Seebodenalp, Switzerland	June–July 2004	TGM	^{222}Rn-tracer	−0.2 ± 0.3 ng m^{-2} h^{-1}[m]	Stable NBL occurred ~35% of the nights sampled.	Obrist et al.[20]
				MBR	−1.7 ± 0.4 ng m^{-2} h^{-1}	Nights with turbulent conditions	

(*Continued on next page*)

TABLE 2. A summary of air-surface mercury flux measurements for various marine, limnological, and terrestrial ecosystems reported in the literature. The flux values are in general given as mean, mean ± standard deviation or as a min–max range if not otherwise stated. *(Continued)*

Surface/source	Location	Season	Species[a]	Method	Flux	Remarks	Citation
Subalpine grassland	Fruebuel, Switzerland	September 2005–October 2006	TGM	AER MBR	−42–29 ng m^{-2} h^{-1} −68–82 ng m^{-2} h^{-1}	Near zero-fluxes during snow cover, net dry deposition during vegetation period.	Fritsche et al.[136]
Temperate montane grasslands	Fruebuel, Switzerland Neustift, Austria Oensingen, Switzerland	July 2006 June 2006 September 2006	TGM	MBR/ AER	−14 –14/ −27–14 ng m^{-2} h^{-1} −76 –37/ −41–26 ng m^{-2} h^{-1} −18–30/ −33–29 ng m^{-2} h^{-1}	Small net dry deposition observed at all of the sites. Nighttime deposition likely the result of Hg code position with condensing water. TGM at Neustift tend to be low (< 1 ng m^{-3}) during mid-day	Fritsche et al.[94]
Subalpine grassland	Eastern flank of Mt. Gongga area, Sichuan, China	December 2005, April 2006, August 2006	TGM	DFC	−25.1– -6.4 ng m^{-2} h^{-1} −4.9–25.1 ng m^{-2} h^{-1} −10.7–51.3 ng m^{-2} h^{-1}	Hg-tot soil concentration 0.17 μg g^{-1}. Elevated TGM conc. 6.2–8.3 ng m^{-3}. TGM conc. 4.2– 6.2 ng m^{-3}. 3 plots w/ Hg-tot soil conc. 0.14 μg g^{-1}.	Fu et al.[262]
			Arid surfaces				
Desert	Mohave, CA, USA Hungry Valley, NV, USA	Dark Light Dark Light	TGM	DFC	0.2 ± 0.02 ng m^{-2} h^{-1} 0.9 ± 0.10 ng m^{-2} h^{-1} 0.0 ± 0.03 ng m^{-2} h^{-1} 0.4 ± 0.05 ng m^{-2} h^{-1}	Four plots with Hg-tot soil concentrations 0.012–0.032 μg g^{-1} Five plots with Hg-tot soil concentrations <0.01–0.022 μg g^{-1}	Ericksen et al.[54]

				Snow surfaces			
Snowpack	Barrow, AK, USA	Spring periods 2001–2004	GOM[ii]	REA	−2.4 ng m^{-2} h^{-1}	Dry deposition as well as emission events of GOM were observed. Upward flux attributed to chemical formation of GOM at/near snow.	Skov et al.[116]
		Spring melt 2002	TGM	DFC	<1–>600 ng m^{-2} h^{-1}	Emission was enhanced both by increased air temperatures and by solar radiation.	Schroeder et al.[265]
		March–April 2003	Hg^0	MBR	3.0 ± 0.6 ng m^{-2} h^{-1}[jj]	Gradients measured with Δz = 20 m during a period of intermittently low air Hg^0 and high GOM conc.	Brooks et al.[266]
Snowpack	Ny-Ålesund, Spitsbergen, Svalbard	May 2002	TGM	DFC	~8 ng m^{-2} h^{-1}[kk]	Snow surface temperature biased by DFC. High flux in presence of wet surface snow inside chamber. Evidence for photo-stimulated emissions in conjunction to depletion events from gradient and DFC measurements.	Sommar et al.[234]
		April–May 2003			~0–230 ng m^{-2} h^{-1}	Maximum flux after a low air Hg^0 event. Generally flux <50 ng m^{-2} h^{-1}	Ferrari et al.[267]
		February-June 2008		AER	−113–694 ng m^{-2} h^{-1}	Net dry deposition until late March. The period towards mid-May with low air Hg^0 event characterized by significant net evasion.	Steen et al.[155]

(*Continued on next page*)

TABLE 2. A summary of air-surface mercury flux measurements for various marine, limnological, and terrestrial ecosystems reported in the literature. The flux values are in general given as mean, mean ± standard deviation or as a min–max range if not otherwise stated. *(Continued)*

Surface/source	Location	Season	Species[a]	Method	Flux	Remarks	Citation
Snowpack	Alert, Nunavut, Canada	February–June 2005	TGM	AER	−0.003±0.03 ng m^{-2} s^{-1}[ll]	Dry deposition prevalent during polar night. Near zero fluxes during polar spring. Significant fluxes with diel patterns during snow melt.	Cobbett et al.[152]
		Julian day 31–62			−0.01 ± 0.1 ng m^{-2} s^{-1}[ll]		
		Julian day 63–94			−0.0001 ± 0.004 ng m^{-2} s^{-1}[ll]		
		Julian day 95–174			0.0003 ± 0.02 ng m^{-2} s^{-1}[ll]		
				Canopy vegetation			
Mature deciduous forest	Walker Branch, TN, USA	Summer-Fall1993	TGM	MBR	−230–290 ng m^{-2} h^{-1}	Daytime. Site close to local sources, emission more frequent than dry deposition. Data indicating dry deposition frequently statistically non-significant.	Lindberg et al.[131]
		September 1992, August 1995	GOM[mm]	MBR	−55–21 ng m^{-2} h^{-1}	Limited number of gradient samples.	Lindberg and Stratton[139]
Plantation with young pine trees	Wartburg, TN, USA	Fall 1994	TGM	MBR	6–86 ng m^{-2} h^{-1}	Daytime. Data indicating dry deposition statistically non-significant.	Lindberg et al.[131]
Red maple forest	Coventry, CT, USA	Early fall 2005	TGM	REA	21.9 ± 32.6[nn] ng m^{-2} h^{-1}	Bimodal emission pattern	Bash and Miller[91]
		Spring 2006			−4011[oo] ng m^{-2} h^{-1}	Dry deposition in the presence of advected air rich in TGM.	Bash and Miller[268]
		2004–2005			−5.6 ± 2.5 μg m^{-2}[pp]	Trend from net dry deposition in early summer to net evasion in the late summer and on before complete senescence.	Bash and Miller[97]

Sugar maple foliage	St. Anicet, Québec, Canada	July–October 2004	TGM	DFB[bb]	−0.39 ± 0.38 ng m^{-2} h^{-1}	Tree branch accounting for 80 healthy maple leaves enclosed. Compensation point ~0.6 ng m^{-3}	Poissant et al.[37]
Mixed vegetation in a high-elevation meadow	Shenandoah National Park, VA, USA	August, 2008 November 2008 February 2009 May 2009	TGM	AER MBR	2.5 ng m^{-2} h^{-1} 0.3 ng m^{-2} h^{-1} 4.1 ng m^{-2} h^{-1} −4.8 ng m^{-2} h^{-1}	Poor agreement between the two methods during the fall and winter seasons.	Converse et al.[157]
Coniferous tree foliage Black spruce Jack Pine	Experimental Lakes Area (ELA), Ontario, Canada	2001–2003	TGM	DFB[bb]	 −24.2–38.5 ng m^{-2} h^{-1} −19.1–39.8 ng m^{-2} h^{-1}	Compensation point 2–3 ng m^{-3}	Graydon et al.[36]

[a]Hg^0 refers optical detection techniques applied on gas samples without pre-concentration or with preconcentration after total removal of GOM and Hg-p. The acronym TGM (Total Gaseous Mercury) is applied for studies using the general gold trap sampling technique. GOM and Hg-p should by rights be assigned as fractions of airborne mercury rather than regular species. MeHg represents monomethyl mercury species (CH_3HgX, where X is single charged anion) and Me_2Hg is an abbreviation of dimethyl mercury.
[b]Box or Gaussian plume model with meteorological data and TGM conc. measurements up- and down-wind the landfill as inputs.
[c]Data segregated into evasion and dry deposition respectively.
[d]Typical average range reported.
[e]Range of individual plot flux mean values from multiplot study.
[f]Refers to Twin Creeks mine only.
[g]Surface diffusion model (see section "Enclosure methods").
[h]Static flux chamber.
[i]Two-layer gas transfer model adopted from Liss and Slater,[175] k_{water} = 9 cm h^{-1}.
[j]Dissolved Organic Carbon.
[k]Mass transfer velocity set at 1.5 and 2.0 cm h^{-1}, respectively. TGM was not measured and set at 2.0 ng m^{-3}.

(*Continued on next page*)

TABLE 2. A summary of air-surface mercury flux measurements for various marine, limnological, and terrestrial ecosystems reported in the literature. The flux values are in general given as mean, mean ± standard deviation or as a min–max range if not otherwise stated. *(Continued)*

[l]Exchange parameterization by Wanninkhof et al.[184] Also see section "Bulk methods for Hg flux measurements over water surfaces."
[m]Data calculated during stable nocturnal conditions (>6 h) when ^{222}Rn showed an approximately linear accumulation in NBL.
[n]Median flux.
[o]Median ± IQR flux.
[p]Exchange parameterization by Wanninkhof.[182]
[q]Exchange parameterization by Liss and Merlivat,[181] Wanninkhof,[182] and Asher et al.[236]
[r]Mean value for night and day, respectively.
[s]Gas transfer velocities 0.5–1.0 m day^{-1}.
[t]Calculated at an averaged wind speed of 8.1 m s^{-1} and for Scheldt Estuary, North Sea Southern bight and German bight a TGM conc. of 3.4, 1.8, and 1.2 ng m^{-3}, respectively.
[u]Exchange parameterization by Borges et al.[243]
[v]Exchange parameterization by Nightingale et al.[183]
[w]Gas exchange velocity of 3.7 cm h^{-1} used.
[x]Thin-film model (see section "Bulk methods for Hg flux measurements over water surfaces").
[y]Transfer velocity 0.5–1.0 m day^{-1} and a TGM conc. 1.9 ng m^{-3} utilized.
[z]Exchange parameterization by Weiss et al.[255]
[aa]Area-weighted average flux.
[bb]The flux calculation is based on leaf area.
[cc]Mean range from sampling campaign divided into five vegetative periods.
[dd]Two DFC systems were used in parallel. One system was kept stationary, while the other was in mobile status. Data for the stationary DFC tabulated.
[ee]Unit: ng m^{-2} h^{-1}.
[ff]Bare field.
[gg]Corn canopy present.
[hh]Median range.
[ii]Sampled by annular denuder method Landis et al.[124]
[jj]Based on a cumulative flux reported for a 2-week period.
[kk]Average flux. Maximum flux ~70 ng m^{-2} h^{-1} after enhanced Hg deposition.
[ll]Unit incorrectly given as ng m^{-2} h^{-1} in original paper.
[mm]Sampled by mist chamber method (Lindberg and Stratton[122]).
[nn]Median flux
[oo]Maximum deposition following a peak of 7.01 ng m^{-3} in TGM.
[pp]Growing season net flux.

called the surface layer (SL) or Prandtl layer. The variability of flux with height in SL is low and thus fluxes in the SL, for many reasons, are treated as constant with height. The constant flux layer concept represents the basis for several micrometeorological (MM) flux measurement techniques. The time averaged statistics of air flow in SL over homogeneous surfaces are described by Monin-Obukhov similarity theory (MOST; see section "Turbulent transport in the planetary boundary layer"). However, it has been known for decades that MOST formulae fail near rough surfaces such as urban areas, vegetation canopies or surface waves. The failure is most often that turbulent fluxes are higher than MOST would predict from the observed mean gradients. Even a homogeneous surface has roughness elements that create characteristic concentration and windfield patterns around them and therefore SL has to be divided into inertial and roughness sub-layer.[28] Due to the strong friction effects, the airflow is mainly laminar within few mm above surface structures (quasi-laminar boundary layer) while the roughness sublayer above including a chaotic time-mean streamline pattern is called Lagrangian turbulence.[29] Figure 2shows a visualization of PBL.

Similar to trace gases, energy in different forms is absorbed or emitted at the surface. The energy exchange is of special importance for the understanding and determination of the trace gas fluxes for several reasons. First, it determines the microclimatic state of a vegetated surface (e.g., radiation, humidity, leaf, and soil temperature) and the overlying air layers (thermal turbulence production) and, thus, influences the exchange processes decisively. Secondly, the transport of mass related (sensible and latent) energy in the air is supposed to be analogous to the transport of trace compounds.[30] This analogy is helpful for the determination of exchange characteristics, because the energy content of the air can usually be measured more easily and accurately than trace gas concentrations. Moreover, there are independent methods for the determination and verification of energy fluxes, which do not exist for trace compounds. In contrast to trace gases, energy can be transported in several different forms. The energy balance equation at Earth's surface is:

$$H + \lambda E = R_n - G - \Delta S \tag{2}$$

where R_n is net radiation, G is conductive heat flux into soil, H and λE are turbulent transport flux of sensible (enthalpy, appearing as temperature change) and latent (evaporation of water) heat respectively with the air through the top of the canopy. ΔS describes the energy storage change within the canopy (the SI (le système International d'unités) unit for the individual terms is W m^{-2}). Short-wave radiation from the sun is the main external controlling factor for the surface energy budget and creates a characteristic diurnal variation. Energy forms may also be transferred in reversed, which mainly happens during night when no solar radiation is coming in. The Earth's surface

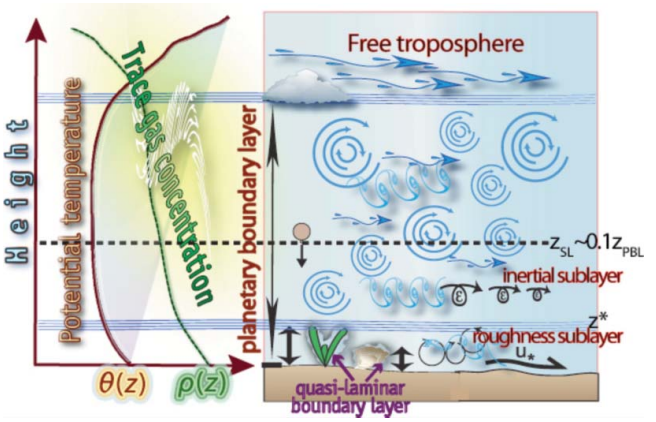

FIGURE 2. Structure of planetary boundary layer (PBL). The surface layer (the lowest 10% of PBL) is divided into roughness sublayer (influenced by single roughness elements) and inertial sublayer (vertically and horizontally constant flux). For the definition of potential temperature, θ, See section "Turbulent transport in the planetary boundary layer" (Color figure available online).

also emits thermal radiation in the long-wave range according to its temperature and absorption/emission properties. Whether it is transported mainly as sensible or as latent heat strongly depends on the vegetation type and activity as well as on the availability of water. The Bowen-ratio ($\beta = H/\lambda E$ [31]) is, therefore, a widely used parameter for characterizing vegetated surfaces. The closure of the energy budget (i.e., the validity of Eq. 2) can be used to test the quality of flux measurements if all components are determined individually. Alternatively, one unknown energy flux can be calculated as residual of Eq. 2.

ENCLOSURE METHODS

Chambers (and mass balance) methods rely on the conservation of mass and therefore the most intuitive compared to the MM methods, which are based on theories of turbulent transport in the atmosphere and have limitations when meteorological conditions are unfavorable. However, chambers are intrusive per se and modify the local meteorological conditions over the plot studied. Eq. 3 shows the law of mass conservation:

$$V\frac{\partial}{\partial t}\langle C_{Hg}\rangle = \sum_{i=0}^{m} A_i \cdot F_{Hg,i} \tag{3}$$

The mass change (where C_{Hg} is the Hg vapor concentration, typically in ng m^{-3}) in a reference volume V is equal to the net inward flux through

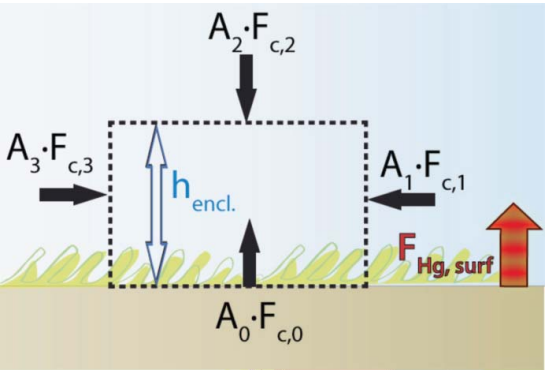

FIGURE 3. Illustration of the mass conservation of a trace gas with concentration ρ_c within a reference volume V directly above the surface; $F_{Hg,\,surf}$ surface exchange flux, $F_{c,i}$ fluxes through volume boundary areas A_i. Modified from Ammann.[119] (Color figure available online).

its boundary areas A_i. The triangular brackets around C_{Hg} signify a spatial average over V. For an enclosure volume directly above the surface, Eq. 1 can be rearranged for the surface exchange flux $F_{Hg,\,surf}$, which is defined upward by convention (i.e., the flux into the volume V through the bottom area A_0, unit m^2):

$$F_{Hg,\,surf} = F_{Hg,0} = \frac{1}{A_0}\left\{V\frac{\partial}{\partial t}\left\langle C_{Hg}\right\rangle_v - \sum_{i=1}^{m} A_i \cdot F_{Hg,i}\right\} \tag{4}$$

This is depicted in Figure 3. The simplest application of Eq. 4 is represented by the so-called static chamber method. The chamber is placed on the investigated surface and is closed against the surrounding air:

$$F_{Hg,\,surface} = \frac{V}{A_0}\cdot\frac{\partial}{\partial t}\left\langle C_{Hg}\right\rangle_v = h_{encl}\cdot\frac{\partial}{\partial t}\left\langle C_{Hg}\right\rangle_v \tag{5}$$

In Hg research, however, flow-through (dynamic) rather than closed (static) enclosures have been employed by numerous groups since the seminal work by Schroeder et al.[32] and Xiao et al.[33] In general, the flow-through dynamic flux chambers (DFCs) employed are of small size and cover a surface area of $\leq$0.1 m^2. The temporal derivative in Eq. 4 is, for this application, set to zero by creating stationary conditions inside the enclosure. This is obtained by a continuous flushing of the chamber at an appropriate rate, replacing the air volume typically one or more times per minute.[34] More specifically, Eckley et al.[35] recommended DFC turnover times of 0.3–0.8 min. Enclosure techniques may not only be applied to bare soil, water or surfaces with low vegetation but also to surfaces of individual plants (canopies, etc.). The enclosures of the latter group (dynamic flux bags [DFB]) have typical dimensions to include the canopy of a small plant or a section of a larger

one.[36–39] Concerning the application of DFC to bare soil surfaces, the investigation by Gillis and Miller[40] showed that insertion of the chamber edges 1 cm into the soil provided a reliable seal against air intrusion. Nevertheless, the specific manipulation undertaken to achieve ground-chamber contact differs between operators (e.g., Carpi and Lindberg,[34] Gustin et al.,[41] Rinklebe et al.,[42] Wallschläger et al.[43]), while it is in many publications vaguely described or unaccounted for. Improper deployment of a DFC as a source of bias has received little attention in studies concerning Hg. However, the broader literature covering enclosure studies of trace gas exchange address this matter in more detail.[44] The airflow in and out of the enclosure can be guided through tubes, where the volume flow rate Q (typically in the unit $m^3\ h^{-1}$) and the Hg vapor concentrations can be easily measured, are maintained by a constant flow rate (Q) of outside air through it. Generally air is sucked through the chamber by a pump, but there are designs in which air is pushed through.[36] Eq. 4 is, in this case, approximated by:

$$F_{Hg,\,surface} \cong \frac{Q}{A_0} \cdot \left(C_{Hg,out} - C_{Hg,in} - blank\right) \tag{6}$$

where the indices in and out represent air entering and exit the enclosure respectively. The operation of a DFC can readily be automatized by directing air to a Hg vapor analyzer using time-controlled magnetic switches in such a way that samples for in and out air are collected sequentially.[45] The blank term represents the spurious adsorption/desorption of Hg vapor at inner walls. For DFCs, it is determined by sealing the open bottom to a clean surface. The magnitude of the system blank (frequently reported in the interval 0.1–0.5 ng $m^{-2}\ h^{-1}$) sets a lower limit of the flux possible to resolve by the method. In field measurements over substrates with very low Hg content, observed fluxes are often at or below the DFC system detection limit.[46] Most enclosure studies employ mass flow controllers (MFCs in the Hg analyzer as well as to regulate main flow) calibrated with dry air (at T_0 and P_0, STP (standard temperature and pressure, 273.15 K and 100 kPa)). If this is the case, concerning a DFC/DFB, a correction term for the density effect of ambient air water vapor of $1.85 R_d T_0 \overline{C_{Hg}} F_{H_2O}/P_0$ should be added to Eq. 6 following Lee[47] (R_d is the ideal gas law constant for dry air, P_0 and T_0 are the pressure and temperature at 100 kPa and 0°C, respectively, $\overline{C_{Hg}}$ is the average ambient air Hg^0 mass concentration (at STP) over the flux averaging interval and F_{H2O} is the corresponding water vapor flux). Only if moisture is removed can this correction be avoided. Analogous to all methods involving non-synchronous gas analysis, deriving fluxes from temporarily separated $C_{Hg,in}$ and $C_{Hg,out}$ sample collection are subject to significant uncertainties under restrictive conditions, such as a high variability in ambient air Hg^0 concentration. Consequently, Eckley et al.[35] proposed the criteria to accept a flux measurement only when $|C_{Hg,\,out} - C_{Hg}| > |\Delta C_{Hg,\,in}|$, where $\Delta C_{Hg,\,in}$

represents the difference between the two $C_{Hg,in}$ samples surrounding a $C_{Hg,out}$ sample in time. Chamber materials with low blanks (i.e., after appropriate cleaning procedures) and high radiation transmission properties are generally chosen, such as FEP Teflon durafilm[34,48], Propafilm-C,[36] Tedlar,[38] quartz,[49] Plexiglas,[50–52] polypropane,[53] and polycarbonate.[54, 55] Carpi et al.[56] advocated Teflon films considering the low blanks and transmission properties at shortwave radiation (UV-B (ultraviolet B, 280–315 nm)) in preference to less expensive polycarbonate that, however, gained broad acceptance in groups most active in this field.[55,57,58] UV-B radiation has been implicated as the wavelength band that is most significant in the soil emission process. Graydon et al.[36] used intermittently film filters (for UV-A (ultraviolet A, 315–400 nm) and UV-B) that draped highly transparent Propafilm-C chambers to determine the importance of UV wavelengths on Hg flux.

As pointed out by Eckley et al.,[35] a standard operating protocol and design for DFCs does not exist, and as a result there is a large diversity in methods described in the literature. The theory of flux chamber measurements demands that the air moves through the chamber without a vertical component,[59] and ideally in the form of a plug so that no stagnant air zones are present. The layouts of DFC (for non-plant applications) are generally rectangular parallelepiped (cylindrical and hemispherical designs have also been used), where the difference in V and Q used spanned over an order of magnitude and the resulting chamber turnover times varied by over 2-orders of magnitude.[35] A general observation by many researchers is that $F_{Hg,surf}$ increases with Q. Zhang et al.[60] and Lindberg et al.[61] applied a two-resistance exchange interface model to simulate DFC measurement of the flux process and recommended high Q ($\sim$1–2.5 $m^3\ h^{-1}$) and high V/A_0 ratios not to underestimate flux. Engle et al.[62] pointed out that low Q is acceptable when sampling from a low Hg content substrate. Other than the different characteristics of the soil substrates being measured, there are two major issues causing uncertainties:

- Different flow rates yield different flux results for the same soil substrate. Eckley et al.[35] suggested the choice of an optimum Q coinciding with the emergence of a regime of constant $C_{Hg,out} - C_{Hg,in}$.
- The chamber design and the materials used for the chamber construction affect the chamber aerodynamic behavior. In general, less attention has been paid to facilitate a uniform air-flow over the surface investigated, thereby eliminating zones of stagnant air.

Recently, Lin et al.[63] implemented a DFC of novel design for measuring Hg^0 flux over soil that enabled precise control of internal shear properties by the flow-through rate. In turn, a methodology that utilizes the measured DFC flux to infer the flux under atmospheric conditions was proposed (see section “Results of field measurements of Hg flux”).

Another category of enclosures was primary developed to investigate Hg in soil or snow gas in order to potentially estimate air-substrate Hg^0 flux. Up to date, the number of studies in this field is comparatively scarce[42, 52, 64–69] involving background and contaminated substrates. The devices, ranging from wells and tube probes to flasks and chambers, are semistatic or operated by actively drawing air from the substrate. In order to sample the interstitial Hg^0 vapor present in pores and avoid significant dilution by the intrusion of ambient air, the collection requires low gas-flow rates or small gas samples. Johnson et al.[65] inserting Teflon wells to two depths (~20 and ~40 cm) of contaminated soil and withdrawing 50 mL soil gas samples with gas-tight glass syringes for Hg^0 analysis. Hg^0 flux was calculated by the soil profile method initially applied for CO_2[70] with measured soil Hg gas gradient ($\partial C_{Hg(g),\,soil}/\partial z$) and soil characteristics influencing the effective diffusion coefficient ($D_{Hg^0,\,\text{soil air}}$ typical unit $cm^2\ s^{-1}$) as input:

$$F_{Hg} = D_{Hg^0,\,soil\,air} \cdot \frac{\partial C_{Hg(g),\,soil}}{\partial z} \tag{7}$$

The soil Hg^0 efflux calculated from DFC was more than one order of magnitude higher than and not correlated with that obtained from the diffusion model, indicating that the process was not diffusion-controlled. Sigler and Lee[68] modified a flask sampling technique previously used for CO_2[71] to sample (at ~30 mL min^{-1}) and analyze Hg^0 at depth in soil. Soil gas Hg^0 concentrations at ~2-cm depth were correlated with Hg^0 flux measured by a DFC unit. The study of Sigler and Lee[68] revealed clear Hg^0 soil gas gradients, where large changes were observed in the shallow layers (<10 cm) underscore the importance of a fine, vertical resolution. In addition to the application of a regular Plexiglas DFC, Wallschläger et al.[52] measured Hg (Hg^0 + $(CH_3)_2Hg$) in contaminated floodplain soil gas by drawing air (at 1.5 L min^{-1}) through Teflon-coated steel tubes directly into an Hg vapor analyzer. The measured Hg concentrations were diluted by the intrusion of ambient air due to the high flow rate and sample volume. In order to compensate for this effect, an extrapolated Hg-soil gas concentration $C_{Hg(g),\,soil}$ (to zero sampling volume) was obtained from consecutive samples at a specific plot depth showing a systematic concentration trend. A surface film approach was used to semiquantitatively estimate Hg air-soil flux deriving from laminar diffusion:

$$F_{Hg} = \frac{D_{Hg^0,\,soil\,air} \cdot \left(C_{Hg(g),\,soil} - C_{Hg,\,air}\right)}{z} \tag{8}$$

where z (typical unit cm) is the thickness of the laminar boundary film and finally $C_{Hg,\,soil}$ is the surface air concentration at the top of the film. In studies of Hg volatilization from heavily contaminated floodplain soils along the river Elbe, Böhme et al.[64] applied a "gas suck-up chamber" to estimate the

potential for Hg emissions of a site. More recently, Rinklebe et al.[42] modified this setup without ambient air inlet to a closed chamber equipped with an air circulating system including a loop through Hg sampling traps during sampling duration (1–2 hr). The chamber was fixed via a Teflon gasket to an in-ground cylinder that prevents lateral flow of soil gas in to the sampling plot. This method has some points in common with that of Di Francesco et al.,[72] which is restricted to heavy contaminated soil. For the sampling of vertical profiles of gaseous Hg in snowpacks, Dommergue et al.[69,73] developed a tube probe device and observed elevated concentrations of Hg^0 in the firn air of a snowpack compared to those of ambient air during the annual melting period in Canadian sub-Arctic. Snow-air fluxes were calculated with a laminar diffusion approach (see Eq. 7) using the Hg^0 concentration gradient in the upper 40 cm of the snowpack. For a closed chamber using a conventional MFC to regulate air circulation, correction for air density effects should be implemented following Lee.[47] This formula also applies for corresponding micro-meteorological systems.

OPEN-PATH LASER OPTICAL SPECTROSCOPIC METHODS

Hg is the only noninert pollutant that exists in the atmosphere in atomic form. Background mixing ratios are in the order of sub-parts per trillion (ppt). Because the whole transition oscillator strength is aggregated in a single line apart from isotopic shifts and hyperfine structures at ~254 nm (resonance transition $6s^1S_0 \rightarrow 6p^3P_1$) rather than distributed on thousands of vibrational-rotational transitions in a molecule (e.g., $HgCl_2$), even such low concentrations can be assessed by long-path optical spectroscopy.[74] Several commercial Hg vapor analyzers utilizing pulsed Zeeman modulation of the 254-nm resonance transition in Hg^0 (Z-AAS) have similar detection limit,[75] in addition the interference of other species exhibiting high optical cross section at this line with the determinations of Hg^0 was eliminated. Besides laboratory-based less portable apparatus for small volume "point" measurements of ambient Hg^0 concentrations with laser powered ring-down cavity enhanced techniques[76] and 2-Photon LIF,[77] more versatile mobile LIDAR systems[78–81] have been developed by the Svanberg group at Lund University of Technology, Sweden, to study geophysical Hg^0 vapor emissions from area sources (mining sites, geothermal sites, fumaroles, etc.). In optical remote sensing measurements of fugitive emissions from Hg-cell chlor-alkali plants, in addition to DIAL[82] recently also commercial systems (Opsis AB, Furulund, Sweden) utilizing UV-DOAS have been employed.[83]

DIAL and DOAS measurements of Hg^0 evasive flux are performed in absorption and the Beer–Lambert law yields a simple connection between the absorbed light fraction and the path integrated concentration profile. After the light, with an intensity of I_0, has travelled a path length L, $I_0(\lambda, L)$

is reduced to $I(\lambda, L)$ as expressed from Eq. 9 using the Beer–Lambert law:

$$I(\lambda, L) = I_0(\lambda, L) \cdot e^{-\int_{\ell=0}^{\ell=L} (\sigma_{Hg}(\lambda,p,T) \cdot \rho_{Hg}(\ell) + \varepsilon_R(\lambda,\ell) + \varepsilon_M(\lambda,\ell))d\ell} + N(\lambda) \qquad (9)$$

where σ_{Hg} (λ, p, T) is the absorption cross-section (cm^2 atom^{-1}) of Hg^0, which depends on the wavelength λ (nm), the pressure p (hPa) and the temperature T (K), $\rho_{Hg}(\ell)$ the number density (cm^{-3}) at the position ℓ along the light path of total length L (cm). Light scattering by Rayleigh-extinction and Mie-extinction are described by the ε_R and ε_M coefficients respectively. $N(\lambda)$ is the photon noise dependent on $I(\lambda, L)$.

In a DIAL system housed in a vehicle, a tuneable optical parametric oscillator laser system that is pumped at 20 Hz by a frequency-tripled injection seeded neodymium-yttrium-aluminum-garnet (Nd:YAG) laser and equipped with doubling and mixing crystal units is employed as a light source.[81] In a DIAL system designed to measure sub-ppt levels of Hg^0, Nayuki et al.[84] used the third harmonic of a tuneable dye laser with LDS 765 dye pumped by the second harmonic of an Nd:YAG laser as the source for the emitted light beam. DIAL-Hg is performed using two wavelength, one on the $6s^1S_0 \rightarrow 6p^3P_1$ absorption line ($\lambda_{\mathrm{on}} = 253.65$ nm) and the other slightly off (λ_{off}). The latter is at a longer wavelength to avoid interference with a close-lying, weak oxygen absorption line.[79] An internal calibration unit using small Hg-vapor saturated cells with known lengths and temperatures was used to monitor and compensate for small laser wavelength and line width changes. The outgoing laser beam is directed coaxially with a vertically mounted telescope and transmitted into the atmosphere via a large flat mirror in a retractable transmitting/receiving dome on the roof. Stepping motors are used to turn the dome and to tilt the mirror. The LIDAR signal was then collected time-resolved to obtain a range-resolved measurement. By forming the ratio between the on and off signals $I(\lambda_{on})/I(\lambda_{off})$, a DIAL curve is obtained, being flat where no Hg is present and sloping downwards in the presence of Hg. As visualized in Figure 4, each DIAL measurement, in a certain direction, gives the range-resolved Hg concentration along the laser beam. Two-dimensional images of the Hg distribution in the spreading plume can be produced by scanning the laser beam in a vertical plane. Such a sweep gathered in 3–5 min, yielding a cross-section of the distribution of Hg in the air mass, which in-turn is area-integrated. Several sweeps with a horizontal reference plane are required to enclose a point or an areal well-defined Hg source. In order to calculate a flux integrated over an area, the surficial Hg^0 concentrations have to be multiplied by the wind field orthogonal to the corresponding plane. In Bennett et al.,[85] the preferences using a Doppler LIDAR system versus anemometer measurements of the wind profile is discussed. In addition, wind directions within a 20–30° sector of the scanning beam are less favorable for the flux calculation.

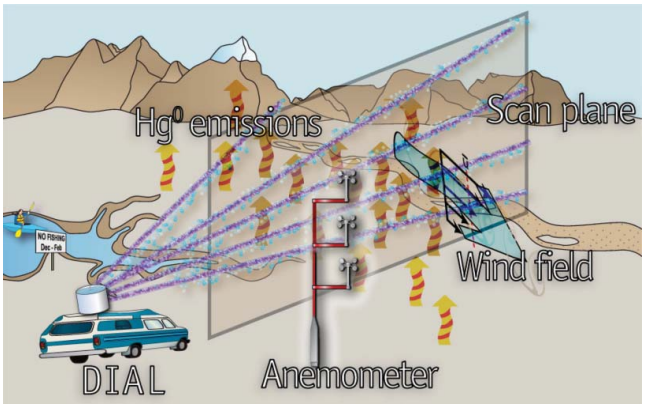

FIGURE 4. A Schematic of the operation of a differential absorption LIDAR system. Depicted is a mobile DIAL when scanning with the laser beam in a vertical plane in order to obtain a concentration cross-section of the mercury plume. The mercury flux is estimated by area integration of the concentration and multiplication by the wind speed component perpendicular to the cross-section surface. To contain a source with areal extension, sweeps over different sections of horizontal reference plane are required (Color figure available online).

MICROMETEOROLOGICAL (MM) TECHNIQUES

The MM techniques for flux measurements depend on transport processes in the atmosphere and are affected by conditions of atmospheric stability. In this section, the driving force of turbulent transport in PBL, its relation to atmospheric stability, and the measurement area of interest are elaborated. This is followed by a discussion of various MM techniques that have been applied for Hg flux measurement to date.

Turbulent Transport in the Planetary Boundary Layer

Persisting atmospheric turbulence mainly occurs near the ground because the surface provides the principal forcing effects for turbulent motion.[30] The first driving force is shear stress in the mean horizontal air motion that is produced by friction at the surface, which depends on windspeed and surface roughness and being associated with the mean vertical gradient in the windspeed profile ($\partial\bar{u}/\partial z$), where u (m s^{-1}) is the horizontal wind. The second driving force for turbulence is buoyancy effect due to air density variations with height. It occurs mainly during daytime, when the surface, together with the lowest air layers, is heated by solar radiation. The warmer air at the ground is less dense than the layers above and rises to induce a turbulent turnover. This process is called *thermal turbulence production* or *free convection*. The buoyancy of an air parcel depends not only on its temperature (T), but also on the pressure (p) and the humidity conditions. Over land surfaces, the influence of humidity is usually small and often ignored.[86] Therefore, the

buoyancy can be quantified by the potential temperature θ (K) referring to a standard pressure $p_0 = 1000$ hPa: $\theta = T \cdot (p_0/p)^{0.286}$. The mean vertical gradient of the potential temperature ($\partial\bar{\theta}/\partial z$) determines the static stability of an air layer. Thermal turbulence production occurs only if the gradient is negative (unstable stratification). A zero gradient indicates neutral and a positive gradient stable stratification. In the latter case, with dense cold air at the ground and warmer layers above, the negative buoyancy force dampens or even inhibits vertical turbulent mixing.

Turbulent motions can be decomposed into a mean part $\bar{a}$ and a random fluctuating part a'. The application requires averaging rules (Reynold's postulates), such as $\overline{a \cdot b} = \bar{a} \cdot \bar{b} + \overline{a' \cdot b'}$ that is, in-turn, the basis for Eddy Covariance technique described below in the following section ("Footprint (source area) of MM-techniques") According to the MOST,[87] the statistics of SL turbulence with respect to z (height above surface), g/T (buoyancy parameter, vertical acceleration due to density variations), $\overline{u'w'}$(vertical surface flux of momentum; mechanical turbulence), $\overline{w'T'}$(vertical surface flux of sensible heat; thermal turbulence) as dependent variables with length, time and temperature as independent dimensions can be described by the single dimensionless parameter z/L. The characteristic length scale L (m) is called the Obukhov length. Here expressed with air density correction due to water vapor content:

$$L = -\frac{u_*^3 \cdot T \cdot \rho_{air} \cdot c_p}{k \cdot g \cdot H} \tag{10}$$

where u_* (m s^{-1}) is the friction velocity $\sqrt{\tau/\rho_{air}}$ (τ being the flux of momentum between the atmosphere and the surface), ρ_{air} (kg m^{-3}) is the density of air, k is von Kármán's constant (~0.4, representing the ratio between the effective turbulent mixing length and the distance to the surface), g (m s^{-2}) is the acceleration due to gravity, T (K) is ambient air temperature, c_p (J kg^{-1} K^{-1}) is the specific heat of air at constant pressure, H (W m^{-2}) is the vertical flux of sensible heat. In neutral conditions, $z/L = 0$; in stable conditions, $z/L > 0$; in unstable conditions, $z/L < 0$. Obukhov length represents the height of an air column in which the production ($L < 0$) or loss ($L > 0$) of turbulent kinetic energy by buoyancy force is equal to the dynamic production of turbulent kinetic energy per volume unit at any measuring height z multiplied by z. L is thus proportional to the height of the inertial sublayer but not identical to it.[25]

Footprint (Source Area) of MM Techniques

The most direct physical approach for the measurement of turbulent trace gas fluxes is the application of Eq. 1 for a horizontal reference plane on a certain height (z) with a vertical wind component (w) within the constant

flux layer. However, the irregularity of turbulent motion implies a strong variation of the instantaneous vertical transport in time as well as in space. Hence certain averaging procedures have to be applied in order to get useful flux estimates. Ideally, an ensemble average should be determined:

$$F_{Hg} = \langle w(z) \cdot C_{Hg}(z) \rangle_{ens} \cong \langle w(z) \cdot C_{Hg}(z) \rangle_{spatial} \cong \langle w(z) \cdot C_{Hg}(z) \rangle_{temporal} \tag{11}$$

under stationary conditions, where turbulent motion over a homogeneous surface represents an *ergodic* system, signifying that the ensemble average is about equal to the respective spatial or temporal average. In MM-flux studies, the time average is typically applied, since it allows determining a representative flux with a sensor system fixed at one single point within the inertial sublayer. The contribution of sources at different distances from the sensor "footprint" is a complex function of the sensor height, surface roughness length and canopy structure together with meteorological conditions (wind speed and direction, turbulence intensity and atmospheric stability).[88] A simple rule of thumb is the concept of cumulative footprint[89,90] that uses analytical solutions of the diffusion equation for near-neutral conditions and averaged wind velocity ($\bar{u}$, m s^{-1}). In this ideal simplified case for low canopies, the cumulative normalized contribution to flux measurements (CNF, %) can be expressed as:

$$CNF(x_L) = \int_0^{x_L} \frac{\bar{u}(z-d)}{u_* k x^2} e^{-\bar{u}(z-d)/k u_* x} dx = e^{-\bar{u}(z-d)/k u_* x_L} \tag{12}$$

where x_L is distance from the sensor (m), z is measurement height (m), u_* is friction velocity (m s^{-1}), d is displacement height (m; see section "Aerodynamic (AER) method"), k is von Kármán's constant. Eq. 12 roughly predicts 80–85% of the flux "seen" at z comes from within a distance (x_L) of $100 \cdot z$ upwind, with the largest contribution occurring at a distance x_L $\sim 10 \cdot z$; in unstable conditions $z/L < 0$, the footprint is somewhat smaller and in stable conditions $z/L > 0$, considerably larger. In most MM studies on Hg flux, it is not specifically stated if a footprint model is utilized (e.g., for compensating for limited fetch). If so,[41,50,91–94] Gaussian dispersion estimates were generally applied.[89,90,95,96] In long-term studies of Hg^0 flux over forest canopies, Bash and Miller[91,97] used the footprint climatology by Amiro,[98] relying on observations of the stratification and the standard deviation of the lateral wind component. Both long-term and short-term observations have changing atmospheric conditions in the data set. Every new atmospheric condition leads to a different footprint and there is a need for a large set of footprint calculations. Fritsche et al.[94] used the model of Kljun et al.,[99] which presents a scaling procedure that provides a tool to estimate footprint variations in time for a given measuring height and roughness length, without

the need to re-calculate the footprint every time the atmospheric conditions change. The model can be retrieved online.[100]

Eddy Covariance (Eddy Correlation) Technique

The eddy covariance (or eddy correlation [EC]) technique estimates Hg flux according to Eq. 11 as the integral covariance of the time series $w(t)$ and $C_{Hg}(t)$ over a suitable time interval Δt:

$$F_{Hg} = \overline{w'C'_{Hg}} = \overline{cov\left(w, C_{Hg}\right)} \cong \frac{1}{\Delta t}\int_{\Delta t} w(t)C_{Hg}\,dt = \tag{13}$$

$$= \frac{1}{N-1}\sum_{k=0}^{N-1}\left[\left(w_k - \overline{w_k}\right)\left(C_{Hg,k} - \overline{C_{Hg,k}}\right)\right]$$

$$= \frac{1}{N-1}\left[\sum_{k=0}^{N-1} w_k C_{Hg,k} - \frac{1}{N}\left(\sum_{k=0}^{N-1} w_k \sum_{k=0}^{N-1} C_{Hg,k}\right)\right]$$

To apply Eq. 13, the distribution of the different eddy sizes (fluctuation periods) and their contribution to turbulent mixing must be known. The time average interval Δt has to be long enough to cover the contribution of the largest eddies while keeping the temporal resolution of the measurements sufficiently high (typically at 10 Hz) to detect the contribution of the smallest eddies. The choice for Δt is depending on stratification and measurement height. However, using a constant averaging time of 30 min during the whole day will not introduce significant error and is now in general recommended.[25] Hence, a turbulence frequency spectrum over more than four orders of magnitude (~0.0005–10 Hz) has to be resolved. This is accomplished by a fast three-axis sonic open-path anemometer that determines the direction of vertical wind velocity. Such a three-dimensional (3D) anemometer is required as knowing all three orthogonal wind components (u, v, w) provides the capability to align EC measurements with the mean wind streamlines, forcing $\bar{v}$ and $\bar{w}$ to zero (planar-fit method[101]). Today there is fast (>10 Hz), sensitive, portable, and reliable equipment for measuring only a few trace gas fluxes (with open-path, e.g., CO_2, H_2O, CH_4, and with closed path laser system, e.g., N_2O, O_3) by EC. The strict requirements for an Hg^0 analyzer of high sensitivity, temporal resolution and precision combined with compactness to make it viable for EC application have turned out be extremely challenging to all fulfill. Although advocated by Bauer et al.[77,102] with 2-photon laser induced fluorescence (LIF) technique, its application as an Hg sensor for Hg^0–EC flux has so far not been realized.[103] Recently, Faïn et al.[76] and Pierce et al.[104] reported progress towards using a cavity ring-down spectroscopic (CRDS) sensor for a future Hg^0-EC flux application.

Relaxed Eddy Accumulation (REA) Technique

The lack of a fast response and sensitive Hg vapor sensor for the EC method can be substituted by using fast response solenoid valves in a conditional technique named relaxed eddy accumulation (REA). REA is a simplified version of eddy accumulation (EA[105]). The basic idea of EA is to interpret the vertical turbulent covariance flux (Eq. 13) as a weighted mean concentration with the vertical windspeed (w) as weighting factor. Since w shows positive (updrafts, ↑) and negative (downdrafts, ↓) values, they must be separated in order to obtain the net weighting factors:

$$F_{Hg} = \overline{w' C'_{Hg}} = \frac{1}{N}\left(\sum_{w>0} |w| \cdot C_{Hg} - \sum_{w<0} |w| \cdot C_{Hg}\right) \tag{14}$$

Air associated with updrafts and downdrafts is sampled by a pump into two bins at a flow rate proportional to $|w|$. Introducing weighted mean concentration for each of the bins $\overline{C^w_{Hg,\uparrow}}$ and $\overline{C^w_{Hg,\downarrow}}$ measured at the end of the sampling period with high resolution (but not necessarily fast response) Hg analyzer or extracted online onto manually handled traps. Since $\sum_{w>0} |w| = \sum_{w<0} |w| = \frac{1}{2}\sum_{i=1}^{N} |w_i| = \frac{N}{2}|\bar{w}|$, Eq. 14 can be rewritten:

$$F_{Hg} = \frac{|\bar{w}|}{2}\left(\overline{C^w_{Hg,\uparrow}} - \overline{C^w_{Hg,\downarrow}}\right) \approx 0.4\sigma_w\left(\overline{C^w_{Hg,\uparrow}} - \overline{C^w_{Hg,\downarrow}}\right) \tag{15}$$

where the last term is valid for a Gaussian distribution ($|\bar{w}|/\sigma_w = \sqrt{2/\pi} \approx 0.798$) and σ_w (m s^{-1}) represents the standard deviation of w. In practice, technical limitations in valve technology make EA hard to apply. Therefore, a "relaxed" version of EA was introduced,[106] where the average concentration of updraft and downdraft air is determined without a weighting by the vertical windspeed. The flow control is more easily handled compared to EA, where the performance of proportional sample flow control solenoids is not able to meet all requirements. Equation 14 has also been adopted for REA and the effect of the non-proportional sampling was expressed through an empirical factor b:

$$F_{Hg} = b \cdot \sigma_w\left(\overline{C_{Hg,\uparrow}} - \overline{C_{Hg,\downarrow}}\right) \tag{16}$$

The b-factor is well defined with a value of 0.627 ($\sqrt{2\pi}/4$) for an ideal Gaussian joint frequency distribution (JFD) of w and C.[107] However, turbulent transport, especially over rough surfaces, often violates the underlying assumption of a linear relationship between w and C.[108] Excursions from the linear relation occur due to non-Gaussian behavior of turbulence and result in smaller b-factors in the parameterization.[109] For many experimental data, b was found to range from 0.54 to 0.60,[110–113] which restricts the use of a fixed factor. Therefore, most investigators determine b in situ from EC and

REA measurements of a suitable scalar quantity χ (e.g., sensible heat flux (H) or CO_2 flux) according to:

$$b_\chi = \frac{\overline{w'\chi'}}{\sigma_w \left(\overline{\chi_\uparrow} - \overline{\chi_\downarrow}\right)} \tag{17}$$

The loss of proportional sampling in the REA technique—compared to the original EA concept—results in an increase of the coefficient in Eqs. 16 to 17 from 0.4 to approximately 0.6. Hence the concentration difference that has to be measured is reduced by a factor of about 1.5. This effect can be partly or fully compensated by the use of a threshold (*deadband*) at $w = 0$ (alternatively at the mean value for vertical wind calculated from e.g. moving average filters), where neither the up-draft nor downdraft sampling is active. The wind-deadband is normally recursively scaled with σ_w and $\leq \alpha \cdot |w/\sigma_w|$, where α is typically 0.5 (*dynamic* deadband). In addition to diminishing the relative contribution of error from the chemical analysis, the use of a deadband reduces the frequency of valve switching that improves sample segregation significantly and alleviate the potential risk of smearing of small eddies inside the sample tubing. In addition to reducing the numerical value of *b,* employment of a dynamic deadband also makes the value largely independent on the friction velocity and atmospheric stability, resulting in an approximately constant b[114]:

$$F_{Hg} \cong 0.42\sigma_w \left(\overline{C_{Hg,\uparrow}(w > \sigma_w/2)} - \overline{C_{Hg,\downarrow}(w < -\sigma_w/2)}\right) \tag{18}$$

The fast response vertical anemometry to sense upward and downward air motions is in REA combined with fast switching of intake air to isolate the air from the upward and downward motions. The concentration scalar material carried in the isolated upward and downward moving air is then accumulated into separate reservoirs or sampled from the isolated lines. Three basic criteria need to be fulfilled:

1. Sampling must be done at constant flow rate,
2. Sample segregation must be at an accurate timing, and
3. Addition due to contamination or loss of the Hg form of interest (e.g., Hg^0, GOM) due to reaction-absorption during sample passage in the system should be minimized.

During the past decade, REA was applied toward measuring Hg^0 fluxes over soils and canopies[91, 92, 97, 115] and measuring GOM fluxes during polar Hg depletion events in the Arctic.[116] The REA-system employed by Bash and Miller[91] is a modified version of that of Cobos et al.[115] according to a suggestion of Bowling et al.[117] and Nie et al.[118] to eliminate negative pressure

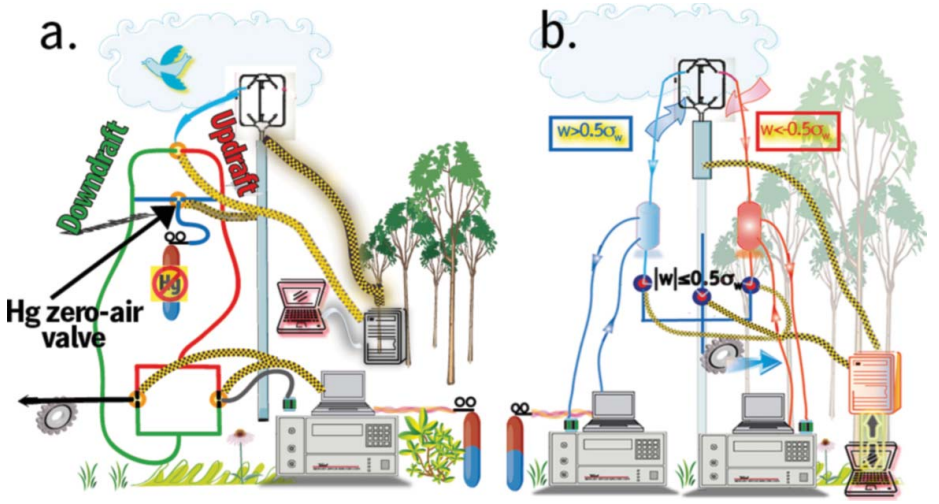

FIGURE 5. Schematics of the Hg^0-REA system employed by Bash and Miller[89] (a) and by Olofsson et al.[90] (b). The Bash and Miller[89] system is modified from that of Cobos et al.[113] The location of Hg zero-air injection valve introduced by Bash and Miller[89] is indicated. (Color figure available online).

that builds up behind the sampling valve. In a simple sketch of Bash and Miller[91] system (left panel of Figure 5), the additional valve marked as 3b is a zero Hg concentration air three-way valve. The twin 2L Teflon reservoir tanks used by Cobos et al.[115] to minimize fluctuations in pressure caused by the valve switching become obsolete in the set-up of Bash and Miller.[91] These REA-systems are of a design with one inlet and without the capability of allowing the isolation of a wind-deadband. By using a combination of two three-way solenoid valves, controlled by a relay driver connected to an automatized Hg vapor analyzer (e.g., Tekran 2537A, Tekran Instruments Corp., Toronto, Canada), one sample line is routed through the analyzer while the other is vented out of the system through a vacuum pump, then the REA measurement can be accomplished. The non-simultaneous (sequential) sample collection and chemical analysis leading to that the numerical strength of updraft versus downdraft samples is separated over the averaging period $\Delta t = 30$ min. Cobos et al.[115] set the b-factor to a constant $b = 0.56$ during experiments while Bash and Miller[91] used three months of sensible heat flux (H) data from the experimental site to calculate $b = 0.474$ ($R^2 \sim 0.96$) according to Eq. (17).

Cobos et al.[115] studied the evolution of Hg^0 flux over agricultural soil in Minnesota planted with corn, while Olofsson et al.[92] investigated modified (Hg contaminated) soil substrates in western Sweden (chlor-alkali waste repository and sewage sludge amended salix field). Both studies report diurnal patterns in Hg vapor fluxes correlated with solar radiation. The work of Bash and Miller[91] is oriented toward long-term Hg^0 REA measurements

from a 40-m tower over a red maple (*Acer rubrum*) forest in Connecticut. During the growing season, there is a trend from net dry deposition in early summer to net evasion in the late summer and early fall before complete senescence.[97] The REA-system employed by Olofsson et al.,[92] shown in the right panel of Figure 5, used separate inlets for updraft and downdraft air samples and in addition a valve for wind-dead band. Every 30 seconds, the band threshold = $0.5 \cdot |w/\sigma_w|$ was updated using wind data from the last 5 minutes. This system is in this aspect identical to earlier reports,[95, 119, 120] exhibiting an approximately constant *b*-factor of 0.42 as repetitively derived from momentum or sensible heat fluxes. In contrast to the setup of Bash and Miller,[91] they (Olofsson et al.) used sub-sample loops that continuously circulate air to the automized Hg vapor analyzers (Tekran® 2537A) from each of the reservoirs buffering segregated air from updrafts and downdrafts, respectively. The analyzer flow rates (0.75 L min^{-1}) were considerably smaller than the main sampling flow rate.[121] Hence, simultaneous and synchronous sample collection and chemical analysis for Hg^0 were obtained. By using two chemical analyzers working in tandem, where one is dedicated for updraft and the other for downdraft analysis only, the performance of the instruments needs to be carefully investigated in order to assess errors of three types:

1. Dissimilar performance of the two Hg sampling cartridges for each instrument,
2. Bias between the instruments (instruments tend to have greater relative accuracy [precision] than absolute accuracy[122]), and
3. Spurious contribution from the sampling system due to light- and/or temperature induced degassing/adsorption of Hg^0.

Sommar et al.[123] found that a dual analyzer system was unpropitious since it suffered from an inherent variability and drift of sensitivity of the Hg^0 analyzers, which was unpractical to compensate by calibration measures. In turn, they developed a system of whole-air type drawing air at high velocity to the Hg^0-REA sampling apparatus, where only a sub-stream was conditionally sampled, thus allowing for the rejection of samples associated with *w*-fluctuations around zero (dead-band). Conditional sampling was executed with 10-Hz resolution by two fast-response three-way solenoid valves in parallel configuration connected to zero Hg^0 air through their normally open ports (see Figure 6).

The relative concentration difference measured by the REA technique is directly related to the respective flux-concentration ratio (w_d) in the following way:

$$\left|\overline{C_{Hg,\uparrow}} - \overline{C_{Hg,\downarrow}}\right| / C_{Hg,amb} = \frac{1}{b\sigma_w} \frac{F_{Hg}}{C_{Hg,amb}} \tag{19}$$

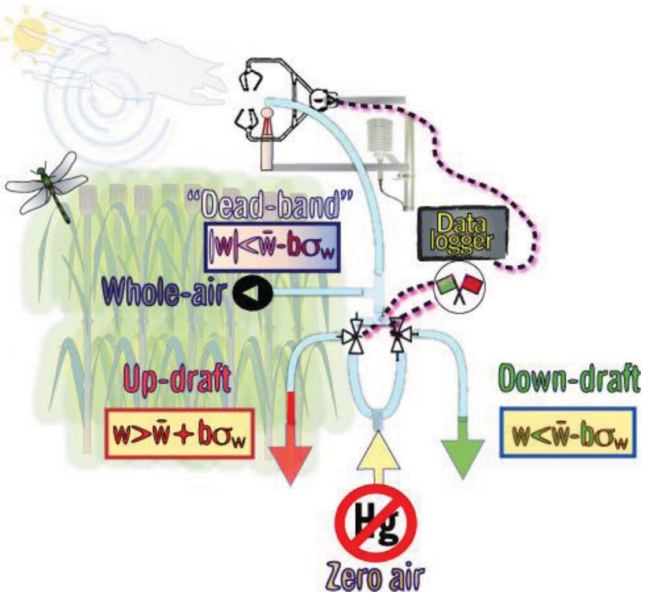

FIGURE 6. Schematics of the Hg^0-REA design employed by Sommar et al.[123] (Color figure available online).

In contrast to Hg^0 with low w_d, GOM exhibits high dry deposition velocities approaching those of strong acids (HNO_3 or HCl) with almost negligible surface resistance (R_c).[8] Given the typical variability of the b-factor and of σ_w, Eq. 19 predicts satisfactory prerequisite of GOM for REA measurements. In this case, REA concentration gradients exceeding 3% should be observed that are resolvable by annular denuder samplers.[124] In the REA-system developed by Skov et al.[116] for GOM, the accumulation devices were placed directly as air inlets before the conditional sampling valves, as indicated in Figure 7. Hence GOM could be sampled without first passing long tubes, valves, or pumps. However, with such an arrangement the accumulating units experience a fluctuating airflow. The performance of the impregnated annular denuder to matrix GOM relying on diffusive transport through a narrow cylindrical slit. In order to accomplish diffusive transport rather than a turbulent one, the flow has to be laminar. The time it takes the build up laminar flow put an upper limit of the sampling frequency of the 3D-anemometer. As an optimum compromise between the meteorological measurements and chemical sample collection, Skov and co-workers[116] used an eddy capture frequency of 1 Hz and a dynamic deadband threshold of $(1/\alpha)\cdot|w/\sigma_w|(\alpha = 2 \text{ or } 3)$. The estimated uncertainty in the REA flux calculation was ~50%. Primarily, the GOM-REA set-up was designed to study the behavior and fate of GOM produced from atmospheric surface layer Hg^0 by reactions involving

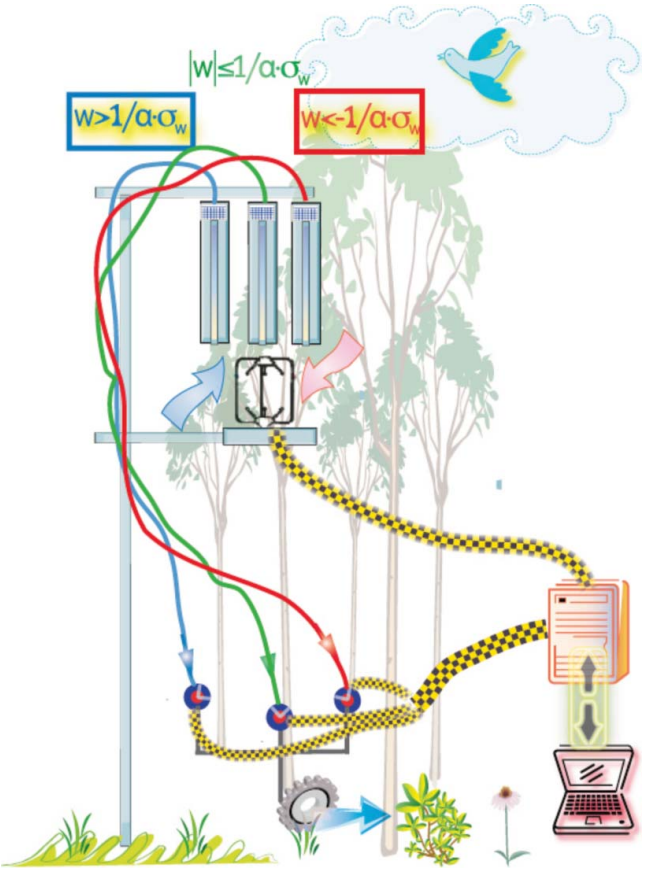

FIGURE 7. Simplified sketch of the REA-system used by Skov et al.[114] to sample GOM flux. (Color figure available online).

reactive bromine species during polar spring. Rather unexpectedly, both dry deposition and emission of GOM were encountered. The emissions were attributed to chemical formation of GOM at or near the snow surface (see Table 2).

Micrometeorological Flux-Gradient Methods

MOST may be used to relate turbulent fluxes to mean quantities (mean profiles and gradients) that can be measured accurately enough with slow response instruments. According to MOST, mean vertical concentration gradient $\partial \bar{C}/\partial z$ can be expressed as:

$$\frac{\partial \bar{C}}{\partial z} \cdot \frac{k \cdot z}{C^*} = \Phi_C\,(z/L) \tag{20}$$

where C^* is the trace gas concentration scale ($-\overline{w'C'}/u_*$) and Φ_C are functions valid for stable ($z/L > 0$) and unstable ($z/L < 0$) conditions, respectively. They were found to be generally equal for scalar quantities (gases Φ_C, potential temperature Φ_H), but not for momentum (Φ_m) in unstable conditions. An often-used form of Φ_m is $1/\sqrt[4]{1+\gamma\,(z/L)}$, called Dyer-Businger relations,[125,126] where the coefficient γ is determined experimentally. Under unstable conditions, $\Phi_C \approx \Phi_H \approx \Phi_m^2$. To get an analytical formula for the profile $C(z)$, the differential relationship in Eq. 20 has to be integrated over z. It is only meaningful to integrate between two heights (z_1 and z_2) within the inertial sublayer and therefore in general only a relationship for a profile difference is obtained. In the simple case of neutral stability ($z/L = 0$), a logarithmic profile function is obtained:

$$\Delta\bar{C} = \frac{C^*}{k} \cdot \int_{z_1}^{z_2} \frac{dz}{z} = \frac{C^*}{k} ln(z_2/z_1) \tag{21}$$

The corresponding logarithmic expression for momentum flux from a height z_0 up to a height z is

$$u(z) - u(z_0) = u(z) = \frac{u_*}{k} ln(z/z_0) \tag{22}$$

where z_0 is the height of the extrapolated logarithmic wind profile where $u(z_0) = 0$ as illustrated in Figure 8. This is the so-called "roughness length/height." The general (non-neutral) profile function contains additional terms, which represent the deviation from the ideal logarithmic shape:

$$\Delta\bar{C} = \frac{C^*}{k} [ln(z_2/z_1) - \Psi_C\,(z_2/L) + \Psi_C\,(z_1/L)] \tag{23}$$

where Ψ-functions are called integrated "stability correction functions" representing the deviation from the neutral logarithmic profile (Eq. 21). The turbulent trace gas fluxes can be related to a measured profile difference by solving Eq. 23 for the scaling quantity C^* and inserting it into the definition of trace gas concentration scale. This results in an integral flux-profile-relationship:

$$\overline{w'C'} = -\underbrace{\left(\frac{u_* \cdot k}{ln(z_2/z_1) - \Psi_C\,(z_2/L) + \Psi_C\,(z_1/L)}\right)}_{v_{tr}} \Delta\bar{C} \tag{24}$$

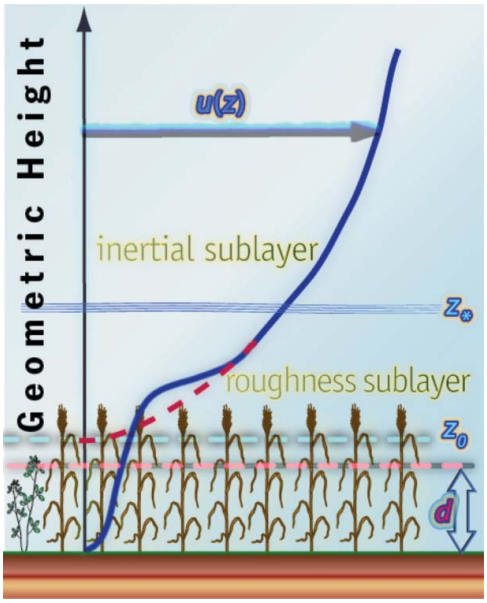

FIGURE 8. Schematic profile of wind speed $u(z)$ in the inertial and roughness sublayer (height z^*) above and within a crop canopy, with indication of the displacement height d and the roughness length z_0. Solid blue line = real profile; dashed red line = ideal extrapolated near-logarithmic profile function. (Color figure available online).

where v_{tr} is called "transfer velocity" since it has the unit of m s^{-1}. The corresponding differential flux-profile-relationship has the form:

$$\overline{w'C'} = -\underbrace{\left(\frac{u_* \cdot k \cdot z}{\Phi_C\,(z/L)}\right)}_{K_C} \cdot \frac{\partial \bar{C}}{\partial z} \tag{25}$$

where K_c (m^2 s^{-1}) in analogy to the similar form in Fick's law for molecular diffusion is called 'turbulent diffusion coefficient' or 'eddy diffusivity'. The relationship between Ψ_c and Φ_c is:

$$\Psi_C\,(z/L) = \int_{z_0/L}^{z/L} \left[1 - \Phi_C\,(\varsigma)\right] \frac{d\varsigma}{\varsigma} \tag{26}$$

Two techniques for the measurement of Hg vapor fluxes according to Eq. 20 have been employed, namely the aerodynamic (pure profile) method and the modified Bowen ratio (scalar analogy) method. These techniques differ in the way v_{tr}/K_c is determined and will be discussed later.

The choice of appropriate measurement heights for the gradient techniques requires careful consideration. First, the measurement level should

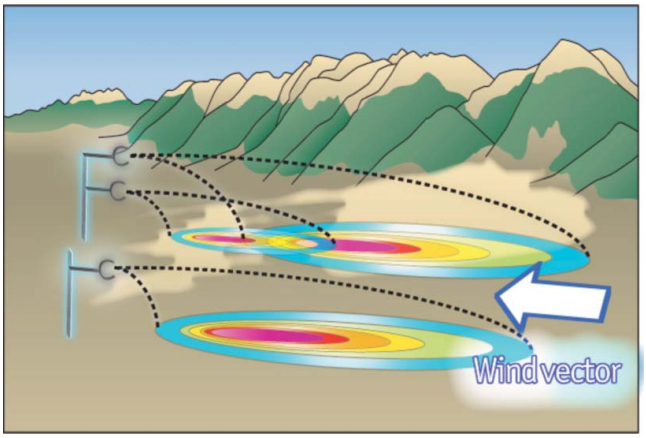

FIGURE 9. Schematic source areas for a single point (EC, REA) and a profile (MBR, AER) MM measurement system (Color figure available online).

have a large vertical distance in order to obtain sufficiently large concentration differences that can be resolved accurately with the available sensors. According to the near logarithmic profile shapes (Eq. 21) the differences are largest near the surface and decrease quickly with height. Therefore, it would be desirable to set the lower measurement level close to the surface. However, all MM measurements should be made above the roughness sublayer height z^* (see Figures 2 and 8), which depends strongly on the size, form, and distribution of roughness elements and has for tall vegetation and forests a thickness ~1.5−2.5 of the canopy height (h).[127] Consequently, tall vegetation,such as forests, the lowest level in the gradient methods often has to be set within the roughness sublayer due to limitations of tower height and sensor resolution. Below the roughness sublayer the profile equation (Eq. 20) is not valid and has to be corrected.[28] A main problem for the gradient methods is that each measurement level has its own distinct source footprint. As shown in Figure 9, it is smaller and closer to the tower for low profile levels than for the higher ones. Under spatial inhomogeneous conditions, the profile levels may sense different surface types and no meaningful flux may result.

5.5.1. Modified Bowen-Ratio (MBR) Technique

Modified Bowen-ratio (MBR) technique is performed under the assumption of equality among the scalar transfer velocities (scalar analogy hypothesis):

$$-v_{tr} = \frac{\overline{w'T'}}{\Delta\overline{\theta}} = \frac{\overline{w'C'_{H_2O}}}{\Delta\overline{C_{H_2O}}} = \frac{\overline{w'C'_{CO_2}}}{\Delta\overline{C_{CO_2}}} = \frac{F_{Hg}}{\Delta\overline{C_{Hg}}} \tag{27}$$

MBR typically requires the measurement of the flux of some reference scalar quantity (χ) on which EC can be performed (e.g., H, CO_2, λE, H_2O), and the two-height concentration gradient of that same quantity and Hg^0. Turbulent transport coefficients for the non-Hg^0 quantity (χ) are determined from the scalar fluxes and concentration gradients:

$$F_{Hg} = \frac{\overline{w'\chi'}}{\Delta\bar{\chi}}\Delta\overline{C_{Hg}} \tag{28}$$

From Eq. 28 it is obvious that the MBR application is problematic, when the reference flux is small.[128] MBR has been employed by in measuring Hg^0 fluxes over both contaminated[93] and background forest soils,[129], over a boreal forest lake,[130] over young and mature forest canopies,[131] and over wetland vegetation.[132] In earlier works, researchers collected up to six replicate manual samples from each level in Hg^0 gradient measurements with a limited resolution of 1–3 hr with a precision of 1.4 ± 0.3%,[129] but eventually employed an automated approach for which inlet bias were typically <0.01 ng m^{-3} using appropriately cleaned sampling lines and a single Hg analyzer sampling sequentially at two heights.[133] Given the uncertainties in the transfer velocity (v_{tr}) determined for H_2O and CO_2, the probable error in MBR Hg^0 gradient measurements was estimated at ~15%,[128,133] Two groups at the Nevada Study and Tests of the Release of Mercury From Soil (STORMS) flux intercomparison campaign (see section "Results of field measurements of Hg flu") also used MBR to quantify Hg^0 fluxes over naturally enriched desert soil.[41,134] In an adjacent area (Carson River superfund site), Gustin et al.[135] utilized automatized Hg^0 and auxiliary MBR measurements at 2–4 heights to estimate Hg^0 emissions from, for example, reprocessed mill tailings (0–150 ng m^{-2} h^{-1}). Poissant et al.[122] used a gradient setup installed on the prow of a ship cruising coastal Lake Ontario and upper St. Lawrence River during July 1998. Using intakes at ~2.7 and ~4.2 m above water surface level, small median gradients (≤0.04 ng m^{-3}) were observed for all of the cruise sections. Fritsche et al.[94,136] employed both MBR and aerodynamic (AER) methods to assess Hg^0 flux over temperate grassland along the Alps. CO_2 was used as a reference species measured with EC. Vertical concentration profiles were established by measuring at 5 heights. Tubings of equal length were connected to a five-port solenoid switching unit and downstream a Hg vapor analyzer (at 5 min per sample) was connected in series with a closed path infrared gas (CO_2, H_2O) analyzer (at 1 Hz). Duplicate samples of $C_{Hg}(z)$ were obtained in the sequence z_1-z_4-z_2-z_5-z_3, where z_1 and z_5 represent the lowest and highest level respectively, translating into a complete profile measurements every 50 min. A minimum resolvable gradient for Hg^0 was determined to 0.02 ng m^{-3}. Using the same instrument to determine the concentrations at all levels removes the influence from the Hg analyzer's systematic detection limit bias

(typically ~0.1 ng m^{-3} for Tekran 2537 using 5-min sampling) on the resolvable gradient,[137] but mentioned previously, a flux determination based on gas sampling not overlapping in time are sensitive to fluctuating conditions within the averaging period. For such MM-measurements, for example non-stationarity in turbulence and intermitted concentration variations are thus of concern. A general presentation of QC-QA (Quality Control-Quality Assurance) measures for MM-systems including e.g. tests of developed turbulence can be found elsewhere.[25,86,138]

Considering speciated Hg (GOM and Hg-p) flux, Lindberg and Stratton[139] utilized mist chamber technique to sample GOM gradients at a grassland and a forest site in connection with MBR technique. The mist chamber technique has since then been found less suitable to determine GOM and has in general been replaced by a KCl-impregnated annular quartz denuder technique.[124] Poissant et al.[140] carried out synchronous gradient measurements of GOM and Hg-p by means of automated Hg speciation systems (Tekran®) operating in tandem at 1.5 and 3.0 m, respectively, as input for MBR-technique using water vapor as a reference component to assess exchange flux over a wetland adjacent to St. Lawrence River.

AER Method

In AER method, v_{tr} is calculated according to Eq. 24 as a function of u_* and L. Generally EC technique is used for determining u_* and L is in turn calculated from Eq. 8. For a vegetated area, the zero-level for the wind field is no longer the ground but within the plant foliage. Instead of the geometric scale z, an effective aerodynamic scale z' is introduced with $z'(d) = 0$ and consequently $z = z' + d$. The (a priori) unknown parameter d is called the displacement height d. For low vegetation with a canopy height of h, Eq. 22 is in geometric scale given by:

$$u(z) = (u_*/k) \ln\left(\frac{\mathrm{z} - \mathrm{d}}{\mathrm{z}_0 - \mathrm{d}}\right) \tag{29}$$

where $u(z_0 + d) = 0$ and z_0 can be roughly determined by $z_0 \approx [z_0 + d] - 2h/3$.

Two groups at the Nevada STORMS flux campaign 1999 used the AER method in connection with chambers[41,50] to measure Hg^0 fluxes over naturally enriched desert soil. The Gustin group utilized Hg vapor measurements at four heights, air temperature and wind velocity at six heights to estimate flux according to the Thornthwaite-Holzman's gradient-flux equation (see Eq. 32) yielding a fetch of ~250 m. The Edwards group choose two low heights above the surface $z_1 = 0.1$ m and $z_2 = 0.4$ m to look at small footprints, typically <50 m of fetch. The flux was calculated according to

Eq. 30:

$$F_{Hg} = \frac{u_* k \left(C_{Hg}(z_1) - C_{Hg}(z_2)\right)}{[ln(z_2/z_1) - \Psi_H(z_2/L) + \Psi_H(z_1/L)]} \tag{30}$$

The stability correction functions Ψ from Businger et al.[125] used in Eq. 30 have numerical forms depending on stability: $\Psi = -4.7 \cdot (z/L)$ for $z/L > 0$, $\Psi = 2 \cdot \ln((1 + x^2)/2)$ and $x = \sqrt[4]{1 - 15(z/L)}$ for $z/L < 0$. A more detailed account on the design and evaluation of this AER system is given in Edwards et al.[137] Two-, three-, and four-point profiling systems were employed during the various field studies. They intermittently imposed a correction factor of ~1.3 on F_{Hg} according to Eq. 30.[141] The gradient gas sampling and measurement system was lined with Teflon (solenoid valve, needle valve, pump, etc.). To avoid the creation of an artificial flux due to flow distortion, the intakes were designed to decrease flow by splitting the intakes into four inlets. The air sample was dried by Nafion bundle (Perma Pure Inc., Toms River, NJ, USA) prior to chemical analysis. Hence, the requirement for correction of water vapor content was avoided.[47] Edwards and co-workers reported a gradient resolution of ~0.01 ng m^{-3} translating into a method detection limit (MDL) of ~1.5 ng m^{-2} h^{-1} ($u_* = 0.1$ m s^{-1}, $z_1 = 0.15$ m and $z_2 = 0.4$ m). Typically, flux was calculated with an averaging time of 90 min. Lee et al.[142] used AER in a biannual study of Hg^0 flux over coastal saltmarsh vegetation in New England. Similar to Edwards et al.,[50] the use of a solenoid valve enabled two height levels sampling (here $\Delta z \sim 1.9$ m) by an automated Hg vapor analyzer (Tekran®). A resistance approach including an aerodynamic resistance was used in the flux calculation:

$$F_{Hg} = -K(z)\frac{\partial C_{Hg}}{\partial z} = -\int_{z_1}^{z_2} dC_{Hg} \Big/ \int_{z_1}^{z_2} \frac{dz}{K(z)} = \left(C_{Hg}(z_1) - C_{Hg}(z_2)\right) \Big/ \int_{z_1}^{z_2} \frac{dz}{K(z)} \tag{31}$$

where K (m^2 s^{-1}) was determined with the EC data with correction for air stability following the functions of Businger and Dyer. The effect of sequential compared to continuous sampling of the gradient was simulated for sensible heat flux, whereby AER was found biased high with 6%. Mean flux bias were estimated to 0.4 and 0.6 ng m^{-2} h^{-1} for the two consecutive years based on an averaged $1/dz/\int_{z_1}^{z_2} dz/K(z)$ of 0.06 m s^{-1}. In eastern Asia, Kim et al.[143,144] performed AER measurements of Hg^0 flux over a vast rice paddy located on an island proximate to the Yellow Sea. Hourly measurements at two heights

($z_1 = 1$ m and $z_2 = 5$ m) were accomplished by two automatized Hg analyzers (AM-2, Nippon Instruments Co., Japan) during spring of two consecutive years. Kim's group has also investigated fluxes over landfills[145,146] and urban settings[145] with this technique. Kim and Kim[147] introduced the percent gradient concept $100\left[\left(C_{Hg}(z_1) - C_{Hg}(z_2)\right)/C_{Hg}(z_1)\right]$ to readily assess if the gradient observations exceeded the precision of their system of typically ~ 2%. The Reinfelder group applied AER to study volatilization of Hg^0 in maritime settings of New Jersey. Goodrow et al.[148] (part of the Reinfelder Group) investigated the contribution of the land-applied stabilized dredged material originated from New York/New Jersey harbor to local Hg emission budget while Smith and Reinfelder[149] studied Hg vapor flux from tidally exposed salt marshes with sparse low vegetation. These authors used a modified Thornthwaite-Holzman's gradient-flux equation[150] to calculate Hg^0 flux:

$$F_{Hg} = ku_* \left(C_{Hg}(z_1) - C_{Hg}(z_2)\right)/\left[\varphi_w(z/L) \cdot \ln(z_2/z_1)\right] \tag{32}$$

where φ_w is a atmospheric stability correction factor accounting for the change in curvature of the wind profile away from neutral conditions for water vapor used as a proxy for Hg vapor. The gradient resolution reported range from $\leq$0.02 to 0.09 ng m^{-3} using a Tekran® 2537 analyzer. The substrates investigated exhibited significant light-driven volatilization of Hg^0.

Marsik et al.[151] employed gradient measurements at two heights with an average inlet bias of 0.01 ng m^{-3} over a mixed sawgrass/cattail marsh in the Everglades, Florida. Van Heyst and co-workers used a similar system to that of Edwards et al.[135] to quantify Hg^0 fluxes over a snow surface in Nunavut, Canada,[152] and an agricultural field (soya bean/corn) amended with biosolids.[153,154] During the first half of 2008, Steen et al.[155] investigated Hg^0 flux over a snow-covered surface under polar night and day at a site in the European high Arctic impacted by Hg depletion events (MDEs).[17,156] For a system similar to that of Edwards et al.,[137] Steen et al.[155] reported a MDL of ~5 ng m^{-2} h^{-1}. The measurements were biased by inconsistent Hg^0 concentration profiles ($z \leq 0.5$ m) explained by a non-stationary turbulence regime. AER and MBR methods have been compared for a full year over a sub-alpine grassland in central Switzerland.[94,136] The time series of AER and MBR Hg^0 fluxes compared favorably in general. However, during spring and summer AER fluxes were consistently higher, which derives from the very small H_g0 gradients measured. The computation of the GEM fluxes with the AER and the MBR methods yielded random errors in the order of 43% and 14%, respectively. Nevertheless, it was suggested that the AER method yields more reliable Hg^0 fluxes than the MBR method. Converse et al.[157] used AER and MBR technique to measure gaseous Hg fluxes over mixed vegetation in a high-elevation meadow in seasonal campaigns during one year. Comparable

fluxes were reported during spring and summer campaigns. However, when the reference (H_2O, evapotranspiration) flux for MBR was low during fall and winter the AER method was found to be more reliable.

CONSERVATIVE TRACERS FOR NONTURBULENT CONDITIONS

The very stable boundary layer with prevalence during nighttime eludes modeling attempts due to the limitation of existing formulations of turbulence. An additional measurement method, the so-called $^{222}Rn/Hg^0$ method, has recently been used for the measurement of Hg^0 fluxes at a grassland site in Seebodenalp, Switzerland, and at the city center of Basel, Switzerland.[20] It was used during periods with a stable nocturnal boundary layer (NBL) and was found to be an effective method for the measurement of Hg^0 fluxes in situations where the atmospheric conditions are nonturbulent, the fluxes are small, or the surface is highly heterogeneous. One of the assumptions of the method are that the lower NBL is reasonably well mixed so that potentially different source areas for ^{222}Rn (emitted primarily from soils) and Hg^0 (emitted and exchanged by soils, plants, and anthropogenic sources such as combustion processes) would not accumulate in different heights in the NBL. The noble gas ^{222}Rn is a decay product of ^{238}U, has a relatively constant emission rate from soils,[158] and has a half-life time of ~4 days. Accumulation of ^{222}Rn in the air is indicative of reduced vertical mixing in the atmospheric boundary layer. Air concentrations of Hg^0 and ^{222}Rn were sequentially sampled with a 5-min resolution, whereby Hg^0 flux was calculated as the ratio of Hg^0 to ^{222}Rn concentration change in the NBL multiplied by the ^{222}Rn source strength:

$$F_{Hg} = \frac{\Delta\overline{C_{Hg}}}{\Delta\overline{C_{^{222}Rn}}} \cdot F_{^{222}Rn} \tag{33}$$

The latter quantity ($F_{^{222}Rn}$) was measured with a small static enclosure connected to a ^{222}Rn ionization chamber. Periods with significant linear accumulation of ^{222}Rn were used to delineate stable NBLs and to calculate Hg^0 fluxes. Linear regression analysis of ^{222}Rn concentration change over >6 h was employed.

BULK METHODS FOR HG FLUX MEASUREMENTS OVER WATER SURFACES

Methods for estimating air-water exchange of Hg (Hg^0) are generally bulk or enclosure approaches although MM techniques have been used in a few cases. Examples of the application of the both latter techniques for

air-water exchange studies have been given in previous sections. The bulk methods are discussed below. The flux of a trace gas between air and water is controlled by two main factors: the difference in concentration (ΔC_{Hg0}) of the gas in air and in water and the overall gas transfer velocity (k_{tot}, typically in cm h^{-1}):

$$F_{Hg} = k_{tot}\Delta C_{Hg^0} = k_{tot}\left(C_{Hg^0,\,water} - C_{Hg^0,\,air}/H_{Hg^0}\right) = \frac{k_{tot}C_{Hg^0,\,air}}{H_{Hg^0}}\left(\frac{S}{100} - 1\right) \quad (34)$$

The right term in Eq. 34 including ΔC_{Hg0} is expressed as function of the Hg^0 saturation level (S in %), where H_{Hg0} is the (dimensionless) Henry's law coefficient for Hg^0. This coefficient has recently been experimentally determined as function of water temperature (T, K) and salinity.[159] A salting-out effect was observed for Hg^0 in 1.5 M NaCl solution, where $\ln(H_{Hg0}) = 5.28 - 1871.6/T$. For pure water, the determination by Andersson et al.[159] compares favorably with that of Sanemasa.[160]

In the two-film model originally proposed by Lewis and Whitman,[161] it is common to express the total resistance as a sum of air and water resistances:

$$R_{tot} = R_{water} + R_{air};\ 1/k_{tot} = 1/k_{water} + 1/(k_{air}H) \quad (35)$$

For a sparingly soluble gas such as Hg^0, R_{water} is the dominant resistance and k_{tot} in Eq. 34&35 can be approximated by the water-transfer velocity (k_{water}). In the seminal work by Fitzgerald et al.[162] and Kim and Fitzgerald[163] estimating Hg^0 flux over the equatorial Pacific, k_{water} is calculated from Fickian molecular diffusion of Hg^0 ($D_{Hg^0,\mathrm{water}}$, $cm^2\ s^{-1}$) across a stagnate surface film (thickness z_d):

$$k_{water} = D_{Hg^0,water}/z_d,\ \ Sc_{Hg^0} = \nu/D_{Hg^0,water} \quad (36)$$

Sc is the Schmidt number, which is the ratio of momentum diffusivity (kinematic viscosity of water, ν) to $D_{Hg^0,\mathrm{water}}$. The aqueous diffusion coefficient $D_{Hg^0,\mathrm{water}}$ has not been experimentally determined and as such has to be approximated by empirical molecular volume- or mass-based methods. Kim and Fitzgerald[163] used the Othmer-Thakar equation[164] while numerous of later works on air-water exchange[165–168] rely on the Wilke-Chang methodology described in Reid et al.[169] Poissant et al.[122] estimated Sc_{Hg0} from a linear and an exponential function for ν[170] and $D_{Hg^0,\mathrm{water}}$,[163] respectively, which is similar to the approach of Costa and Liss.[171] This simplistic approach has been implemented in an early version of the GEOS-Chem global 3-D model for Hg[172] but in a later version,[173] it was revised to include the Wilke-Chang approximation. Schroeder et al.[174] applied a mass-based approximation proposed by Liss and Slater[175] for low molecular gases on Hg^0, accordingly $D_{Hg^0,\mathrm{water}}$ is inversely proportional to the molecular mass.

Kuss et al.[176] performed molecular dynamic simulations of the diffusivity of Hg^0 yielding $D_{Hg^0,water}$ ($cm^2\ s^{-1}$) in freshwater and seawater fitted by Arrhenius expressions of 0.01768 · exp(-2042.22/T(K)) and 0.02293 · exp(-2136.03/T(K)), respectively. Their results fall in-between those obtained with the volume and the mass approximations, which in-turn being significantly higher and lower (~83 and ~78% at 20°C), respectively. Moreover, in fresh water, the predicted Sc_{Hg0} was found to compare well with experimentally derived Sc_{CO2}[177] in the temperature range of 10–25°C.

It is evident that the surface film model oversimplifies the gas exchange dynamics.[178] Baeyens et al.[179] and Baeyens and Leermakers[180] used a classical shear turbulence model and a wave breaking model to calculate air-sea exchange of Hg over the North Sea and adjacent waters. Later works on Hg^0-gas exchange over (large) water surfaces using concurrent measurements of $C_{Hg^0,air}$ and $C_{Hg^0,water}$ normally rely on parameterizations of k_{water} obtained from proxy tracers formulated in terms of wind speed at 10 m height under neutral air boundary condition (u_{10n}). Of these parameterizations, the three most frequently used for sea surfaces are the three-segment, piecewise linear u_{10n} relation developed by Liss and Merlivat,[181] the quadratic u_{10n} function proposed by Wanninkhof[182] and grade two polynomial u_{10n} function of Nightingale et al.[183] For shallow water bodies (lakes, etc.), gas exchange parameterizations, such as that of Wanninkhof et al.,[184] obtained empirically from SF_6 tracer experiments over a lake are preferred. See Table 2 for the gas exchange model used in the specific studies. The transfer velocity k_{water} (u_{10n}) is in practice calculated normalized for CO_2 at 20°C in either freshwater ($Sc = 600$; k_{600}) or in seawater ($Sc = 660$; k_{660}). The species-specific k_{water} for Hg^0 is subsequently calculated (here in the case of sea water) from:

$$k_{water}(Hg^0) = k_{660}\left(\frac{Sc_{Hg^0}}{660}\right)^{-n} \tag{37}$$

where $Sc_{Hg}{}^0$ is given at the appropriate temperature and if relevant recalculated to apply for seawater according to Wanninkhof.[182] The exponent n in Eq. 37 is usually set at 0.5 (2/3 for the smooth segment in the model of Liss and Merlivat[181]). A recent review has suggested that the model developed by Nightingale et al.[183] best represents the simulations made for Hg evasion.[14]

During the last decade, methods have been developed to obtain near real-time analysis of $C_{Hg^0,water}$ (dissolved gaseous Hg, DGM) in discrete water samples, flow-through devices or *in-situ* the surface water. They rely either on quantitative Hg^0 extraction procedures (using Hg^0 free purging gas)[185–187] or by utilizing the phase partitioning equilibrium of Hg^0 between air and water.[188–191] The automatized DGM sampling systems developed by

Andersson et al.[191] and Kuss and Schneider[190] have been operated during extensive oceanographic cruises.[192,193] The former system includes a jacketed cylindrical extractor, which being continuously pumped by a high flow of surface water entering at the top of the inner cylinder. A stream of pressurized ambient air with considerably lower flow rate is dispersed as tiny bubbles at the bottom of this water column by using a pore size P0 glass frit. The contact time obtained between the streams by the opposite flow operation was sufficient for the gas exiting the system with respect to Hg^0 vapor to attain phase equilibrium with the water. Moreover, the downstream water in the outer cylinder acts insulating on the media in the inner one with respect to heat transfer from surrounding air (at room temperature). The concentration of Hg^0 in the outgoing air (C_{eq}) is analyzed and used to calculate $C_{Hg^0,\,water}$ according to:

$$C_{Hg^0,\,water} = C_{eq} \big/ H(T_w) \tag{38}$$

where T_w is the temperature of the surface water conserved during the extraction procedure. Using an automatized Hg vapor analyzer (Tekran®), an analytical cycle for DGM is typically completed every 10 min. The sampling efficiency of DGM was stated to ~99%. The latter system[190,194] employs a static air head-space continuously sprayed with surface water in a glass bottle equipped with a water drain during 1-h equilibrium time. Subsequently, the drain is closed and the rising water level supply equilibrated air for Hg^0 analysis without dilution or contamination by ambient air. Again, Eq. 38 is utilized to calculate $C_{Hg^0,\,water}$ corresponding to a time resolution of 75 min of DGM determinations.

RESULTS OF FIELD MEASUREMENTS OF HG FLUX

There have been a substantial number of field studies of Hg fluxes over various surface types using several different measurement methods. In Table 2, a large selection of such investigations reported in the literature has been listed with brief supplementary information and sorted by substrate type. The data sets vary largely in time duration from sporadic samples during a short period to full-seasonal studies. Further on in this section, it is appropriate to talk over intercomparisons of field flux methods. A number of groups have made side-by-side comparison of the flux-gradient MM techniques.[94,136,157] An extensive field intercomparison campaign (Nevada STORMS) involving four groups using both MM and DFC techniques in one cluster and three groups using DFCs only in another was conducted during fall of 1997.[195] The MM techniques compared favorably (averaged fluxes within 15% of each other) with the exception one setup consistently recording much lower fluxes. Given the highly

heterogeneous soil concentration in the landscape, the result has been explained largely by spatial differences in fetch.[41,50] The comparison of DFCs with various design and standard operating procedures during the same campaign showed that calculated Hg fluxes using different chambers varied over an order of magnitude.[43,195] The significant difference ($p < 0.05$) between DFCs was partially explained by substrate heterogeneity. Rinklebe et al.[42] and Magarelli and Fostier[196] deployed replicate chambers in multiple site studies and found a general high coefficient of variability between site replicates (maximum 137–250%). The spatial variability has also been assessed by monitoring flux from two colocated polycarbonate DFC systems interfaced by automatized Hg analyzers and subsequently moving one system around while having one remain stationary.[197,198] In studies of litter-covered background soils in the eastern United States, Kuiken et al.[197] found fluxes observed with the non-stationary DFC in comparison were slightly more variable and for three out of six sites the mean flux observed by the two systems exhibited statistically significant differences. The MM systems applied during Nevada STORMS campaign measured diurnal Hg fluxes about 3 times higher than those measured with DFCs,[41] while a subsequent intercomparison study involving dry and wet conditions at the site showed that fluxes derived from a small-volume polycarbonate DFC (air turnover time 0.2 min) were not significantly different ($p < 0.05$) from those derived simultaneously and within the footprint of a MBR system.[13] One of the participating groups of Nevada STORMS had previously found that MBR and a novel designed DFC applied over a rural grassland in southern Quebec in general were well correlated with a slight discrepancy during night.[199] Carpi and Lindberg[200] reported agreeable Hg^0 fluxes derived from MBR and DFC over a sludge amended field. In multisite study over Canada, Edwards et al.[137] achieved a good comparison between DFC and AER methods concerning low-emitting homogeneous substrate sites. Gillis and Miller[40] pointed out that airflow rates through the chamber and chamber exposure to ambient wind could potentially account for the poor agreement between DFC flux and that derived from MM techniques. Moreover, Wallschläger et al.[43] found a significant correlation between ambient wind speed and flux despite the fact that chambers exclude most wind. Recently, polycarbonate DFCs with aerodynamic design to create a regular air-flow field over the flux measurement zone have been fabricated by two groups and verified by computational fluid dynamics computational simulations.[63,201] Assuredly of similar shape, the DFC design of Lin et al.[63] nevertheless comparatively enables an appreciably more uniform flow field to establish. Capitalizing on the predictable surface shear properties inside this type of DFC (with a internal height and a length of 3 cm and 30 cm, respectively), a scaling procedure using overall mass transfer coefficients to link the measured flux (F_{DFC}) to atmospheric surface layer flux (F_{atm})

was introduced:

$$F_{atm} = F_{DFC}\frac{k_{atm}}{k_{DFC}} = \frac{Q\left(C_{Hg,\,out} - C_{Hg,\,in}\right)}{A}\frac{\left[4.86 + \frac{3.625\cdot10^{-6}\left(u_*/z_0 D_{Hg,\,air}\right)}{1+3.911\cdot10^{-5}\left(u_*/z_0 D_{Hg,\,air}\right)^{2/3}}\right]}{\left[4.86 + \frac{3.633\cdot10^{-2}\left(Q/D_{Hg,\,air}\right)}{1+1.818\cdot10^{-2}\left(Q/D_{Hg,\,air}\right)^{2/3}}\right]} \quad (39)$$

where k_{DFC} (m s^{-1}) is the overall mass transfer coefficient in DFC, k_{atm} (m s^{-1}) is the corresponding coefficient under atmospheric conditions and $D_{Hg,air}$ is the diffusion coefficient of Hg^0 in air (1.194×10^{-5} m^2 s^{-1}).

SUMMARY

Hg is the only noninert element that besides the noble gases is predominantly in the gaseous atomic form in the atmosphere. Long-path optical laser spectroscopy can be used to detect Hg^0 at high frequency to levels approaching the ambient sub-ppt background mixing ratios. For decades, the DIAL technique has proven to be efficient tool for 3D mapping of atmospheric Hg^0 in Hg impacted sites yielding reliable integrated flux determinations. The DIAL technique is however too imprecise for measurements of background diffuse areal Hg^0 fluxes, for which enclosure or conditional MM techniques and additionally bulk methods for water surfaces being employed. Benefiting from smaller and easily field deployable equipment, the standard procedure of sampling ambient air Hg^0 is by enhancement collection onto collectors containing gold in manual or automated systems. Moreover, background monitoring of Hg^0 without preconcentration can be performed by Z-AAS instruments (e.g. Lumex RA-915AM, Lumex Ltd., St. Petersburg, Russia[75,202]). Interfacing a flux sampling system with automatized Hg gas analyzer alleviates the otherwise tedious and time consuming work with processing a large number of manual traps analytically. This implementation is however associated with a significant cost, for which the expense of the analyzer is a few to several times that of the essential flux system (see Table 1).

Enclosures, representing the smallest scale ($\ll$1 m^2), are by far the most common tools in terrestrial field research. Open flow-through DFCs are the most frequently employed. In contrast to many other trace gases (CH_4, N_2O, etc.), closed (static or dynamic) enclosures have so far received very limited attention for Hg^0. In their simplest form including manual Hg gas analysis by traps, enclosure methods are of relatively low cost. The enclosures are portable and permit process studies and experiments with many treatments. However, they also suffer from several disadvantages, including their intrusive nature, influence on the microclimate over the plot studies ("greenhouse effect"), isolation from outside air. Given the small footprint of enclosures and that Hg^0 gas exchange fluxes over terrestrial surfaces are profoundly

variable in space and time, replication measurements are thus preferred but often not carried out (see section "Results of field measurements of Hg flux"). Another issue is that no standard design and corresponding operation procedures have been implemented for field studies with DFCs. Although a large number of field investigations with this technique have been performed, many of the various flux data sets are not readily comparable due to divergent operating parameters.

Given the lack of a fast response ambient Hg^0 sensor precluding the possibility to perform Hg^0-EC flux, the MM techniques employed for measuring Hg gas fluxes on large landscape scales are restricted to REA and flux–gradient methods. EC is the micrometeorologist's preferred technique because it is a direct measurement at a point. There is no problem with different footprints for different measurement heights as there can be for flux–gradient techniques, it is not impaired by a number of the simplifying assumptions as other MM approaches such as similarity between the eddy diffusivities for different entities, and it is independent of atmospheric stability.

REA technique substitutes fast-response solenoid valves for a fast-response gas sensor. Air is sampled at a constant rate at a point and is directed into "up" and "down" bins (reservoirs) depending on the direction of the vertical wind. The gas flux is calculated as the product of the standard deviation of w and the concentration difference between the bins, multiplied by an in situ determined or empirical coefficient. Advantages of the method include its insensitivity to different footprints for different sensor heights and stability conditions, and the ability of preconditioning the air samples before analysis. However, the implementation of fast response solenoid valves, if not carefully configured, can introduce severe fluctuation in sampling flow that violates the fundamental requirements of the REA measurement. Other sources of systematic error are the potential offset in w-measurements and improper time delay between the wind speed measurement and corresponding conditional sampling (execution of fast-response valves). The applicability of MM technique in measuring background Hg^0 fluxes is strongly dependent on the minimum resolvable concentration difference (gradient) that can be achieved. It is thus very important to exercise a stringent QA/QC-protocol on the gas sampling and chemical analytical system. For REA, when the precision of the chemical analyzer is limited, it is viable to increase the concentration difference between the updraft and downdraft bins by disposal of air in a wind deadband (i.e., for $w < |w_0|$).

In flux–gradient approaches, fluxes are calculated as the product of the eddy diffusivity and the vertical concentration gradient of Hg^0 or transfer velocity and the difference in Hg^0 concentration between two heights (AER method), or in the case of MBR-method as the product of a tracer flux (typically that of heat, water vapor or CO_2 measured with EC) and the ratio of concentration differences of tracer and Hg^0 between two heights

measured simultaneously. In the AER method, the eddy diffusivity/transfer velocity can be inferred from turbulence measurements made with a fast response 3D anemometer. Corrections are needed to account for the effects of atmospheric stability.

Precautions are ordered in applying flux–gradient techniques over (high) canopies. In principle, measurements need to be conducted above the roughness sublayer height. However, given small gradients in this zone and limitations of tower height, often at least the lowest level has to be set within the roughness sublayer to satisfy a limited chemical sensor precision. In addition, the application of AER technique requires knowledge of d and z_0, which is not the case for MBR. On the other hand, in periods where the tracer flux is small, AER tends to be more reliable than the MBR-technique. Flux–gradient systems for Hg^0 normally employ interchange gear to measure concentrations at different heights with the same instrument resulting in non-synchronous concentration measurements. However, the resolvable concentration gradient obtained by employing two instruments operating in tandem is often insufficient because the individual instrumental (squared) errors are added in the calculation.

In contrast to enclosure techniques, the MM techniques allow spatially averaged measurements over a large area without disturbing ambient conditions and may serve as independent tests of process-based models, but are in-turn technically more demanding and require detailed knowledge of the prevailing micrometeorological conditions and the source area (see Table 1). The personal expense for technical maintenance and support of a MM system is likely to be higher. In general, enclosures can detect fluxes that are smaller than the lower limit for MM techniques. Moreover, the flux measured with a MM system will be the same as that at the bulk surface only if the flux is constant with height. Changes of fluxes with height are expected to be of consideration when obstructions exist in the upwind fetch, the surface has non-uniform vegetation or roughness or if adjacent strong point sources are present. Therefore, a MM sampling site must be chosen with care, still often compromises are necessary in the measurements such as excluding wind sectors and unfavorable meteorological conditions (inclusive of precipitation events during which the essential wind anemometer may exhibit frequent malfunction). Obviously, MM techniques are best suited for estimating terrestrial net ecosystem Hg gas exchange as the measured flux includes the contribution from the all present various surface (vegetation, soil, etc.) processes. Given the biomes complexity, however, a broad seasonal record of data is preferred to temporarily limited studies. As only dry deposition can be measured by MM techniques, co-located sampling of wet deposition is required to provide complementary information about inputs in order to judge if an ecosystem acts as a sink or as a source of Hg. Contrary to enclosures, there are thus site conditions and logistical considerations for which MM techniques are not appropriate. Enclosure techniques have their main

niche to gauge fluxes over defined surfaces or at spatial scales below the resolution possible with MM techniques. Nevertheless, by combining data from appropriate sampling allocations, enclosure measurements can potentially be used to estimate net Hg gas exchange over a large area.

Hg^0 is ubiquitous in the surface waters of the oceans and of fresh water systems in concentrations exceeding those expected as if it were in equilibrium with the atmosphere. In water, enclosures can only be used during relatively calm conditions, which make direct surveys of the influence of wind and waves on the Hg^0 gas exchange less viable. This is particularly of concern for the application for seawater surface, where the transfer of gases between water and atmosphere is largely governed by events associated with high wind speed and breaking waves. For larger water bodies, bulk methods have been widely applied. They generally combine measurements of Hg^0 in air and surface water with gas transfer-wind speed relationships obtained for studies of proxy tracers. A significant source of uncertainty stems from the aqueous diffusion coefficient of Hg^0, which has not been experimentally determined. The methods used in the literature for estimation produce largely divergent results. In recent years, progress has been made to measure Hg^0 in surface water with automated techniques to better match the time-resolution permissible by using on-line instrument for monitoring Hg^0 in ambient air.

ACKNOWLEDGMENTS

This study was supported by National Research Program of China (2013CB430003) as well as by Chinese Academy of Sciences through an instrument development program (YZ200910) and of Natural Science Foundation of China through grants 41030752 and 40825011. The authors express their gratitude to the three anonymous reviewers who provided helpful comments and suggestions to significantly improve the manuscript.

REFERENCES

[1] Mergler, D., Anderson, H. A., Chan, L. H. M., Mahaffey, K. R., Murray, M., Sakamoto, M., and Stern, A. H. (2007). Methylmercury exposure and health effects in humans: A worldwide concern. *Ambio* 36(1), 3–11.

[2] Lindqvist, O., and Rodhe, H. (1985). Atmospheric mercury—A review. *Tellus Series B—Chemical and Physical Meteorology* 37(3), 136–159.

[3] Lin, C. J., and Pehkonen, S. O. (1999). The chemistry of atmospheric mercury: A review. *Atmospheric Environment* 33 (13), 2067–2079.

[4] Primeau, F. W., and Holzer, M. (1996). The ocean's memory of the atmosphere: Residence-time and ventilation-rate distributions of water masses. *Journal of Physical Oceanography*; 36, 1439–1456.

[5] Smith-Downey, N. V., Sunderland, E. M., and Jacob, D. J. (2010). Anthropogenic impacts on global storage and emissions of mercury from terrestrial

soils: Insights from a new global model. *Journal of Geophysical Research* 115, G03008, doi: 10.1029/2009jg001124.

[6] Pirrone, N., Cinnirella, S., Feng, X., Finkelman, R. B., Friedli, H. R., Leaner, J., Mason, R., Mukherjee, A. B., Stracher, G., Streets, D. G., and Telmer, K. (2009). Global Mercury Emissions to the Atmosphere from Natural and Anthropogenic Sources. In N. Pirrone and R. Mason (Eds.), *Mercury fate and transport in the global atmosphere*, (pp.1–47). Springer, New York.

[7] Gustin, M., and Jaffe, D. (2010). Reducing the uncertainty in measurement and understanding of mercury in the atmosphere. *Environmental Science & Technology* 44(7), 2222–2227.

[8] Zhang, L., Wright, L. P., and Blanchard, P. (2009). A review of current knowledge concerning dry deposition of atmospheric mercury. *Atmospheric Environment* 43(37), 5853–5864.

[9] Feng, X. B., Fu, X. W., Sommar, J., Lin, J., Shang, L. H., and Qiu, G. L. (2011). Earth surface natural mercury emission: Research progress and perspective. *Chinese Journal of Ecology*; 30(5), 845–856.

[10] Mason, R. P. (2009). Mercury emissions from natural processes and their importance in the global mercury cycle. In N. Pirrone and R. Mason (Eds.), *Mercury fate and transport in the global atmosphere* (pp. 173–191). Springer, New York.

[11] Gustin, M. S. and Lindberg, S. E. (2005). Terrestrial Hg Fluxes: Is the Next Exchange Up, Down, or Neither? In N. Pirrone and K. R. Mahaffey (Eds). *Dynamics of mercury pollution on regional and global scales* (pp. 241–259), Springer, New York.

[12] Gustin, M. S., Lindberg, S. E., and Weisberg, P. J. (2008). An update on the natural sources and sinks of atmospheric mercury. *Applied Geochemistry*; 23(3), 482–493.

[13] Gustin, M. S. (2011). Exchange of mercury between the atmosphere and terrestrial ecosystems. In Y. Cai, G. Liu, and N. J. O'Driscoll (Eds.), *Advances in environmental chemistry and toxicology of mercury*. John Wiley & Sons, Hoboken, NJ, USA, 423–452.

[14] Qureshi, A., MacLeod, M., Sunderland, E., and Hungerbühler, K. (2011). Exchange of elemental mercury between the oceans and the atmosphere. In Y. Cai, G. Liu, and N. J. O'Driscoll (Eds.), *Advances in environmental chemistry and toxicology of mercury*. John Wiley & Sons, Hoboken, NJ, USA, 389–422.

[15] Sprovieri, F., Pirrone, N., Mason, R. P., and Andersson, M. (2009). Spatial coverage and temporal trends of over-water, air-surface exchange, surface and deep sea water mercury measurements. In N. Pirrone and R. Mason (Eds.), *Mercury fate and transport in the global atmosphere* (pp. 323–380). Springer, New York.

[16] Durnford, D., and Dastoor, A. (2011). The behavior of mercury in the cryosphere: A review of what we know from observations. *Journal of Geophysical Research* 116, D06305, doi: 10.1029/2010jd014809.

[17] Steffen, A., Douglas, T. A., Amyot, M., Ariya, P. A., Aspmo, K., Berg, T., Bottenheim, J., Brooks, S., Cobbett, F., Dastoor, A., Dommergue, A., Ebinghaus, R., Ferrari, C. P., Gårdfeldt, K., Goodsite, M. E., Lean, D. R., Poulain, A. J.,

Scherz, C., Skov, H., Sommar, J., and Temme, C. (2008). A synthesis of atmospheric mercury depletion event chemistry linking atmosphere, snow and water *Atmospheric Chemistry and Physics* 8(6), 1445–1482.

[18] Nriagu, J. O., and Becker, C. (2003). Volcanic emissions of mercury to the atmosphere: Global and regional inventories. *Science of the Total Environment* 304(1–3), 3–12.

[19] Friedli, H. R., Arellano, A. F., Cinnirella, S., and Pirrone, N. (2009). Mercury emissions from global biomass burning: Spatial and temporal distribution. In N. Pirrone and R. Mason (Eds.), *Mercury fate and transport in the global atmosphere* (pp. 193–220). Springer, New York.

[20] Obrist, D., Conen, F., Vogt, R., Siegwolf, R., and Alewell, C. (2006). Estimation of Hg^0 exchange between ecosystems and the atmosphere using ^{222}Rn and Hg^0 concentration changes in the stable nocturnal boundary layer. *Atmospheric Environment* 40(5), 856–866.

[21] Li, Z. G., Feng, X., Li, P., Liang, L., Tang, S. L., Wang, S. F., Fu, X. W., Qiu, G. L., and Shang, L. H. (2010). Emissions of air-borne mercury from five municipal solid waste landfills in Guiyang and Wuhan, China. *Atmospheric Chemistry and Physics* 10(7), 3353–3364.

[22] Lindberg, S. E., Southworth, G. R., Bogle, M. A., Blasing, T. J., Owens, J., Roy, K., Zhang, H., Kuiken, T., Price, J., Reinhart, D., and Sfeir, H. (2005). Airborne emissions of mercury from municipal solid waste. I: New measurements from six operating landfills in Florida. *Journal of the Air & Waste Management Association* 55(7), 859–869.

[23] Lindberg, S. E., and Price, J. L. (1999). Airborne emissions of mercury from municipal landfill operations: A short-term measurement study in Florida. *Journal of the Air & Waste Management Association* 49(5), 520–532.

[24] Denmead, O. T. (2008). Approaches to measuring fluxes of methane and nitrous oxide between landscapes and the atmosphere. *Plant and Soil* 309(1–2), 5–24.

[25] Foken, T. (2008). *Micrometeorology*, Berlin, Heidelberg: Springer-Verlag.

[26] Friedli, H. R., Arellano, A. F., Cinnirella, S., and Pirrone, N. (2009). Initial estimates of mercury emissions to the atmosphere from global biomass burning. *Environmental Science & Technology* 43(10), 3507–3513.

[27] Stull, R. B. (1988). *An introduction to boundary layer meteorology*, Dordrecht, Boston, London: Kluwer Academic Publisher.

[28] Garratt, J. R. (1992). *The atmospheric boundary layer*, Cambridge, UK: Cambridge University Press.

[29] Raupach, M. R., Finnigan, J. J., and Brunet, Y. (1996). Coherent eddies in vegetation canopies—The mixing layer analogy. *Boundary-Layer Meteorology* 78, 351–382.

[30] Campbell, G. S., and Norman, J. M. (1998). *An introduction to environmental biophysics*, New York: Springer.

[31] Bowen, I. S. (1926). The ratio of heat losses by conduction and by evoporation from any water surface. *Physical Review* 27, 779–787.

[32] Schroeder, W. H., Munthe, J., and Lindqvist, O. (1989). Cycling of mercury between water, air and soil compartments of the environment. *Water Air and Soil Pollution* 48 (3–4), 337–347.

[33] Xiao, Z. F., Munthe, J., Schroeder, W. H., and Lindqvist, O. (1991). Vertical fluxes of volatile mercury over forest soil and lake surfaces in Sweden. *Tellus Series B-Chemical and Physical Meteorology* 43(3), 267–279.

[34] Carpi, A., and Lindberg, S. E. (1998). Application of a Teflon™ dynamic flux chamber for quantifying soil mercury flux: Tests and results over background soil. *Atmospheric Environment* 32(5), 873–882.

[35] Eckley, C. S., Gustin, M., Lin, C. J., Li, X., and Miller, M. B. (2010). The influence of dynamic chamber design and operating parameters on calculated surface-to-air mercury fluxes. *Atmospheric Environment* 44(2), 194–203.

[36] Graydon, J. A., St Louis, V. L., Lindberg, S. E., Hintelmann, H., and Krabbenhoft, D. P. (2006). Investigation of mercury exchange between forest canopy vegetation and the atmosphere using a new dynamic chamber. *Environmental Science & Technology*, 40(15), 4680–4688.

[37] Poissant, L., Pilote, M., Yumvihoze, E., and Lean, D. (2008). Mercury concentrations and foliage/atmosphere fluxes in a maple forest ecosystem in Quebec, Canada. *Journal of Geophysical Research-Atmospheres* 113, D10307, doi: 10.1029/2007jd009510.

[38] Zhang, H. H., Poissant, L., Xu, X., and Pilote, M. (2004). Explorative and innovative dynamic flux bag method development and testing for mercury air-vegetation gas exchange fluxes. *Atmospheric Environment* 38, 7481–7493.

[39] Fay, L., and Gustin, M. S. (2007). Investigation of mercury accumulation in cattails growing in constructed wetland mesocosms. *Wetlands* 27 (4), 1056–1065.

[40] Gillis, A., and Miller, D. R. (2000). Some potential errors in the measurement of mercury gas exchange at the soil surface using a dynamic flux chamber. *Science of the Total Environment* 260(1–3), 181–189.

[41] Gustin, M. S., Lindberg, S., Marsik, F., Casimir, A., Ebinghaus, R., Edwards, G., Hubble-Fitzgerald, C., Kemp, R., Kock, H., Leonard, T., London, J., Majewski, M., Montecinos, C., Owens, J., Pilote, M., Poissant, L., Rasmussen, P., Schaedlich, F., Schneeberger, D., Schroeder, W., Sommar, J., Turner, R., Vette, A., Wallschläger, D., Xiao, Z., and Zhang, H. (1999). Nevada STORMS project: Measurement of mercury emissions from naturally enriched surfaces. *Journal of Geophysical Research-Atmospheres* 104(D17), 21831–21844.

[42] Rinklebe, J., During, A., Overesch, M., Wennrich, R., Stark, H. J., Mothes, S., and Neue, H. U. (2009). Optimization of a simple field method to determine mercury volatilization from soils—Examples of 13 sites in floodplain ecosystems at the Elbe River (Germany). *Ecological Engineering*; 35(2), 319–328.

[43] Wallschläger, D., Turner, R. R., London, J., Ebinghaus, R., Kock, H. H., Sommar, J., and Xiao, Z. F. (1999). Factors affecting the measurement of mercury emissions from soils with flux chambers. *Journal of Geophysical Research-Atmospheres* 104(D17), 21859–21871.

[44] Livingston, G. P., and Hutchinson, G. L. (1995). Enclosure-based measurement of trace gas exchange: applications and sources of error. In P. A. Matson, R. C.

Harriss (Eds), *Biogenic trace gases: Measuring emissions from soil and water* (pp. 14–51). Oxford: Blackwell.

[45] Gårdfeldt, K., Feng, X. B., Sommar, J., and Lindqvist, O. (2001). Total gaseous mercury exchange between air and water at river and sea surfaces in Swedish coastal regions. *Atmospheric Environment* 35(17), 3027–3038.

[46] Kuiken, T. (2007). *Mercury air/surface exchange over terrestrial background surfaces of the eastern United States and its policy implications*. Ph.D. thesis, Tennessee Technological University, Cookeville, TN.

[47] Lee, X. H. (2000). Water vapor density effect on measurements of trace gas mixing ratio and flux with a massflow controller. *Journal of Geophysical Research-Atmospheres* 105(D14), 17807–17810.

[48] Kim, K. H., and Lindberg, S. E. (1995). Design and initial tests of a dynamic enclosure chamber for measurements of vapor-phase mercury fluxes over soils. *Water Air and Soil Pollution* 80(1–4), 1059–1068.

[49] Feng, X. B., Wang, S. F., Qiu, G. A., Hou, Y. M., and Tang, S. L. (2005). Total gaseous mercury emissions from soil in Guiyang, Guizhou, China. *Journal of Geophysical Research-Atmospheres* 110, D14306, doi: 10.1029/2004jd005643.

[50] Edwards, G. C., Rasmussen, P. E., Schroeder, W. H., Kemp, R. J., Dias, G. M., Fitzgerald-Hubble, C. R., Wong, E. K., Halfpenny-Mitchell, L., and Gustin, M. S. (2001). Sources of variability in mercury flux measurements. *Journal of Geophysical Research-Atmospheres* 106(D6), 5421–5435.

[51] Garcia-Sanchez, A., Contreras, F., Adams, M., and Santos, F. (2006). Atmospheric mercury emissions from polluted gold mining areas (Venezuela). *Environmental Geochemistry and Health* 28(6), 529–540.

[52] Wallschläger, D., Kock, H. H., Schroeder, W. H., Lindberg, S. E., Ebinghaus, R., and Wilken, R. D. (2002). Estimating gaseous mercury emissions from contaminated floodplain soils to the atmosphere with simple field measurement techniques. *Water Air and Soil Pollution* 135(1–4), 39–54.

[53] Bouchet, S., Tessier, E., Monperrus, M., Bridou, R., Clavier, J., Thouzeau, G., and Amouroux, D. (2011). Measurements of gaseous mercury exchanges at the sediment-water, water-atmosphere and sediment-atmosphere interfaces of a tidal environment (Arcachon Bay, France). *Journal of Environmental Monitoring* 13(5), 1351–1359.

[54] Ericksen, J. A., Gustin, M. S., Xin, M., Weisberg, P. J., and Fernandez, G. C. J. (2006). Air-soil exchange of mercury from background soils in the United States. *Science of The Total Environment* 366, 851–863.

[55] Engle, M. A., Gustin, M. S., and Zhang, H. (2001). Quantifying natural source mercury emissions from the Ivanhoe Mining District, north-central Nevada, USA. *Atmospheric Environment* 35(23), 3987–3997.

[56] Carpi, A., Frei, A., Cocris, D., McCloskey, R., Contreras, E., and Ferguson, K. (2007). Analytical artefacts produced by a polycarbonate chamber compared to a Teflon chamber for measuring surface mercury fluxes. *Analytical and Bioanalytical Chemistry* 388(2), 361–365.

[57] Eckley, C. S., and Branfireun, B. (2008). Gaseous mercury emissions from urban surfaces: Controls and spatiotemporal trends. *Applied Geochemistry* 23(3), 369–383.

[58] Choi, H. D., and Holsen, T. M. (2009). Gaseous mercury fluxes from the forest floor of the Adirondacks. *Environmental Pollution* 157(2), 592–600.
[59] Gao, F., Yates, S. R., Yates, M. V., Gan, J. Y., and Ernst, F. F. (1997). Design, fabrication, and application of a dynamic chamber for measuring gas emissions from soil. *Environmental Science & Technology* 31(1), 148–153.
[60] Zhang, H., Lindberg, S. E., Barnett, M. O., Vette, A. F., and Gustin, M. S. (2002). Dynamic flux chamber measurement of gaseous mercury emission fluxes over soils. Part 1: Simulation of gaseous mercury emissions from soils using a two-resistance exchange interface model. *Atmospheric Environment* 36(5), 835–846.
[61] Lindberg, S. E., Zhang, H., Vette, A. F., Gustin, M. S., Barnett, M. O., and Kuiken, T. (2002). Dynamic flux chamber measurement of gaseous mercury emission fluxes over soils: Part 2—Effect of flushing flow rate and verification of a two-resistance exchange interface simulation model. *Atmospheric Environment* 36(5), 847–859.
[62] Engle, M. A., Gustin, M. S., Goff, F., Counce, D. A., Janik, C. J., Bergfeld, D., Rytuba, J. J. (2006). Atmospheric mercury emissions from substrates and fumaroles associated with three hydrothermal systems in the western United States. *Journal of Geophysical Research-Atmospheres* 111, D17304, 10.1029/2005jd006563.
[63] Lin, C.-J., Zhu, W., Li, X., Feng, X., Sommar, J., and Shang, L. (2012). Novel dynamic flux chamber for measuring air-surface exchange of Hg^0 from soils. *Environmental Science & Technology* 46(16), 8910–8920.
[64] Böhme, F., Rinklebe, J., Stark, H. J., Wennrich, R., Mothes, S., and Neue, H. U. (2005). A simple field method to determine mercury volatilization from soils. *Environmental Science and Pollution Research* 12(3), 133–135.
[65] Johnson, D. W., Benesch, J. A., Gustin, M. S., Schorran, D. S., Lindberg, S. E., and Coleman, J. S. (2003). Experimental evidence against diffusion control of Hg evasion from soils. *Science of the Total Environment* 304(1–3), 175–184.
[66] Kyllonen, K., Hakola, H., Hellen, H., Korhonen, M., and Verta, M. (2012). Atmospheric mercury fluxes in a southern boreal forest and wetland. *Water, Air and Soil Pollution* 223, 1171–1182.
[67] Moore, C. W., Castro, M. S., and Brooks, S. B. (2011). A simple and accurate method to measure total gaseous mercury concentrations in unsaturated soils. *Water Air and Soil Pollution* 218(1–4), 3–9.
[68] Sigler, J. M., and Lee, X. (2006). Gaseous mercury in background forest soil in the northeastern United States. *Journal of Geophysical Research-Biogeosciences* 111, G02007, doi: 10.1029/2005jg000106.
[69] Dommergue, A., Ferrari, C. P., and Boutron, C. F. (2003). First investigation of an original device dedicated to the determination of gaseous mercury in interstitial air in snow. *Analytical and Bioanalytical Chemistry* 375(1), 106–111.
[70] de Jong, E., and Schappert, H. J. V. (1972). Calculation of soil respiration and activity from CO_2 profiles in the soil. *Soil Science* 113, 328–333.
[71] Fang, C., and Moncrieff, J. B. (1998). Simple and fast technique to measure CO_2 profiles in soil. *Soil Biology & Biochemistry* 30(14), 2107–2112.

[72] Di Francesco, F., Ferrara, R., and Mazzolai, B. (1998). Two ways of using a chamber for mercury flux—A simple mathematical approach. *Science of the Total Environment* 213(1–3), 33–41.
[73] Dommergue, A., Ferrari, C. P., Gauchard, P.-A., Boutron, C. F., Poissant, L., Pilote, M., Jitaru, P., and Adams, F. C. (2003). The fate of mercury species in a sub-arctic snowpack during snowmelt. *Geophysical Research Letters* 30, 1621.
[74] Edner, H., and Svanberg, S. (1991). LIDAR measurements of atmospheric mercury. *Water Air and Soil Pollution* 56, 131–139.
[75] Fu, X., Feng, X., and Zhang, H. (2011). Atmospheric total gaseous concentration in Guiyang: Measurement intercalibration with Lumex RA-915AM and Tekran 2537A. *Chinese Journal of Ecology* 30(5), 939–943.
[76] Faïn, X., Moosmuller, H., and Obrist, D. (2010). Toward real-time measurement of atmospheric mercury concentrations using cavity ring-down spectroscopy. *Atmospheric Chemistry and Physics* 10(6), 2879–2892.
[77] Bauer, D., Campuzano-Jost, P., and Hynes, A. J. (2002). Rapid, ultra-sensitive detection of gas phase elemental mercury under atmospheric conditions using sequential two-photon laser induced fluorescence. *Journal of Environmental Monitoring* 4(3), 339–343.
[78] Aldén, M., Edner, H., and Svanberg, S. (1982). Remote measurements of atmospheric mercury using differential absorption LIDAR. *Optics Letters* 7(5), 221–223.
[79] Edner, H., Faris, G. W., Sunesson, A., and Svanberg, S. (1989). Atmospheric atomic mercury monitoring using differential absorption LIDAR techniques. *Applied Optics* 28(5), 921–930.
[80] Guan, Z. G., Lundin, P., Mei, L., Somesfalean, G., and Svanberg, S. (2010). Vertical LIDAR sounding of atomic mercury and nitric oxide in a major Chinese city. *Applied Physics B—Lasers and Optics* 101(1–2), 465–470.
[81] Sjöholm, M., Weibring, P., Edner, H., and Svanberg, S. (2004). Atomic mercury flux monitoring using an optical parametric oscillator based LIDAR system. *Optics Express* 12(4), 551–556.
[82] Grönlund, R., Sjöholm, M., Weibring, P., Edner, H., and Svanberg, S. (2005). Elemental mercury emissions from chlor-alkali plants measured by LIDAR techniques. *Atmospheric Environment* 39(39), 7474–7480.
[83] Thoma, E. D., Secrest, C., Hall, E. S., Jones, D. L., Shores, R. C., Modrak, M., Hashmonay, R., and Norwood, P. (2009). Measurement of total site mercury emissions from a chlor-alkali plant using ultraviolet differential optical absorption spectroscopy and cell room roof-vent monitoring. *Atmospheric Environment* 43(3), 753–757.
[84] Nayuki, T., Marumoto, K., Fujii, T., Fukuchi, T., Nemoto, K., Shirakawa, A., and Ueda, K. (2004). Development of a differential-absorption LIDAR system for measurement of atmospheric atomic mercury by use of the third harmonic of an LDS-dye laser. *Applied Optics* 43(35), 6487–6491.
[85] Bennett, M., Edner, H., Grönlund, R., Sjöholm, M., Svanberg, S., and Ferrara, R. (2006). Joint application of Doppler LIDAR and differential absorption LIDAR to estimate the atomic mercury flux from a chlor-alkali plant. *Atmospheric Environment* 40(4), 664–673.

[86] Kaimal, J. C., and Finnigan, J. J. (1994). *Atmospheric boundary layer flows*. New York, Oxford: Oxford University Press.

[87] Monin, A. S., and Obukhov, A. M. O. (1958). Fundamentale Gesetzmaßigkeiten der turbulenten Vermischung in der bodennahen Schicht der Atmosphere. In H. Göring (Ed.), *Sammelband zur statistischen Theorie der Turbulenz* (pp. 199–226). Berlin: Deutsche Akademie der Wissenschaften zu Berlin.

[88] Vesala, T., Kljun, N., Rannik, Ü., Rinne, J., Sogachev, A., Markkanen, T., Sabelfeld, K., Foken, T., and Leclerc, M. Y. (2008). Flux and concentration footprint modelling: State of the art. *Environmental Pollution* 152(3), 653–666.

[89] Gash, J. H. C. (1986). A note on estimating the effect of a limited fetch on micrometeorological evaporation measurements. *Boundary-Layer Meteorology* 35(4), 409–413.

[90] Schuepp, P. H., Leclerc, M. Y., MacPherson, J. I., and Desjardins, R. L. (1990). Footprint prediction of scalar fluxes from analytical solutions of the diffusion equation. *Boundary-Layer Meteorology* 50(1–4), 355–373.

[91] Bash, J. O., and Miller, D. R. (2008). A relaxed eddy accumulation system for measuring surface fluxes of total gaseous mercury. *Journal of Atmospheric and Oceanic Technology* 25(2), 244–257.

[92] Olofsson, M., Sommar, J., Ljungström, E., and Andersson, M. (2005). Application of relaxed eddy accumulation technique to quantify Hg^0 fluxes over modified soil surfaces. *Water Air and Soil Pollution* 167, 331–354.

[93] Lindberg, S. E., Kim, K. H., Meyers, T. P., and Owens, J. G. (1995). Micrometeorological gradient approach for quantifying air-surface exchange of mercury-vapor-tests over contaminated soils. *Environmental Science & Technology* 29(1), 126–135.

[94] Fritsche, J., Wohlfahrt, G., Ammann, C., Zeeman, M., Hammerle, A., Obrist, D., and Alewell, C. (2008). Summertime elemental mercury exchange of temperate grasslands on an ecosystem-scale. *Atmospheric Chemistry and Physics* 8(24), 7709–7722.

[95] Olofsson, M., Ek-Olaussson, B., Ljungström, E., and Langer, S. (2003). Flux of organic compounds from grass measured by relaxed eddy accumulation technique. *Journal of Environmental Monitoring* 5, 963–970.

[96] Wong, E. K. (1999). *Development and assessment of measurement approaches and a footprint model for trace gas emissions*. MSc. Thesis, University of Guelph, Guelph, Ontario, Canada.

[97] Bash, J. O., and Miller, D. R. (2009). Growing season total gaseous mercury (TGM). Flux measurements over an *Acer rubrum* L. stand. *Atmospheric Environment* 43(37), 5953–5961.

[98] Amiro, B. D. (1998). Footprint climatologies for evapotranspiration in a boreal catchment. *Agricultural and Forest Meteorology* 90(3), 195–201.

[99] Kljun, N., Calanca, P., Rotachhi, M. W., and Schmid, H. P. (2004). A simple parameterisation for flux footprint predictions. *Boundary-Layer Meteorology* 112(3), 503–523.

[100] Kljun, N. A simple parameterisation for flux footprint predictions. Retrieved from http://footprint.kljun.net/ [accessed May 15, 2013].

[101] Wilczak, J. M., Oncley, S. P., and Stage, S. A. (2001). Sonic anemometer tilt correction algorithms. *Boundary-Layer Meteorology* 99(1), 127–150.

[102] Bauer, D., Swartzendruber, P. C., and Hynes, A. J. (2010). Deployment of a compact sequential 2 Photon LIF detection system for gaseous elemental mercury at ambient levels. *Geochimica Et Cosmochimica Acta* 74(12), A60–A60.

[103] Hynes, A. J., Bauer, D., Swartzendruber, P., Evenhart, S., Tuatum-Ernest, C., and Ter Schure, A. Measurements of gaseous elemental mercury and reactive gaseous mercury using laser-based spectroscopic techniques. *In Proceedings of 10th International Conference on Mercury as a Global Pollutant, Halifax, Canada, 2011* (available free online, www.mercury2011.org/program_and_abstracts).

[104] Pierce, A., Faïn, X., Obrist, D., and Moosmüller, H. Atmospheric mercury concentration measurements using cavity ring-down spectroscopy. In *Proceedings of 10th International Conference on Mercury as a Global Pollutant, Halifax, Canada, 2011* (available free online, www.mercury2011.org/program_and_abstracts).

[105] Desjardins, R. L., Buckley, D., and St Amour, G. (1984). Eddy flux measurements of CO_2 above corn using a microcomputer system. *Agricultural and Forest Meteorology* 32, 257–265

[106] Businger, J. A., and Oncley, S. P. (1990). Flux Measurement with Conditional Sampling. *Journal of Atmospheric and Oceanic Technology* 7(2), 349–352.

[107] Baker, J. M., Norman, J. M., and Bland, W. L. (1992). Field-scale application of flux measurement by conditional sampling. *Agricultural and Forest Meteorology* 62(1–2), 31–52.

[108] Katul, G. G., Finkelstein, P. L., Clarke, J. F., and Ellestad, T. G. (1996). An investigation of the conditional sampling method used to estimate fluxes of active, reactive, and passive scalars. *Journal of Applied Meteorology* 35(10), 1835–1845.

[109] Milne, R., Mennim, A., and Hargreaves, K. (2001). The value of the beta coefficient in the relaxed eddy accumulation method in terms of fourth-order moments. *Boundary-Layer Meteorology* 101(3), 359–373.

[110] Ammann, C., and Meixner, F. X. (2002). Stability dependence of the relaxed eddy accumulation coefficient for various scalar quantities. *Journal of Geophysical Research-Atmospheres* 107(D7–D8), art. no. 4071.

[111] Beverland, I. J., Oneill, D. H., Scott, S. L., and Moncrieff, J. B. (1996). Design, construction and operation of flux measurement systems using the conditional sampling technique. *Atmospheric Environment* 30(18), 3209–3220.

[112] Bowling, D. R., Delany, A. C., Turnipseed, A. A., Baldocchi, D. D., and Monson, R. K. (1999). Modification of the relaxed eddy accumulation technique to maximize measured scalar mixing ratio differences in updrafts and downdrafts. *Journal of Geophysical Research-Atmospheres* 104(D8), 9121–9133.

[113] Oncley, S. P., Delany, A. C., Horst, T. W., and Tans, P. P. (1993). Verification of Flux Measurement Using Relaxed Eddy Accumulation. *Atmospheric Environment Part a-General Topics* 27(15), 2417–2426.

[114] Grönholm, T., Haapanala, S., Launiainen, S., Rinne, J., Vesala, T., and Rannik, Ü. (2008). The dependence of the beta coefficient of REA system with dynamic deadband on atmospheric conditions. *Environmental Pollution* 152(3), 597–603.

[115] Cobos, D. R., Baker, J. M., and Nater, E. A. (2002). Conditional sampling for measuring mercury vapor fluxes. *Atmospheric Environment* 36(27), 4309–4321.

[116] Skov, H., Brooks, S. B., Goodsite, M. E., Lindberg, S. E., Meyers, T. P., Landis, M. S., Larsen, M. R. B., Jensen, B., McConville, G., and Christensen, J. (2006). Fluxes of reactive gaseous mercury measured with a newly developed method using relaxed eddy accumulation. *Atmospheric Environment* 40(28), 5452–5463.

[117] Bowling, D. R., Turnipseed, A. A., Delany, A. C., Baldocchi, D. D., Greenberg, J. P., and Monson, R. K. (1998). The use of relaxed eddy accumulation to measure biosphere- atmosphere exchange of isoprene and of her biological trace gases. *Oecologia* 116(3), 306–315.

[118] Nie, D., Kleindienst, T. E., Arnts, R. R., and Sickles, J. E. (1995). The design and testing of a relaxed eddy accumulation system. *Journal of Geophysical Research-Atmospheres* 100(D6), 11415–11423.

[119] Christensen, C. S., Hummelshøj, P., Jensen, N. O., Larsen, B., Lohse, C., Pilegaard, K., and Skov, H. (2000). Determination of the terpene flux from orange species and Norway spruce by relaxed eddy accumulation. *Atmospheric Environment* 34(19), 3057–3067.

[120] Gaman, A., Rannik, Ü., Aalto, P., Pohja, T., Siivola, E., Kulmala, M., and Vesala, T. (2004). Relaxed eddy accumulation system for size-resolved aerosol particle flux measurements. *Journal of Atmospheric and Oceanic Technology* 21(6), 933–943.

[121] Ammann, C. (1998). *On the applicability of relaxed eddy accumulation and common methods for measuring trace gas surface fluxes*. PhD thesis, Swiss Federal Institute of Technology (ETH), Zürich, Switzerland.

[122] Poissant, L., Amyot, M., Pilote, M., and Lean, D. (2000). Mercury water-air exchange over the Upper St. Lawrence River and Lake Ontario. *Environmental Science & Technology* 34(15), 3069–3078.

[123] Sommar, J., Zhu, W., Shang, L., Feng, X., and Lin, C.-J. (2012). *Vertical fluxes of mercury vapour (Hg^0).measured by a relaxed eddy accumulation (REA). System coupled to a cold vapour atomic fluorescence spectrophotometric (CVAFS). Analyser. Tellus B.* Manuscript submitted for publication.

[124] Landis, M. S., Stevens, R. K., Schaedlich, F., and Prestbo, E. M. (2002). Development and characterization of an annular denuder methodology for the measurement of divalent inorganic reactive gaseous mercury in ambient air. *Environmental Science & Technology* 36(13), 3000–3009.

[125] Businger, J. A., Wyngaard, J. C., Izumi, Y., and Bradley, E. F. (1971). Flux-profile relationships in the atmospheric surface layer. *Journal of Atmospheric Science* 28, 181–189.

[126] Dyer, A. J. (1974). A review of flux-profile-relationships. *Boundary-Layer Meteorology* 7, 363–372.

[127] Arya, S. P. (2001). *Introduction to micrometeorology*, San Diego: Academic Press.

[128] Meyers, T. P., Hall, M. E., Lindberg, S. E., and Kim, K. (1996). Use of the modified Bowen-ratio technique to measure fluxes of trace gases. *Atmospheric Environment* 30(19), 3321–3329.

[129] Kim, K. H., Lindberg, S. E., and Meyers, T. P. (1995). Micrometeorological measurements of mercury-vapor fluxes over background forest soils in eastern tennessee. *Atmospheric Environment* 29(2), 267–282.

[130] Lindberg, S. E., Meyers, T. P., and Munthe, J. (1995). Evasion of mercury vapor from tee surface of a recently limed acid forest lake in Sweden. *Water Air and Soil Pollution* 85(2), 725–730.

[131] Lindberg, S. E., Hanson, P. J., Meyers, T. P., and Kim, K. H. (1998). Air/surface exchange of mercury vapor over forests—The need for a reassessment of continental biogenic emissions. *Atmospheric Environment* 32(5), 895–908.

[132] Lindberg, S. E., Dong, W. J., and Meyers, T. (2002). Transpiration of gaseous elemental mercury through vegetation in a subtropical wetland in Florida. *Atmospheric Environment* 36(33), 5207–5219.

[133] Lindberg, S. E., and Meyers, T. P. (2001). Development of an automated micrometeorological method for measuring the emission of mercury vapor from wetland vegetation. *Wetlands Ecology and Management* 9(4), 333–348.

[134] Poissant, L., Pilote, M., and Casimir, A. (1999). Mercury flux measurements in a naturally enriched area: Correlation with environmental conditions during the Nevada Study and Tests of the Release of Mercury From Soils (STORMS). *Journal of Geophysical Research-Atmospheres* 104(D17), 21845–21857.

[135] Gustin, M. S., Coolbaugh, M. F., Engle, M. A., Fitzgerald, B. C., Keislar, R. E., Lindberg, S. E., Nacht, D. M., Quashnick, J., Rytuba, J. J., Sladek, C., Zhang, H., and Zehner, R. E. (2003). Atmospheric mercury emissions from mine wastes and surrounding geologically enriched terrains. *Environmental Geology* 43(3), 339–351.

[136] Fritsche, J., Obrist, D., Zeeman, M. J., Conen, F., Eugster, W., and Alewell, C. (2008). Elemental mercury fluxes over a sub-alpine grassland determined with two micrometeorological methods. *Atmospheric Environment* 42(13), 2922–2933.

[137] Edwards, G. C., Rasmussen, P. E., Schroeder, W. H., Wallace, D. M., Halfpenny-Mitchell, L., Dias, G. M., Kemp, R. J., and Ausma, S. (2005). Development and evaluation of a sampling system to determine gaseous Mercury fluxes using an aerodynamic micrometeorological gradient method. *Journal of Geophysical Research-Atmospheres* 110, D10306, doi: 10.1029/2004jd005187.

[138] Foken, T., and Wichura, B. (1996). Tools for quality assessment of surface-based flux measurements. *Agricultural and Forest Meteorology* 78(1–2), 83–105.

[139] Lindberg, S. E., and Stratton, W. J. (1998). Atmospheric mercury speciation: Concentrations and behavior of reactive gaseous mercury in ambient air. *Environmental Science & Technology* 32(1), 49–57.

[140] Poissant, L., Pilote, M., Xu, X. H., Zhang, H. H., and Beauvais, C. (2004). Atmospheric mercury speciation and deposition in the bay St. Francois wetlands. *Journal of Geophysical Research* 109, D11301, doi: 10.1029/2003JD004364.

[141] Twine, T. E., Kustas, W. P., Norman, J. M., Cook, D. R., Houser, P. R., Meyers, T. P., Prueger, J. H., Starks, P. J., and Wesely, M. L. (2000). Correcting eddy-covariance flux underestimates over a grassland. *Agricultural and Forest Meteorology* 103(3), 279–300.

[142] Lee, X., Benoit, G., and Hu, X. Z. (2000). Total gaseous mercury concentration and flux over a coastal saltmarsh vegetation in Connecticut, USA. *Atmospheric Environment* 34(24), 4205–4213.

[143] Kim, K. H., Kim, M. Y., Kim, J., and Lee, G. (2002). The concentrations and fluxes of total gaseous mercury in a western coastal area of Korea during late March 2001. *Atmospheric Environment* 36(21), 3413–3427.

[144] Kim, K. H., Kim, M. Y., Kim, J., and Lee, G. (2003). Effects of changes in environmental conditions on atmospheric mercury exchange: Comparative analysis from a rice paddy field during the two spring periods of 2001 and 2002. *Journal of Geophysical Research-Atmospheres* 108, 4607, doi: 10.1029/2003jd003375.

[145] Kim, K. H., Kim, M. Y., and Lee, G. (2001). The soil-air exchange characteristics of total gaseous mercury from a large-scale municipal landfill area. *Atmospheric Environment* 35(20), 3475–3493.

[146] Nguyen, H. T., Kim, K. H., Kim, M. Y., and Shon, Z. H. (2008). Exchange pattern of gaseous elemental mercury in an active urban landfill facility. *Chemosphere* 70(5), 821–832.

[147] Kim, K. H., and Kim, M. Y. (1999). The exchange of gaseous mercury across soil-air interface in a residential area of Seoul, Korea. *Atmospheric Environment* 33(19), 3153–3165.

[148] Goodrow, S. M., Miskewitz, R., Hires, R. I., Eisenreich, S. J., Douglas, W. S., and Reinfelder, J. R. (2005). Mercury emissions from cement-stabilized dredged material. *Environmental Science & Technology* 39(21), 8185–8190.

[149] Smith, L. M., and Reinfelder, J. R. (2009). Mercury volatilization from salt marsh sediments. *Journal of Geophysical Research* 114, G00C09, doi: 10.1029/2009jg000979.

[150] Majewski, M., Desjardins, R., Rochette, P., Pattey, E., Seiber, J., and Glotfelty, D. (1993). Field Comparison of an Eddy Accumulation and an Aerodynamic-Gradient System for Measuring Pesticide Volatilization Fluxes. *Environmental Science & Technology* 27(1), 121–128.

[151] Marsik, F. J., Keeler, G. J., Lindberg, S. E., and Zhang, H. (2005). Air-surface exchange of gaseous mercury over a mixed sawgrass-cattail stand within the Florida everglades. *Environmental Science and Technology* 39(13), 4739–4746.

[152] Cobbett, F. D., Steffen, A., Lawson, G., and Van Heyst, B. J. (2007). GEM fluxes and atmospheric mercury concentrations (GEM, RGM and Hgp) in the Canadian Arctic at Alert, Nunavut, Canada (February–June 2005). *Atmospheric Environment* 41(31), 6527–6543.

[153] Cobbett, F. D., and Van Heyst, B. J. (2007). Measurements of GEM fluxes and atmospheric mercury concentrations (GEM, RGM and Hg-P) from an agricultural field amended with biosolids in Southern Ont., Canada (October 2004–November 2004). *Atmospheric Environment* 41(11), 2270–2282.

[154] Baya, A. P., and Van Heyst, B. (2010). Assessing the trends and effects of environmental parameters on the behaviour of mercury in the lower atmosphere

over cropped land over four seasons. *Atmospheric Chemistry and Physics* 10(17), 8617–8628.

[155] Steen, A. O., Berg, T., Dastoor, A. P., Durnford, D. A., Hole, L. R., and Pfaffhuber, K. A. (2009). Dynamic exchange of gaseous elemental mercury during polar night and day. *Atmospheric Environment* 43(35), 5604–5610.

[156] Schroeder, W. H., Anlauf, K. G., Barrie, L. A., Lu, J. Y., Steffen, A., Schneeberger, D. R., and Berg, T. (1998). Arctic springtime depletion of mercury. *Nature* 394(6691), 331–332.

[157] Converse, A. D., Riscassi, A. L., and Scanlon, T. M. (2010). Seasonal variability in gaseous mercury fluxes measured in a high-elevation meadow. *Atmospheric Environment* 44(18), 2176–2185.

[158] Dörr, H., and Münnich, K. O. (1990). ^{222}Rn flux and soil air concentration profiles in West Germany: Soil ^{222}Rn as tracer for gas transport in the unsaturated soil zone. *Tellus Series B—Chemical and Physical Meteorology* 42, 20–28.

[159] Andersson, M. E., Gårdfeldt, K., Wängberg, I., and Strömberg, D. (2008). Determination of Henry's law constant for elemental mercury. *Chemosphere* 73(4), 587–592.

[160] Sanemasa, I. (1974). The solubility of elemental mercury vapour in water. *Bulletin of the Chemical Society of Japan* 48(6), 1795–1798.

[161] Lewis, W. K., and Whitman, W. G. (1924). Principles of gas absorption. *Industrial and Engineering Chemistry* 16, 1215–1220.

[162] Fitzgerald, W. F., Gill, G. A., and Kim, J. P. (1984). An equatorial Pacific-Ocean source of atmospheric mercury. *Science* 224(4649), 597–599.

[163] Kim, J. P., and Fitzgerald, W. F. (1986). Sea-air partitioning of mercury in the equatorial Pacific-Ocean. *Science* 231(4742), 1131–1133.

[164] Othmer, D. F., and Thakar, M. S. (1953). Correlating diffusion coefficients in liquids. *Industrial and Engineering Chemistry* 45(3), 589–593.

[165] Wängberg, I., Schmolke, S., Schager, P., Munthe, J., Ebinghaus, R., and Iverfeldt, Å. (2001). Estimates of air-sea exchange of mercury in the Baltic Sea. *Atmospheric Environment* 35(32), 5477–5484.

[166] Gårdfeldt, K., Sommar, J., Ferrara, R., Ceccarini, C., Lanzillotta, E., Munthe, J., Wängberg, I., Lindqvist, O., Pirrone, N., Sprovieri, F., Pesenti, E., and Strömberg, D. (2003). Evasion of mercury from coastal and open waters of the Atlantic Ocean and the Mediterranean Sea. *Atmospheric Environment* 37, S73–S84.

[167] Narukawa, M., Sakata, M., Marumoto, K., and Asakura, K. (2006). Air-sea exchange of mercury in Tokyo Bay. *Journal of Oceanography* 62(3), 249–257.

[168] Andersson, M. E., Gårdfeldt, K., Wängberg, I., Sprovieri, F., Pirrone, N., and Lindqvist, O. (2007). Seasonal and daily variation of mercury evasion at coastal and off shore sites from the Mediterranean Sea. *Marine Chemistry* 104(3–4), 214–226.

[169] Reid, R. C., Prausnitz, J. M., and Poling, B. E. (1997). *The properties of gases and liquids*. New York: McGraw-Hill.

[170] Thibodeaux, J. L. (1996). *Environmental chemodynamics: Movement of chemicals in air, water, and soil*. John Wiley & Sons, Inc, New York.

[171] Costa, M., and Liss, P. S. (1999). Photoreduction of mercury in sea water and its possible implications for Hg^0 air-sea fluxes. *Marine Chemistry* 68(1–2), 87–95.

[172] Strode, S. A., Jaegle, L., Selin, N. E., Jacob, D. J., Park, R. J., Yantosca, R. M., Mason, R. P., and Slemr, F. (2007). Air-sea exchange in the global mercury cycle. *Global Biogeochemical Cycles* 21 (1) (GB1017, doi: 10.1029/2006GB002766).

[173] Sørensen, A. L., Sunderland, E. M., Holmes, C. D., Jacob, D. J., Yantosca, R. M., Skov, H., Christensen, J. H., Strode, S. A., and Mason, R. P. (2010). An improved global model for air-sea exchange of mercury: High concentrations over the north Atlantic. *Environmental Science & Technology* 44(22), 8574–8580.

[174] Schroeder, W., Lindqvist, O., Munthe, J., and Xiao, Z. F. (1992). Volatilization of mercury from lake surfaces. *Science of the Total Environment* 125, 47–66.

[175] Liss, P. S., and Slater, P. G. (1974). Flux of gases across the air-sea interface. *Nature* 247(5438), 181–184.

[176] Kuss, J., Holzmann, J., and Ludwig, R. (2009). An elemental mercury diffusion coefficient for natural waters determined by molecular dynamics simulation. *Environmental Science & Technology* 43(9), 3183–3186.

[177] Jähne, B., Heinz, G., and Dietrich, W. (1987). Measurement of the diffusion coefficients of sparingly soluble gases in water. *Journal of Geophysical Research* 92(C10), 10767–10776.

[178] Asher, W., and Wanninkhof, R. (1998). Transient tracers and air-sea gas transfer. *Journal of Geophysical Research-Oceans* 103(C8), 15939–15958.

[179] Baeyens, W., Leermakers, M., Dedeurwaerder, H., and Lansens, P. (1991). Modelization of the mercury fluxes at the air-sea interface. *Water Air and Soil Pollution* 56, 731–744.

[180] Baeyens, W., and Leermakers, M. (1998). Elemental mercury concentrations and formation rates in the Scheldt estuary and the North Sea. *Marine Chemistry* 60(3–4), 257–266.

[181] Liss, P. S., and Merlivat, L. (1986). Air-sea gas exchange rates: Introduction and synthesis. In P. Buat-Ménard (Ed.), *The role of air-sea gas exchange in geochemical cycling* (pp. 113–127). Dordrecht, The Netherlands: D. Reidel.

[182] Wanninkhof, R. (1992). Relationship between wind speed and gas exchange over the ocean. *Journal of Geophysical Research-Atmospheres* 97, 7373–7382.

[183] Nightingale, P. D., Malin, G., Law, C. S., Watson, A. J., Liss, P. S., Liddicoat, M. I., Boutin, J., and Upstill-Goddard, R. C. (2000). In situ evaluation of air-sea gas exchange parameterizations using novel conservative and volatile tracers. *Global Biogeochemical Cycles* 14(1), 373–387.

[184] Wanninkhof, R., Ledwell, J. R., and Broecker, W. S. (1985). Gas exchange-wind speed relationship measured with sulfur hexafluoride on a lake. *Science* 227, 1224–1226.

[185] Lindberg, S. E., Vette, A. F., Miles, C., and Schaedlich, F. (2000). Mercury speciation in natural waters: Measurement of dissolved gaseous mercury with a field analyzer. *Biogeochemistry* 48(2), 237–259.

[186] O'Driscoll, N. J., Siciliano, S. D., and Lean, D. R. S. (2003). Continuous analysis of dissolved gaseous mercury in freshwater lakes. *The Science of The Total Environment* 304(1–3), 285–294.

[187] Amyot, M., Lean, D. R., Poissant, L., and Doyon, M.-R. (2000). Distribution and transformation of elemental mercury in the St. Lawrence River and Lake

Ontario. *Canadian Journal of Fisheries and Aquatic Sciences* 57(3), 155–164.

[188] Amyot, M., Auclair, J. C., and Poissant, L. (2001). In situ high temporal resolution analysis of elemental mercury in natural waters. *Analytica Chimica Acta* 447(1–2), 153–159.

[189] Gårdfeldt, K., Horvat, M., Sommar, J., Kotnik, J., Fajon, V., Wängberg, I., and Lindqvist, O. (2002). Comparison of procedures for measurements of dissolved gaseous mercury in seawater performed on a Mediterranean cruise. *Analytical and Bioanalytical Chemistry* 374(6), 1002–1008.

[190] Kuss, J., and Schneider, B. (2007). Variability of the gaseous elemental mercury sea-air flux of the Baltic Sea. *Environmental Science & Technology* 41(23), 8018–8023.

[191] Andersson, M. E., Gårdfeldt, K., and Wängberg, I. (2008). A description of an automatic continuous equilibrium system for the measurement of dissolved gaseous mercury. *Analytical and Bioanalytical Chemistry* 391(6), 2277–2282.

[192] Andersson, M. E., Sommar, J., Gårdfeldt, K., and Lindqvist, O. (2008). Enhanced concentrations of dissolved gaseous mercury in the surface waters of the Arctic Ocean. *Marine Chemistry* 110(3–4), 190–194.

[193] Kuss, J., Zulicke, C., Pohl, C., and Schneider, B. (2011). Atlantic mercury emission determined from continuous analysis of the elemental mercury sea-air concentration difference within transects between 50 degrees N and 50 degrees S. *Global Biogeochemical Cycles* 25, doi: 10.1029/2010GB003998.

[194] Marks, R. (2002). Preliminary investigation of the mercury saturation in the Baltic Sea winter surface water. *Science of the Total Environment* 299(1–3), 227–236.

[195] Gustin, M. S., Lindberg, S. E., and Allan, M. A. (1999). Special Section: Constraining mercury emissions from naturally enriched surfaces: Assessment of methods and controlling parameters (mercury flux)—Preface. *Journal of Geophysical Research-Atmospheres* 104(D17), 21829–21830.

[196] Magarelli, G., and Fostier, A. H. (2005). Influence of deforestation on the mercury air/soil exchange in the Negro River Basin, Amazon. *Atmospheric Environment* 39, 7518–7528.

[197] Kuiken, T., Gustin, M., Zhang, H., Lindberg, S., and Sedinger, B. (2008). Mercury emission from terrestrial background surfaces in the eastern USA. II: Air/surface exchange of mercury within forests from South Carolina to New England. *Applied Geochemistry* 23(3), 356–368.

[198] Kuiken, T., Zhang, H., Gustin, M., and Lindberg, S. (2008). Mercury emission from terrestrial background surfaces in the eastern USA. Part I: Air/surface exchange of mercury within a southeastern deciduous forest (Tennessee), over one year. *Applied Geochemistry* 23(3), 345–355.

[199] Poissant, L., and Casimir, A. (1998). Water-air and soil-air exchange rate of total gaseous mercury measured at background sites. *Atmospheric Environment* 32(5), 883–893.

[200] Carpi, A., and Lindberg, S. E. (1997). Sunlight-mediated emission of elemental mercury from soil amended with municipal sewage sludge. *Environmental Science & Technology* 31(7), 2085–2091.

[201] Corbett-Hains, H., Walters, N. E., and van Heyst, B. J. (2012). Evaluating the effects of sub-zero temperature cycling on mercury flux from soils. *Atmospheric Environment* 63, doi: 10.1016/j.atmosenv.2012.09.047.

[202] Sholupov, S., Pogarev, S., Ryzhov, V., Mashyanov, N., and Stroganov, A. (2004). Zeeman atomic absorption spectrometer RA-915+for direct determination of mercury in air and complex matrix samples. *Fuel Processing Technology* 85(6–7), 473–485.

[203] Edner, H., Ragnarson, P., and Wallinder, E. (1995). Industrial emission control using LIDAR techniques. *Environmental Science & Technology* 29(2), 330–337.

[204] Wängberg, I., Edner, H., Ferrara, R., Lanzillotta, E., Munthe, J., Sommar, J., Sjöholm, M., Svanberg, S., and Weibring, P. (2003). Atmospheric mercury near a chlor-alkali plant in Sweden. *Science of the Total Environment* 304(1–3), 29–41.

[205] Ferrara, R., Maserti, B. E., Andersson, M., Edner, H., Ragnarson, P., Svanberg, S., and Hernandez, A. (1998). Atmospheric mercury concentrations and fluxes in the Almadén district (Spain). *Atmospheric Environment* 32(22), 3897–3904.

[206] Ferrara, R., Maserti, B. E., Andersson, M., Edner, H., Ragnarson, P., and Svanberg, S. (1997). Mercury degassing rate from mineralized areas in the Mediterranean basin. *Water Air and Soil Pollution* 93(1–4), 59–66.

[207] Ferrara, R., Mazzolai, B., Edner, H., Svanberg, S., and Wallinder, E. (1998). Atmospheric mercury sources in the Mt. Amiata area, Italy. *Science of the Total Environment* 213(1–3), 13–23.

[208] Ferrara, R., Maserti, B. E., Edner, H., Ragnarson, P., Svanberg, S., and Wallinder, E. (1992). Mercury emissions into the atmosphere from a chloralkali complex measured with the LIDAR technique. *Atmospheric Environment Part A—General Topics* 26(7), 1253–1258.

[209] Grönlund, R., Edner, H., Svanberg, S., Kotnik, J., and Horvat, M. (2005). Mercury emissions from the Idrija mercury mine measured by differential absorption LIDAR techniques and a point monitoring absorption spectrometer. *Atmospheric Environment* 39(22), 4067–4074.

[210] Kotnik, J., Horvat, M., and Dizdarevič, T. (2005). Current and past mercury distribution in air over the Idrija Hg mine region, Slovenia. *Atmospheric Environment* 39, 7570–7579.

[211] Coolbaugh, M. F., Gustin, M. S., and Rytuba, J. J. (2002). Annual emissions of mercury to the atmosphere from natural sources in Nevada and California. *Environmental Geology* 42(4), 338–349.

[212] Xin, M., Gustin, M. S., Ladwig, K., and Pflughoeft-Hassett, D. F. (2006). Air-substrate mercury exchange associated with landfill disposal of coal combustion products. *Journal of the Air & Waste Management Association* 56(8), 1167–1176.

[213] Wang, S. F., Feng, X. B., Qiu, G. L., Wei, Z. Q., and Xiao, T. F. (2005). Mercury emission to atmosphere from Lanmuchang Hg-Tl mining area, Southwestern Guizhou, China. *Atmospheric Environment* 39(39), 7459–7473.

[214] Wang, S. F., Feng, X. B., Qiu, G. L., Fu, X. W., and Wei, Z. Q. (2007). Characteristics of mercury exchange flux between soil and air in the heavily air-polluted area, eastern Guizhou, China. *Atmospheric Environment* 41(27), 5584–5594.

[215] Wang, S. F., Feng, X. B., Qiu, G. G., Shang, L. H., Li, P., and Wei, Z. Q. (2007). Mercury concentrations and air/soil fluxes in Wuchuan mercury mining district, Guizhou province, China. *Atmospheric Environment* 41(28), 5984–5993.

[216] Eckley, C. S., Gustin, M., Marsik, F., and Miller, M. B. (2011). Measurement of surface mercury fluxes at active industrial gold mines in Nevada (USA). *Science of the Total Environment*; 409(3), 514–522.

[217] Nacht, D. M., Gustin, M. S., Engle, M. A., Zehner, R. E., and Giglini, A. D. (2004). Atmospheric mercury emissions and speciation at the sulphur bank mercury mine superfund site, Northern California. *Environmental Science & Technology* 38(7), 1977–1983.

[218] Rinklebe, J., During, A., Overesch, M., Du Laing, G., Wennrich, R., Stark, H. J., and Mothes, S. (2010). Dynamics of mercury fluxes and their controlling factors in large Hg-polluted floodplain areas. *Environmental Pollution* 158(1), 308–318.

[219] Boudala, F. S., Folkins, I., Beauchamp, S., Tordon, R., Neima, J., and Johnson, B. (2000). Mercury flux measurements over air and water in Kejimkujik National Park, Nova Scotia. *Water Air and Soil Pollution* 122(1–2), 183–202.

[220] O'Driscoll, N. J., Beauchamp, S., Siciliano, S. D., Rencz, A. N., and Lean, D. R. S. (2003). Continuous analysis of dissolved gaseous mercury (DGM) and mercury flux in two freshwater lakes in Kejimkujik Park, Nova Scotia: Evaluating mercury flux models with quantitative data. *Environmental Science & Technology* 37(10), 2226–2235.

[221] Feng, X. B., Yan, H. Y., Wang, S. F., Qiu, G. L., Tang, S. L., Shang, L. H., Dai, Q. J., and Hou, Y. M. (2004). Seasonal variation of gaseous mercury exchange rate between air and water surface over Baihua reservoir, Guizhou, China. *Atmospheric Environment* 38 (28), 4721–4732.

[222] Feng, X. B., Wang, S. F., Qiu, G. G., He, T. R., Li, G. H., Li, Z. G., and Shang, L. H. (2008). Total gaseous mercury exchange between water and air during cloudy weather conditions over Hongfeng Reservoir, Guizhou, China. *Journal of Geophysical Research-Atmospheres* 113, D15309, doi: 10.1029/2007jd009600.

[223] Fu, X. W., Feng, X. B., Wan, Q., Meng, B., Yan, H. Y., and Guo, Y. N. (2010). Probing Hg evasion from surface waters of two Chinese hyper/meso-eutrophic reservoirs. *Science of the Total Environment* 408(23), 5887–5896.

[224] Zhang, H., Dill, C., Kuiken, T., Ensor, M., and Crocker, W. C. (2006). Change of dissolved gaseous mercury concentrations in a southern reservoir lake (Tennessee). Following seasonal variation of solar radiation. *Environmental Science & Technology* 40, 2114–2119.

[225] Vandal, G. M., Mason, R. P., and Fitzgerald, W. F. (1991). Cycling of volatile mercury in temperate lakes. *Water Air and Soil Pollution* 56, 791–803.

[226] Amyot, M., Lean, D., and Mierle, G. (1997). Photochemical formation of volatile mercury in high Arctic lakes. *Environmental Toxicology and Chemistry* 16(10), 2054–2063.

[227] Amyot, M., Mierle, G., Lean, D., and McQueen, D. J. (1997). Effect of solar radiation on the formation of dissolved gaseous mercury in temperate lakes. *Geochimica Et Cosmochimica Acta* 61(5), 975–987.

[228] Southworth, G., Lindberg, S., Hintelmann, H., Amyot, M., Poulain, A., Bogle, M., Peterson, M., Rudd, J., Harris, R., Sandilands, K., Krabbenhoft, D., and

Olsen, M. (2007). Evasion of added isotopic mercury from a northern temperate lake. *Environmental Toxicology and Chemistry* 26(1), 53–60.

[229] Mason, R. P., and Sullivan, K. A. (1997). Mercury in Lake Michigan. *Environmental Science & Technology* 31(3), 942–947.

[230] Hines, N. A., and Brezonik, P. L. (2004). Mercury dynamics in a small Northern Minnesota lake: Water to air exchange and photoreactions of mercury. *Marine Chemistry* 90(1–4), 137–149.

[231] Tseng, C. M., Lamborg, C., Fitzgerald, W. F., and Engstrom, D. R. (2004). Cycling of dissolved elemental mercury in Arctic Alaskan lakes. *Geochimica Et Cosmochimica Acta* 68(6), 1173–1184.

[232] O'Driscoll, N. J., Poissant, L., Canario, J., Ridal, J., and Lean, D. R. S. (2007). Continuous Analysis of dissolved gaseous mercury and mercury volatilization in the upper St. Lawrence River: Exploring temporal relationships and UV attenuation. *Environmental Science & Technology* 41(15), 5342–5348.

[233] Gabriel, M. C., and Williamson, D. (2008). Some insight into the influence of urban ground surface properties on the air-surface exchange of total gaseous mercury. *Applied Geochemistry* 23(4), 794–806.

[234] Sommar, J., Wängberg, I., Berg, T., Gårdfeldt, K., Munthe, J., Richter, A., Urba, A., Wittrock, F., and Schroeder, W. H. (2007). Circumpolar transport and air-surface exchange of atmospheric mercury at Ny-Ålesund (79°N), Svalbard, spring 2002. *Atmospheric Physics & Chemistry* 7(1), 151–166.

[235] Schroeder, W. H., Beauchamp, S., Edwards, G., Poissant, L., Rasmussen, P., Tordon, R., Dias, G., Kemp, J., Van Heyst, B., and Banic, C. M. (2005). Gaseous mercury emissions from natural sources in Canadian landscapes. *Journal of Geophysical Research-Atmospheres* 110, D18302, doi: 10.1029/2004jd005699.

[236] Asher, W. E., Karle, L. M., Higgins, B. J., Farley, P. J., Leifer, I. S., and Monahan, E. C. (1995). The effect of bubble plume size on the parameterization of air/seawater gas transfer velocities. In B. Jähne, E. C. Monahan (Eds.), *Air-water gas transfer* (pp. 227–238). Aeon Verlag.

[237] Rolfhus, K. R., and Fitzgerald, W. F. (2001). The evasion and spatial/temporal distribution of mercury species in Long Island Sound, CT-NY. *Geochimica Et Cosmochimica Acta* 65(3), 407–418.

[238] Ferrara, R., and Mazzolai, B. (1998). A dynamic flux chamber to measure mercury emission from aquatic systems. *Science of the Total Environment* 215(1–2), 51–57.

[239] Ci, Z. J., Zhang, X. S., and Wang, Z. W. (2011). Elemental mercury in coastal seawater of Yellow Sea, China: Temporal variation and air-sea exchange. *Atmospheric Environment* 45(1), 183–190.

[240] Conaway, C. H., Squire, S., Mason, R. P., and Flegal, A. R. (2003). Mercury speciation in the San Francisco Bay estuary. *Marine Chemistry* 80(2–3), 199–225.

[241] Mason, R. P., Fitzgerald, W. F., Hurley, J., Hanson, A. K., Donaghay, P. L., and Sieburth, J. M. (1993). Mercury biogeochemical cycling in a stratified estuary. *Limnology and Oceanography* 38(6), 1227–1241.

[242] Mason, R. P., Lawson, N. M., Lawrence, A. L., Leaner, J. J., Lee, J. G., and Sheu, G. R. (1999). Mercury in the Chesapeake Bay. *Marine Chemistry* 65, 77–96.

[243] Borges, A. V., Delille, B., Schiettecatte, L. S., Gazeau, F., Abril, G., and Frankignoulle, M. (2004). Gas transfer velocities of CO_2 in three European estuaries (Randers Fjord, Scheldt, and Thames). *Limnology and Oceanography* 49(5), 1630–1641.

[244] Mason, R. P., Rolfhus, K. R., and Fitzgerald, W. F. (1998). Mercury in the North Atlantic. *Marine Chemistry* 61(1–2), 37–53.

[245] Andersson, M. E., Sommar, J., Gårdfeldt, K., and Jutterström, S. (2011). Air-sea exchange of volatile mercury in the North Atlantic Ocean. *Marine Chemistry* 125(1–4), 1–7.

[246] Temme, C., Bakau, J., Schneider, B., Aspmo, K., Fain, X., Ferrari, C., Gauchard, P.-E., and Ebinghaus, R. Air/water exchange of mercury in the North Atlantic Ocean during arctic summer. In *Proceedings of XIII International Conference on Heavy Metals in the Environment, Rio de Janeiro, 2005*.

[247] Mason, R. P., and Sullivan, K. A. (1999). The distribution and speciation of mercury in the south and equatorial Atlantic. *Deep-Sea Research II* 46(937–956).

[248] Mason, R. P., Lawson, N. M., and Sheu, G. R. (2001). Mercury in the Atlantic Ocean: Factors controlling air-sea exchange of mercury and its distribution in the upper waters. *Deep-Sea Research II* 48(13), 2829–2853.

[249] St Louis, V. L., Sharp, M. J., Steffen, A., May, A., Barker, J., Kirk, J. L., and Kell, D. J. A. (2005). Some sources and sinks of monomethyl and inorganic mercury on Ellesmere Island in the Canadian high Arctic. *Environmental Science & Technology* 39, 2686–2701.

[250] Mason, R. P., and Fitzgerald, W. F. (1993). The distribution and biogeochemical cycling of mercury in the equatorial Pacific-Ocean. *Deep-Sea Research I* 40(9), 1897–1924.

[251] Laurier, F. J. G., Mason, R. P., Whalin, L., and Kato, S. (2003). Reactive gaseous mercury formation in the north Pacific Ocean's marine boundary layer: A potential role of halogen chemistry. *Journal of Geophysical Research-Atmospheres* 108, 4529, doi: 10.1029/2003JD003625.

[252] Fu, X. W., Feng, X. B., Zhang, G., Xu, W. H., Li, X. D., Yao, H., Liang, P., Li, J., Sommar, J., Yin, R. S., and Liu, N. (2010). Mercury in the marine boundary layer and seawater of the south China Sea: Concentrations, sea/air flux, and implication for land outflow. *Journal of Geophysical Research-Atmospheres* 115, D06303, doi: 10.1029/2009JD012958.

[253] Ci, Z. J., Zhang, X. S., Wang, Z. W., Niu, Z. C., Diao, X. Y., and Wang, S. W. (2011). Distribution and air-sea exchange of mercury (Hg), in the Yellow Sea. *Atmospheric Chemistry and Physics* 11(6), 2881–2892.

[254] Coquery, M., and Cossa, D. (1995). Mercury speciation in surface waters of the North Sea. *Netherlands Journal of Sea Research* 34(4), 245–257.

[255] Weiss, A., Kuss, J., Peters, G., and Schneider, B. (2007). Evaluating transfer velocity–wind speed relationship using a long-term series of direct eddy correlation CO_2 flux measurements. *Journal of Marine Systems* 66, 130–139.

[256] Lindberg, S. E., Dong, W. J., Chanton, J., Qualls, R. G., and Meyers, T. (2005). A mechanism for bimodal emission of gaseous mercury from aquatic macrophytes. *Atmospheric Environment* 39(7), 1289–1301.

[257] Lindberg, S. E., and Zhang, H. (2000). Air/water exchange of mercury in the Everglades II: Measuring and modeling evasion of mercury from surface waters

in the Everglades Nutrient Removal Project. *Science of the Total Environment* 259(1–3), 135–143.

[258] Poissant, L., Pilote, M., Constant, P., Beauvais, C., Zhang, H. H., and Xu, X. H. (2004). Mercury gas exchanges over selected bare soil and flooded sites in the bay St. Francois wetlands (Quebec, Canada). *Atmospheric Environment* 38(25), 4205–4214.

[259] Zhang, H. H., Poissant, L., Xu, X. H., Pilote, M., Beauvais, C., Amyot, M., Garcia, E., and Laroulandie, J. (2006). Air-water gas exchange of mercury in the Bay Saint Francois wetlands: Observation and model parameterization. *Journal of Geophysical Research-Atmospheres* 111, D17307, doi: 10.1029/2005jd006930.

[260] Zhang, H., Lindberg, S. E., Marsik, F. J., and Keeler, G. J. (2001). Mercury air/surface exchange kinetics of background soils of the Tahquamenon River watershed in the Michigan Upper Peninsula. *Water Air and Soil Pollution* 126(1–2), 151–169.

[261] Hintelmann, H., Harris, R., Heyes, A., Hurley, J. P., Kelly, C. A., Krabbenhoft, D. P., Lindberg, S., Rudd, J. W. M., Scott, K. J., and St Louis, V. L. (2002). Reactivity and mobility of new and old mercury deposition in a Boreal forest ecosystem during the first year of the METAALICUS study. *Environmental Science & Technology* 36(23), 5034–5040.

[262] Fu, X. W., Feng, X. B., and Wang, S. F. (2008). Exchange fluxes of Hg between surfaces and atmosphere in the eastern flank of Mount Gongga, Sichuan province, southwestern China. *Journal of Geophysical Research-Atmospheres* 113, D20306, doi: 10.1029/2008jd009814.

[263] Zhu, J. S., Wang, D. Y., Liu, X. A., and Zhang, Y. T. (2011). Mercury fluxes from air/surface interfaces in paddy field and dry land. *Applied Geochemistry* 26(2), 249–255.

[264] Carpi, A., Lindberg, S. E., Prestbo, E. M., and Bloom, N. S. (1997). Methyl mercury contamination and emission to the atmosphere from soil amended with municipal sewage sludge. *Journal of Environmental Quality* 26(6), 1650–1655.

[265] Schroeder, W. H., Steffen, A., Scott, K., Bender, T., Prestbo, E., Ebinghaus, R., Lu, J. Y., and Lindberg, S. E. (2003). Summary report: First international Arctic atmospheric mercury research workshop. *Atmospheric Environment* 37(18), 2551–2555.

[266] Brooks, S. B., Saiz-Lopez, A., Skov, H., Lindberg, S. E., Plane, J. M. C., and Goodsite, M. E. (2006). The mass balance of mercury in the springtime arctic environment. *Geophysical Research Letters* 33(13), L13812.

[267] Ferrari, C. P., Gauchard, P.-A., Aspmo, K., Dommergue, A., Magand, O., Bahlmann, E., Nagorski, S., Temme, C., Ebinghaus, R., and Steffen, A. (2005). Snow-to-air exchanges of mercury in an Arctic seasonal snow pack in Ny-Ålesund, Svalbard. *Atmospheric Environment* 39(39), 7633–7645.

[268] Bash, J. O., and Miller, D. R. (2007). A note on elevated total gaseous mercury concentrations downwind from an agriculture field during tilling. *Science of the Total Environment* 388, 379–388.